DEVELOPMENT OF CaO-BASED SORBENT FOR HIGH-TEMPERATURE CO_2 SORPTION

By
Mr. Panupong Jamrunroj

A Thesis Submitted in Partial Fulfillment of the Requirements for the Degree
Master of Engineering Program in Chemical Engineering
International Program
Graduate School, Silpakorn University
Academic Year 2015

DEVELOPMENT OF CaO-BASED SORBENT FOR HIGH-TEMERATURE CO_2 SORPTION

By
Mr.Panupong Jamrunroj

A Thesis Submitted in Partial Fulfillment of the Requirements for the Degree
Master of Engineering Program in Chemical Engineering
International Program
Graduate School, Silpakorn University
Academic Year 2015

การพัฒนาตัวดูดซับจากแคลเซียมออกไซด์เพื่อการดูดซับแก๊สคาร์บอนไดออกไซด์ที่อุณหภูมิสูง

โดย

นายภาณุพงศ์ จำรูญโรจน์

วิทยานิพนธ์นี้เป็นส่วนหนึ่งของการศึกษาตามหลักสูตรปริญญาวิศวกรรมศาสตรมหาบัณฑิต

สาขาวิชาวิศวกรรมเคมี

ภาควิชาวิศวกรรมเคมี

บัณฑิตวิทยาลัย มหาวิทยาลัยศิลปากร

ปีการศึกษา 2558

The Graduate School, Silpakorn University has approved and accredited the Thesis title of "DEVELOPMENT OF CaO-BASED SORBENT FOR HIGH-TEMPERATURE CO_2 SORPTION" submitted by MR. Panupong Jamrunroj as a partial fulfillment of the requirements for the degree of Master of Engineering in CHEMICAL ENGINEERING

.....
(Associate Professor Panjai Tantatsanawong, Ph.D.)
Dean of Graduate School
...../...../.....

The Thesis Advisor

Assistant Professor Suwimol Wongsakulphasatch, Ph.D.

The Thesis Examination Committee

..... Chairman
(Assistant Professor Worapon Kiatkittipong, D.Eng.)
...../...../.....

..... Member
(Assistant Professor Chaiwat Prapainainar, Ph.D.)
...../...../.....

..... Member
(Paweena Prapainainar, Ph.D.)
...../...../.....

56404205: MAJOR: CHEMICAL ENGINEERING
KEY WORDS: CaO-BASED SORBENT/ CO_2 SORPTION/ SURFACTANT
PANUPONG JAMRUNROJ: DEVELOPMENT OF CaO-BASED SORBENT FOR HIGH-TEMERATURE CO_2 SORPTION. THESIS ADVISOR: ASST. PROF.SUWIMOL WONGSAKULPHASATCH, Ph.D. 99 pp.

CaO-based sorbent was synthesized and used as sorbent for high-temperature CO_2 sorption. In this work, CaO was obtained from calcination of $CaCO_3$, which was produced by precipitation technique using different precursors of calcium and carbonate. The effect of precursor (both calcium and carbonate precursors), the addition of additive, and synthesis method on CO_2 sorption capacity were investigated. The results show that precursor has an effect on morphology of CaO derived from $CaCO_3$ and also has an influence on CO_2 capture ability. CaO, synthesized from the use of calcium acetate and urea, show large network of connected particles, which resulted in good performance of CO_2 sorption capacity of 0.64 $gCO_2/gCaO$ at 700°C. In addition, the addition of additive during synthesis also show the effect on CaO properties and the ability to adsorb CO_2. The sorbent prepared with the addition of 2 mM of Gemini surfactant provides rod-like structure with rough surface and large surface area (16.3 m^2/g). This sorbent offers CO_2 sorption capacity of 0.29 $gCO_2/gCaO$ at 600°C. In addition, thermal stability of CaO was improved by incorporating CaO with aluminum using different techniques. The results show CaO-based sorbent synthesized by sol-gel technique provides good performance of CO_2 capture at 0.63 $gCO_2/gCaO$ and CO_2 sorption capacity reduced approximately 35% after 10 repeated cycles.

Department of Chemical Engineering Graduate School, Silpakorn University
Student's signature ..... Academic Year 2015
Thesis Advisor's signature .....

56404205 : สาขาวิชาวิศวกรรมเคมี
คำสำคัญ : ตัวดูดซับแคลเซียมออกไซด์/ การดูดซับคาร์บอนไดออกไซด์/ สารลดแรงตึงผิว

ภาณุพงศ์ จำรูญโรจน์ : การพัฒนาตัวดูดซับจากแคลเซียมออกไซด์เพื่อการดูดซับแก๊สคาร์บอนไดออกไซด์ที่อุณหภูมิสูง. อาจารย์ที่ปรึกษาวิทยานิพนธ์ : ผศ.ดร.สุวิมล วงศ์สกุลเภสัช. 99 หน้า.

ตัวดูดซับแคลเซียมออกไซด์ถูกปรับปรุงความสามารถในการดูดซับเพื่อนำมาใช้ในการดูดซับคาร์บอนไดออกไซด์ที่อุณหภูมิสูง ในงานวิจัยนี้ตัวดูดซับแคลเซียมออกไซด์ที่ใช้ได้มาจากการเผาแคลเซียมคาร์บอเนตที่สังเคราะห์ด้วยวิธีการตกตะกอนระหว่างสารตั้งต้นแคลเซียมและคาร์บอเนตที่แตกต่างกัน ผลของการปรับปรุงโดยการเลือกใช้สารตั้งต้นแคลเซียมและคาร์บอเนตที่แตกต่างกัน การเติมสารเติมแต่ง การเลือกใช้วิธีการสังเคราะห์ ได้ถูกนำมาตรวจสอบความสามารถในการดูดซับแก๊สคาร์บอนไดออกไซด์ ผลการทดลองแสดงให้เห็นว่าการเลือกใช้สารตั้งต้นต่างชนิดกันจะทำให้เกิดรูปร่างของแคลเซียมออกไซด์ที่มาจากแคลซียมคาร์บอเนตที่แตกต่างกัน ซึ่งรูปร่างที่แตกต่างกันนั้นส่งผลต่อความสามารถในการดูดซับแก๊สคาร์บอนไดออกไซด์ โดยแคลเซียมออกไซด์ที่สังเคราะห์จากแคลเซียมอะซิเตรทกับยูเรียมีรูปร่างเป็นโครงร่างตาข่ายที่เกิดจากการเชื่อมกันของอนุภาคขนาดเล็กซึ่งแสดงความสามารถในการดูดซับได้ดีคือ 0.64 กรัมคาร์บอนไดออกไซด์ต่อกรัมของแคลเซียมออกไซด์ที่ 700 องศาเซลเซียส ในส่วนของการเติมสารเติมแต่งคือสารลดแรงตึงผิวลงไปในขั้นตอนการสังเคราะห์นั้นพบว่าส่งผลต่อคุณสมบัติของแคลเซียมออกไซด์ และส่งผลต่อความสามารถในการดูดซับ ตัวดูดซับที่ถูกเตรียมโดยการเติมสารลดแรงตึงผิวชนิดเจ็มมินายลงไป 2 มิลิโมลาร์จะมีรูปร่างเหมือนแท่งที่มีผิวขรุขระและมีพื้นที่ผิวที่ 16.3 ตารางเมตรต่อกรัม ตัวดูดซับนี้มีความสามารถในการดูดซับที่ 0.29 กรัมคาร์บอนไดออกไซด์ต่อกรัมของแคลเซียมออกไซด์ที่ 600 องศาเซลเซียส นอกจากนี้ตัวดูดซับแคลเซียมออกไซด์ได้ถูกปรับปรุงความเสถียรทางความร้อนโดยรวมแคลเซียมออกไซด์กับอะลูมินัมด้วยเทคนิคที่แตกต่างกัน ผลการปรับปรุงแสดงให้เห็นว่าการสังเคราะห์โดยวิธีโซลเจลนั้นสารถดูดซับได้ 0.63 กรัมคาร์บอนไดออกไซด์ต่อกรัมของแคลเซียมออกไซด์ และผลการทดสอบการดูดซับในหลายรอบพบว่าความสามารถในการดูดซับลดลง 35 เปอร์เซนต์หลังจากการดูดซับในรอบที่ 10

ภาควิชาวิศวกรรมเคมี บัณฑิตวิทยาลัย มหาวิทยาลัยศิลปากร
ลายมือชื่อนักศึกษา..... ปีการศึกษา 2558
ลายมือชื่ออาจารย์ที่ปรึกษาวิทยานิพนธ์.....

Acknowledgements

I would like to express my sincere gratitude and appreciation to my advisor, Asst. Prof. Dr. Suwimol Wongsakulphasatch, for her valuable suggestions, stimulation and useful discussions throughout this research and devotion to revise this thesis. My appreciation would also go to Professor Suttichai Assabumrungrat for comments and the assistance of experimental equipments. I also would like to thank Dr. Atthaphon Maneedaeng, Mr.Janewit Phromprasit, Miss Piya Pecharaumporn, Miss Chanita wattanasomboon, Miss Siriporn Aeamsuksai, Miss Mintra Aupahad, and Miss Natcha Khunthong for their assistance in the lab.

In particular, I appreciate for the kind comments and suggestions from Asst. Prof. Dr. Worapon Kiatkittipong, Asst. Prof. Dr. Chaiwat Prapainainar, and Dr. Paweena Prapainainar who have been the chairman and members of the thesis committee, respectively.

List of Tables

List of Figures

Table of Contents

CHAPTER I

INTRODUCTION

1.1. Motivation

CaO is used in many applications, for example, catalyst for transesterification reaction [Hai-xin et al. (2009)], reactant of cement [Katsuyama et al. (2005)], additive in paper industrial [Chen and Xiang (2009)], or gas separation [Barker (1973), Olivares-marin et al. (2013)]. One of the most widely applications of CaO is the use as adsorbent for CO_2 capture. CaO is used to adsorb CO_2 through the so-called calcium looping technology as represented in Eqs. (1) and (2):

Carbonation: $CaO + CO_2 \rightarrow CaCO_3$ $\Delta H = -178$ kJ/mole (1)

Calcination: $CaCO_3 \rightarrow CaO + CO_2$ $\Delta H = +178$ kJ/mole (2)

In calcium looping, CaO is reacted with CO_2 to form $CaCO_3$ (Eq. 1).This process is exothermic reaction and called carbonation reaction. The reverse reaction (Eq. 2) is endothermic reaction and named calcination reaction.

Calcium looping technology is widely used in three processes: pre-combustion, post-combustion, and oxy-fuel. In pre-combustion, carbon capture takes place before combustion process, for instance, in steam reforming reaction or water gas shift (WGS). In these processes, CaO is used to separate CO_2 from H_2 for higher H_2 purity. For post-combustion process such as coal combustion or fossil fuel combustion for power generation, large amount of CO_2 is emitted from these processes, calcium looping become an important role for CO_2 capture technology. In oxy-fuel process, pure oxygen is used to combust with fuel for power generation, where CO_2 is needed to lessen before releasing into the environment.

One of the attract attentions for the use of CaO is its abundant in nature; it can be obtained from several resources such as natural lime, egg shell, seashells, and snail shells [Chen et al. (2010)]. However, textural and chemical properties of the natural resources of CaO are diversity and difficult to control for specific industrial requirements. As a consequence, synthetic CaO is developed to improve the properties of CaO to overcome the limitation of natural CaO and for a variety of applications.

In the present study, we attempt to improve properties of CaO-based sorbent for CO_2 sorption specifically for high-temperature of sorption, where an interesting application is found in hydrogen production process. It has been revealed that synthesis method Gupta and Fan (2002), Santos et al. (2012), and Liu et al. (2008), reactants Silaban et al. (1992), Lu et al. (2006), and Lu et al. (2008), the addition of additives Olivares-Marin et al. (2013), Akgsornpeak et al. (2014), and Witoon et al., (2014), etc., can affect morphologies and properties of CaO, which in turn affect CO_2 sorption capacity and stability. As such, in this work, the effects of calcium precursors, the addition of surfactant as a directing agent, and the incorporation of metal ion for the improvement of both capacity and stability of sorbents on high-temperature CO_2 sorption are subjects of interest. Performances of the sorbents on CO_2 sorption will be investigated in terms of sorption capacity and sorbent stability.

1.2. Objective of Research

To study the effect of CaO-based sorbent on both sorption capacity and stability for high-temperature CO_2 capture by investigating the effects of precursors types, type and concentration of additives, and method for metal corporation between CaO and Al_2O_3 on CO_2 sorption performances.

CHAPTER II

LITERATURE REVIEW

CaO-based sorbents are widely used in CO_2 capture and storage due to its availability, high capacity and ability to regenerate. Although, CaO can be found in nature; however, uncontrollable of natural CaO sorbent is the main drawback to use in industrial applications. Synthetic CaO is therefore became an alternative way to improve properties of CaO sorbents. In this section, review of literatures will be focused on factors that affect the properties of synthetic CaO and also the performance of high-temperature CO_2 capture, for example, synthesis method, calcium precursor, the addition of additives and metal oxide.

2.1 Synthesis of $CaCO_3$

CaO sorbent can be prepared by several methods such as precipitation Zhang et al. (2008), Chen and Xiang (2009), hydrothermal Liu et al. (2008), sol-gel Santos et al. (2012), etc. One technique that is widely used to synthesize CaO is the derivation from $CaCO_3$. Precipitation method is a simple technique used to prepare $CaCO_3$ before calcination to CaO. Zhang et al. (2008) synthesized $CaCO_3$ by precipitation method using $Ca(OH)_2$ and CO_2 as precursors. In this work, 2.2 g/L of $Ca(OH)_2$ was reacted with CO_2 under pressure ranging from 4.90-12.04 MPa in autoclave, which placed in water bath at 20^{o}C under vigorous stirring for 1 h. The results showed calcite phase and cubic morphology of $CaCO_3$ were obtained for all CO_2 pressures used. Chen and Xiang (2009) prepared $CaCO_3$ by precipitation method using equimolar (2.5 M) of NH_4HCO_3 and $CaCl_2$. The mixture solution was stirred at 30^{o}C for 45 min. The results showed that the obtained $CaCO_3$ was only vaterite phase and its morphology was mushroom-like of lamellar aggregation. In addition, the effect of precursor ratios of $CaCl_2$ and NH_4HCO_3 on structure of $CaCO_3$ precipitation was also investigated in this work. The concentration ratio $CaCl_2$:NH_4HCO_3 of 1:2 showed lamellar aggregate morphology and polymorph was pure vaterite whereas the molar ratio $CaCl_2$:NH_4HCO_3 of 2:1 showed lamellar hexagonal and the phase of $CaCO_3$ was found to be 79% of vaterite, 19% of aragonite and 1.5% of calcite. Hwang et al. (2011) studied the effect of temperature on precipitation of $CaCO_3$. The equimolar of

$CaCl_2$ and Na_2CO_3 was mixed under vigorous stirring at pH 9 at different temperatures of 25, 40, 60, and 80^oC. The $CaCO_3$ synthesized at 25 and 40^oC showed aggregation of cubic particle. When increasing temperature to 60^oC and 80^oC, the agglomeration of cubic particle was inhibited and tended to form more mono-cubic particle. The polymorph of $CaCO_3$ was calcite phase for all temperatures of the synthesis. Shen et al. (2004) synthesized $CaCO_3$ from $CaCl_2$ and Na_2CO_3 with the use of additives polyvinylpyrrolidone (PVP) and sodium dodecyl benzene sulfonate (SDBS). The PVP (inert of nonionic polymer) additive was added into the solutions of Na_2CO_3 and $CaCl_2$, each concentration was 0.1 M, while SDBS was added only into the Na_2CO_3 solution. The mixture solution was allowed to stir at 200 rpm, pH 7, and 26^oC for 10 h. The results showed that $CaCO_3$ synthesized without the addition of additive showed polydispersity of cubic with small particle morphologies. $CaCO_3$ synthesized with the addition of 100 g/L of PVP showed calcite of rhombohedral morphology and the addition of SDBS surfactant of 50 mM could control morphology to vaterite spherical. Wei et al. (2005) studied effect of anionic surfactants: sodium dodecyl sulfate (SDS), sodium dodecyl sulfonate (DDS), and sodium dodecyl benzenesulfonate (SDBS) on precipitation of $CaCO_3$ from equimolar (0.1 M) of $CaCl_2$ and Na_2CO_3. The surfactant concentration of 0.5 and 5 mM was added into solution of Na_2CO_3 and then the solution of $CaCl_2$ was added in the mixture solution. The mixture solution was allowed to stir at 26^oC and pH 7 for 10 h. The results showed that $CaCO_3$ synthesized with 0.5 mM and 5 mM of DDS showed cubic morphology. $CaCO_3$ synthesized with 0.5 mM of SDS possessed cubic and small amount of spherical formed from cubic aggregation. When concentration of SDS was increased to 5 mM, $CaCO_3$ morphology showed spherical shape. The synthesis of $CaCO_3$ with SDS and DDS formed calcite phase. In case of SDBS additive, $CaCO_3$ morphology showed cubic structure of calcite at 0.5 mM and then converted to spherical of vaterite at SDBS of 5 mM. The authors claimed that the addition of 0.5 mM of all additives yielded cubic structure due to surfactant cannot adsorbed on the surface of $CaCO_3$ at this concentration. The effect of SDS and DDS was explained as SO_3^- of SDS and DDS adsorbed monolayer on the surface of $CaCO_3$ at plane (001) and carbonate were aligned parallel on the plane. The $CaCO_3$ with SDS and DDS of 5 mM showed different morphologies due to different degree of hydroplilicity of surfactant: the SDS ($-OSO_3^-$) is more hydrophilic than DDS ($-SO_3^-$). Yu et al. (2005) used cationic surfactants cetyltrimethylammonium bromide (CTAB) and poly (styrene-alt-maleic acid) (PSMA) as additives in the precipitation of $CaCO_3$ for controlling structure. $CaCO_3$ was synthesized by 0.5 M, 1.5 mL equimolar of $CaCl_2$ and Na_2CO_3. The additive was used at concentration of: CTAB 0.2-5 mM and PSMA 0.5 or 1.5 g/L. In this study, the results showed that CTAB had no obvious effect on morphology and polymorph at room temperature as both $CaCO_3$ without and with CTAB addition showed rhombohedral morphology and pure calcite. On the other hand, the PSMA at concentration of 0.5 and 1.5 g/L provided $CaCO_3$ morphology of

rhombohedral with mixed phase of calcite and vaterite and dumbbell-shape with calcite phase, respectively.

2.2 CaO-based sorbent for CO_2 capture

2.2.1 CaO sorbent for CO_2 capture

Silaban et al. (1992) synthesized CaO by decomposing different $CaCO_3$ precursors by heat. Calcium carbonate ($CaCO_3$) and calcium acetate ($Ca(CH_3COO)_2$) were selected as precursors and they were completely decomposed at 750^oC for 45 min. Comparison structure of CaO from different precursors showed that CaO-$Ca(CH_3COO)_2$ had larger pore size (30 um) than CaO-$CaCO_3$ (0.04 um). The sorbents were tested to adsorb CO_2 at 750^oC for 60 min in 15% v/v CO_2 (balance N_2) and showed that 96% conversion was observed for CaO-$Ca(CH_3COO)_2$ and 78% conversion for CaO-$CaCO_3$. It was claimed that CaO-$Ca(CH_3COO)_2$ had higher capacity than CaO-$CaCO_3$ due to larger surface area. Gupta and Fan (2002) synthesized $CaCO_3$ by precipitation of $Ca(OH)_2$ and CO_2. The concentration of $Ca(OH)_2$ was varied at 8, 16, and 24 times its saturation solubility limit (sat) and reacted with CO_2 for 10 min. The results of surface area of $CaCO_3$ at $Ca(OH)_2$ concentration of 8, 16, and 24-sat showed 13.8, 38.3, and 36.8 m^2/g, respectively. The synthesized $CaCO_3$ was calcined to be CaO and used for CO_2 adsorption. The capacity of CaO sorbents derived from $CaCO_3$ at 16-sat provided 90%, 70%, and 60% conversion at 650, 600, and 550^oC in pure CO_2, respectively. Lu et al. (2006) prepared CaO from calcination of calcium precursors including calcium nitrate ($Ca(NO_3)_2$), calcium oxide (CaO), calcium hydroxide ($Ca(OH)_2$), calcium carbonate ($CaCO_3$), and calcium acetate ($Ca(CH_3COO)_2$) at 750^oC for 30 min in helium atmosphere. The surface area was in the order: CaO-$Ca(CH_3COO)_2$ (20 m^2/g) > CaO-$Ca(OH)_2$ (14 m^2/g) > CaO-$CaCO_3$ (5 m^2/g)> CaO-CaO (4 m^2/g). The conversion of each sorbent was 2.5% CaO- $Ca(NO_3)$, 25% CaO-CaO, 63% CaO-$Ca(OH)_2$, 66% CaO-$CaCO_3$, and 97% CaO-CaAc at carbonation temperature of 600^oC, 30% v/v CO_2 (balanced He). Lysikov et al. (2007) used spherically monodisperse $CaCO_3$ of 3-4 um size, monocrystal of $CaCO_3$ and commercial $CaCO_3$ to calcine at 822^oC under Ar flow for 15 min for the decomposition for CaO. The reactivity for CO_2 capture was tested in isothermal system under 33% v/v of CO_2 (balanced Ar) for 15 min of adsorption. The capacity of sorbent was in the order of $CaCO_3$ commercial (61% conversion) > monodisperse $CaCO_3$ (51% conversion) > monocrystal $CaCO_3$ (34% conversion). From the results, they suggested that CO_2 sorption capacity depends upon morphology structure of sorbents. Florin and Harris (2009) used nano-sized $CaCO_3$ (40 nm) to calcine for the production of CaO at 700^oC under N_2 to investigate CO_2 sorption performances using TGA at 650^oC for 24 h under 15% v/v CO_2 (balance N_2) and also the ability to regenerate at 850^oC for 10 min under N_2 atmosphere. The results showed 90% conversion was observed in the 1st cycle and decreased to 20% in

the 100th cycle. Zhu et al. (2011) used nano $CaCO_3$ to test the adsorption of CO_2. The $CaCO_3$ had morphology of hexagonal calcite with 70 nm of particle size. The $CaCO_3$ was activated by calcination under N_2 (40 ml/min) at 850°C for 10 min. In this work, the activated sorbent was tested for CO_2 sorption in fixed bed reactor at 650°C for 40 min (flow rate of CO_2 was 10 ml/min). The CO_2 sorption capacity was found to be 8 mol/kg (0.35 $gCO_2/gCaO$). Additionally, the grain of CaO was observed that being increased in size for multi-cycles use: the grain size of 47 nm was observed at the 1st cycle and the size became 90 nm after 40 cycles (carbonation 650°C, 40 min under 20% v/v CO_2 (balanced N_2) and calcination at 800°C for 30 min in N_2). Santos et al. (2012) synthesized CaO by sol-gel method where equimolar of calcium nitrate and citric acid were mixed and vigorous stirred at 80°C until a yellow gel was formed. Then the gel was dried at 130°C and calcined at 850°C for 5 h. The morphology of CaO sorbent observed from SEM was found to be an aggregate of rod–shape. CO_2 sorption of the synthetic CaO in thermal gravimetric analysis showed 90% conversion at 700°C for 15% v/v CO_2 (Balanced N_2). Lu et al. (2006) studied the effect of temperature on CO_2 sorption by varying the temperature of 200, 300, 400, 500, 550, 600, 700, and 800 °C. The CaO sorbent was prepared by calcination of calcium acetate at 750°C for 30 min. The sorbent was evaluated its sorption capacity under 30% CO_2 (balanced helium) using Thermal Gravimetric Analysis (TGA). The results showed that increasing temperature enhanced CO_2 sorption capacity; conversion increased from 10% to 97% when carbonation temperature was raised from 200 to 800°C. Olivares-Marín et al. (2013) precipitated $CaCO_3$ from Na_2CO_3 and $CaCl_2$ with the addition of surfactant TX-100 and commercial dish washing liquid detergent (DLD) of 1%v/v. The results showed the precipitated $CaCO_3$ without additive formed rhombohedral calcite and needle aragonite. Addition of TX-100 showed similar morphology to that without additive whereas morphology of $CaCO_3$ with the addition of DLD obtained spherical of vaterite. All $CaCO_3$ sorbents were calcined to CaO at 950°C for 4 h and then tested CO_2 capture performances at condition of 15% v/v CO_2 and 650°C. The results revealed that conversion was 25.66% for $CaCO_3$ without additive, 23.84% for CaO-TX-100, and 18.30% for CaO-DLD. Lower capacity of CaO with the addition of DLD additive was found to be due to large agglomeration of particles. It is noted, however, that capacity of all sorbents showed no correlation between adsorption capacities with surface area. Witoon et al. (2014) synthesized $CaCO_3$ by precipitation of $Ca(NO_3)_2$ and Na_2CO_3 with the addition of chitosan and sodium dodecyl sulfate (SDS). In this work, $Ca(NO_3)_2$ was added into 100-mL solution of chitosan, which was dissolved in 1% v/v acetic acid. The mass ratio of chitosan to Ca^{2+} was varied 0.125:1, 0.25:1, 0.75:1, 1.25:1, and 2.5:1. The results showed that synthetic CaO without additive possessed rhombohedral structure. When the chitosan was added, the $CaCO_3$ formed sheet-like and interconnected of skeleton structure at all concentrations. When concentration of chitosan was increased, the $CaCO_3$ tended to aggregate to form larger particle. In case of adding 50 mmol SDS

surfactant and the mixture of SDS and chitosan (mass ratio 0.75:1), the obtained $CaCO_3$ was spherical structure and flower shape structure, respectively. Capability of CO_2 sorption by CaO sorbents was tested at carbonation temperature of 700°C for 40 min in 15% v/v CO_2 (balanced N_2). In addition, multi-cycles used of the sorbent was also investigated in this work, the sorbent was regenerated by calcination at 850°C for 10 min. The results showed that CaO without surfactant provided 37% conversion in the first cycle and reduced to 30% conversion in the 20th cycle. The optimum condition of adding chitosan was found at 1:0.75 by mass ratio of CaO:chitosan where maximum capacity of 82% and 58% conversion in 1st cycle and 20th cycles, respectively, was observed. CaO with 50 mmol SDS added showed 47% and 20% conversion in the 1st cycle and the 20th cycle, respectively. CaO synthesized with the mix of chitosan (mass ratio of CaO/chitosan was 1:0.75) and 50 mmol of SDS yielded 60% conversion in the 1st cycle and decreased to approximately 20% conversion in the 20th cycle. Akgsornpeak et al. (2014) used sol-gel method with the addition of CTAB to synthesize CaO with the variation of calcium and CTAB concentrations: 5, 10, and 15 mmol for $Ca(NO_3)_2$ and 0, 1.5, 3, 4.5, and 6 mmol for CTAB. Synthesis method was carried out by dissolving CTAB in 60 mL of DI water and then added $Ca(NO_3)_2$ into the solution, where pH was adjusted to 11.1. The mixture was allowed to age for 6 h at 80°C, then dried at 140°C for 24 h when the gel was formed. The final product was obtained by calcination at 700°C for 2 h. The effect of $Ca(NO_3)_2$ concentration was explained that increasing concentration of $Ca(NO_3)_2$ leaded to a decrease in size of particle. The present of CTAB surfactant resulted in both negative and positive effects on morphology and surface area; the negative effect is that CTAB promoted larger agglomerated particle whereas positive effect is high porous and small particle. The CaO sorbent 10$Ca(NO_3)_2$:3CTAB showed the best performance of 76.6% conversion in the 1st cycle and decreased to 63.3% conversion in the 20th cycle.

2.2.2 Incorporation of aluminum oxide with calcium-based sorbent

Although CaO is proved to be a good material for high-temperature CO_2 sorption due to its high sorption capacity; however, low capacity upon multiple cycles use is the main drawback of this material. Therefore, another improvement on applying CaO sorbent for high-temperature CO_2 capture is to improve stability of the material. The addition of metal, synthesis method, and the effect of amount of metal adding are reviewed in this section. Kierzkowska et al. (2013) investigated the effect of precursors and pH of co-precipitation CaO-based on CO_2 sorption performances. $Ca(NO_3)_2$ and $Ca(CH_3COO)_2$ were used as calcium precursors, Na_2CO_3 and $(NH_4)_2CO_3$ were used as carbonate precursors, and $Al(NO_3)_2$ was used as aluminum precursor. The results showed sorbents prepared at pH 7 and 9.7 were not influent CO_2 sorption capacity whereas calcium and carbonate precursors strongly affected CO_2 adsorption. The sorbents synthesized from $Ca(NO_3)_2$, $Al(NO_3)_2$ and $(NH_4)_2CO_3$

at pH 9.7 showed the highest conversion of 83% and 69% in the 1st and 30th cycle, respectively, at carbonation temperature of 750°C in 40% CO_2 (balanced N_2) for 20 min and calcination at 750°C for 20 min in pure N_2. Sorbent from $Ca(CH_3COO)_2$, $Al(NO_3)_2$, and $(NH_4)_2CO_3$ at pH 9.7 had 79% in the 1st cycle and reduced to 69% conversion in the 30th cycle. CaO synthesized by $Ca(NO_3)_2$, $Al(NO_3)_2$, and Na_2CO_3 obtained 80% and 60% conversion in 1st and 30th cycle, respectively, $Ca(CH_3COO)_2$, $Al(NO_3)_2$, and Na_2CO_3 found similar tend with the case of $Ca(NO_3)_2$, which conversion was 77% and 54% in the 1st and 30th cycle, respectively. Xu et al. (2013) synthesized CaO-based alumina sorbent by sol-gel technique. The aluminum isopropoxide was hydrolyzed at 85°C and 500 rpm under reflux for 1.5 h. Then the solution of calcium lactate was added into aluminum solution. The pH of mixture solution was adjusted to 3-4 by acetic acid and the condensation reaction was continued at 90°C under reflux for 24 h. the solution was formed to gel and then dried at 110°C for 12 h and calcined at 900°C for 2 h. Carbonation was tested at 650°C, 30 min, and 15% v/v CO_2 in N_2 and calcination at 800°C for 10 min in N_2. The components of sample were 20% wt of $Ca_9Al_6O_{18}$ and 80% wt of CaO. Sorption capacity in the 1st and 35th cycle was found to be 84% and 83% conversion, respectively. These results indicated that $Ca_9Al_6O_{18}$ is an important factor to keep stability of CaO sorbent by delaying sintering effect. Lao et al. (2011) prepared CaO-based sorbent by mixing $CaCO_3$ with $Al(NO_3)_3$ in DI water. The CaO-based sorbent showed by XRD the formation of an inert support $Ca_{12}Al_{14}O_{33}$ and an active CaO at weight ratio of 80% of CaO and 20% of $Ca_{12}Al_{14}O_{33}$. CO_2 sorption tests were performed in fixed-bed reactor under 100% CO_2 and the results showed 73% conversion in the 1st cycle and reduced to 50% conversion in the 11th cycle. In addition, the same authors were also synthesized CaO-based by sol-gel combustion using $Ca(NO_3)_2$ and $Al(NO_3)_3$ as precursors. The results showed an improvement of both sorption capacity and stability at 76% conversion for 11th cycles. Xu et al. (2013) studied the effect of percent mixed oxide Al_2O_3 to CaO on CO_2 capture performances by sol-gel synthesis. Percent of Al_2O_3 from aluminum isopropoxide were varied from 10% to 30%wt. The resulted CaO-based contained $Ca_9Al_6O_{18}$ and CaO. CO_2 sorption were tested at carbonation temperature of 650°C under 15% v/v CO_2 (balanced N_2) for 30 min and calcination was done at 800°C in N_2 for 10 min. Both 10% and 20% wt of Al_2O_3 provided 80% conversion for all 35 cycles of adsorption whereas 30% wt of Al_2O_3 support yielded 95% conversion in the 1st cycle and reduced to 90% conversion in the 35th cycle. Martavaltzi and Lemonidou (2008b) varied weight ratio of CaO (from $Ca(CH_3COO)_2$)/Al_2O_3 (from $Al(NO_3)_3$) of 65/35, 75/25, and 85/15 and tested for CO_2 capture. The conversion of CaO-based at weight ratio CaO/Al_2O_3 of 65/35 showed the lowest conversion of 23% and 22% in 1st and 45th cycle, respectively, for carbonation at 690°C, 30 min, and 15% v/v CO_2 and calcination at 850°C for 5 min. For similar condition, the results at weight ratio CaO/Al_2O_3 of 75/25 was obtained 35% conversion in the 1st cycle and 30% conversion were found in the

45th cycle. The weight ratio CaO/Al_2O_3 of 85/15 had highest capacity of 45% and 35% conversion in the 1st and the 45th cycle, respectively. The increasing inert metal was found to have two opposite effects: CO_2 sorption ability was decreased due to a decrease amount of active site and high thermal stability of sorbent. Xu et al. (2013) synthesized CaO-based alumina using different calcium precursors:calcium lactate (CL), calcium acetate (CA), calcium citrate (CC), and calcium gluconate (CG) by sol-gel method with the incorporation of aluminum isopropoxide. The results of all precursors showed two components of CaO and $Ca_9Al_6O_{18}$. Carbonation was tested at 650°C, 30 min, and 15%v/v CO_2 in N_2 and calcination at 800°C for 10 min in N_2. The samples have conversion in cycle 1st and 10th of 84% and 95% for CL, 78% and 93% for CG, 76% and 72% for CC, and 74% and 76% for CA. The sorbent showed high performance of CO_2 adsorption and stability because the formation of $Ca_9Al_6O_{18}$ could uniformly distribute among CaO and could reduce the decay rate of CaO due to sintering effect. The authors concluded that the efficiency of CaO-based sorbent mainly caused by smaller grain size and larger surface area. Martavaltzi and Lemonidou (2008a) used CaO derived from calcium acetate and calcium hydroxide precursors to mix with $Al(NO_3)_3$ in the solution of 2-propanol and DI water with weight ratio $CaO:Ca_{12}Al_{14}O_{33}$ of 75:25. The CaO-based sorbent was obtained with the mixing condition at 75°C for 1 h and calcination at 900°C for 1.5 h. The obtained of CaO-based sorbents were tested for CO_2 capture using TGA at carbonation temperature of 690°C, 30 min under 15% v/v CO_2 and the ability to regenerate using calcination temperature of 850°C for 10 min. The results revealed that CaO-based sorbent derived from $Ca(OH)_2$ provided constant capacity of sorbent at 21% conversion for 45 cycles. The CaO-based sorbent derived from $Ca(CH_3COO)_2$ showed 35% conversion in the 1st cycle and decreased to 29% in the 45th cycle. The morphology of calcium alumina was observed unchanged distribution after multiple-cycles, it exhibited that $Ca_{12}Al_{14}O_{33}$ can prevent sintering effect during carbonation and calcination**.**

2.3 Gemini surfactant

Mostly, surfactants are used as structure directing agent in precipitation $CaCO_3$ technique, where $CaCO_3$ is used as precursor for CaO sorbent. In general, surfactants are divided into 3 types: anionic surfactant, cationic surfactant, and nonionic surfactant. In order to act as a directing agent, the concentration of surfactant is used at the minimum value where micelle is formed, which is known as critical micelle concentration (CMC). In general, the critical micelle concentration is in the range of tens mM for single surfactant. To minimize the cost and waste of surfactant used gemini surfactant has emerged as an alternative material because it has lower CMC than that of single surfactant. Gemini surfactant consists of three parts: two single-chain of hydrophobic, two head groups of hydrophilic, and space (connected

head group). To the best of our knowledge, applying gemini surfactant on the synthesis of $CaCO_3$ is rare so in this review the effect of properties of gemini surfactant on CMC is summarized as it has been revealed that concentration of surfactant has effect on structural properties of materials. Wang et al. (2008) studied the effect of spacer and hydrophobic length (C_x) on properties of anionic gemini surfactant. Alkane (p-xylyl $(CH_2)_3$, C_3) and benzene (C_{px}) were used as spacer (C_y), the sample was denoted by $C_xC_yC_x(SO_3)_2$. In this work, hydrophobic length was varied at 8, 10, and 12 atom of carbon. The results of spacer on micelle properties such as critical micelle concentration (CMC), surface tension, and $\Delta H_{micelle}$ for alkane and benzene spacer were similar because both of the spacers are rigid hydrocarbon. The results showed hydrophobic lengths affected CMC and $\Delta H_{micelle}$. The CMC at hydrophobic length of $C_8C_{px}C_8(SO_3)_2$, $C_{10}C_{px}C_{10}(SO_3)_2$, and $C_{12}C_{px}C_{12}(SO_3)_2$ showed 0.91 mM, 0.055 mM and 0.057 mM, respectively. The reason of closely CMC of $C_{10}C_{px}C_{10}(SO_3)_2$ and $C_{12}C_{px}C_{12}(SO_3)_2$ was due to the aggregation of long tail of hydrophobic (critical aggregation concentration, CAC). Yoshimura et al. (2009) synthesized fluorinated gemini surfactants and studied surface properties and morphologies of the aggregate. Anionic gemini surfactant, N,N'-di(3-perfluoroalkyl-2-hydroxypropyl)-N,N'-diacetic acid ethylenediamine (2CFn edda) was used in this study. The properties of hydrophobic gemini surfactants were studied by varying number of carbon (n=4, 6, 8) of 2CFn edda, the results showed that, 2CF6 edda had lower surface tension and CMC than those containing n=4 and 8. This is because when hydrophobic was increased, CMC and surface tension decreased. The 2CF8 edda had CMC higher than 2CF6 because 2CF8 edda aggregate to pre-micelle. The morphology of 2CF4 edda, 2CF6 edda, 2CF8 edda were string-like, cage-like, and large aggregate of bilayer sheets, respectively. Tsubone et al. (2003) synthesized anionic gemini surfactants having Dialkyl Amine, Carboxyl, and Carboxylate group ($(CH_2)_2[N(COC_nH_{2n+1})CH(COOH)\text{-}CH_2COOH].2NaOH$, GA-(n+1)). In this work, hydrophobic at n+1 = 8, 10, 12, 14, and 16 were varied. The monomer GA-12 surfactant (one hydrophobic and one hydrophilic) exhibited critical micelle concentration (CMC) at 4 mM which was higher than GA-12 of 0.00715 mM. The effect of hydrophobic directly influenced on CMC, the CMC was decreased when the length of hydrophobic in the range between 8 and14 was increased. However, the GA-16 showed higher CMC than GA-14 because the GA-16 was formed to micelle before completely reduced surface tension (critical aggregation concentration, CAC).

CHAPTER III

SCOPES AND METHODOLOGY

3.1 Scope of Research

The scope of this research is divided into three parts as follows:

Part 1: Improvement of high-temperature CO_2 sorption capacity of CaO-based sorbent by investigating the effects of $CaCO_3$ which were synthesized from different calcium and carbonate precursors:

- Calcium precursors: calcium acetate ($Ca(CH_3COO)_2$) and calcium chloride ($CaCl_2$)
- Carbonate precursors: sodium carbonate (Na_2CO_3) and urea ($CO(NH_2)_2$).

The effect of calcium and carbonate precursors on $CaCO_3$ morphologies and properties were investigated in this work as it was believed that different morphologies and textural properties of $CaCO_3$ can affect CaO properties and hence CO_2 sorption capacity of sorbent.

Part 2: Improvement of CaO-based sorbent for CO_2 sorption by studying the effect of additive addition on the structure of $CaCO_3$

- Surfactants: commercial surfactant sodium dodecyl sulphate (SDS) and Gemini surfactant (12-3-12)

The effect of surfactant on $CaCO_3$ morphologies and properties were investigated in this work as it was believed that the surfactant can control polymorph and morphology structure of $CaCO_3$ and this effect could improve the properties of CaO sorbent for higher CO_2 sorption capacity.

Part 3: Improvement stability of CaO-based sorbent by investigating the effect of metal incorporation and synthesis method on sorbent properties. The incorporation of metal ion could prevent sintering effect of CaO so multiple cycles use could be improved.

3.2 Methodology

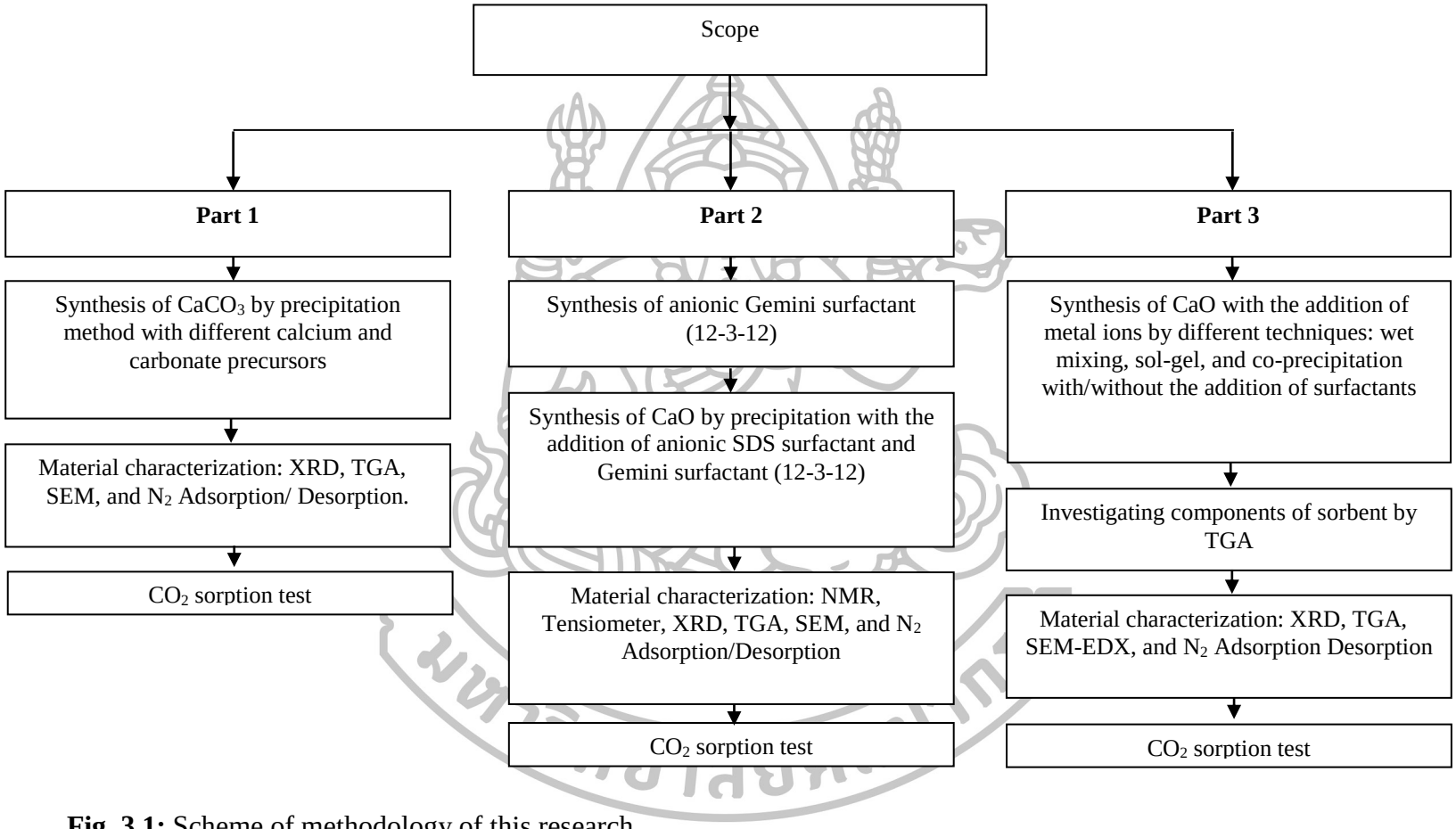

Fig. 3.1: Scheme of methodology of this research

3.3 Contribution of Research

1.) Obtain better potential sorbent for high-temperature CO_2 capture in terms of sorption capacity and sorbent stability.

2.) Understand the mechanism of micelle formation which affect the properties of the synthetic sorbent.

CHAPTER IV

IMPROVEMENT OF CaO DERIVED FROM $CACO_3$ SYNTHESIZED FROM DIFFERENT CALCIUM AND CARBONATE PRECURSORS

4.1 Abstract

Precipitation of $CaCO_3$ by using different calcium and carbonate precursors were studied to investigate the effect on CO_2 capture. Physical and chemical properties were characterized by X-ray diffraction, scanning electron microscopy, thermal gravimetric analysis, and N_2 adsorption/desorption. The morphology of $CaCO_3$ derived from different precursors has the effect on CaO morphology and also influence on CO_2 sorption ability. The sorbent that was synthesized by calcium acetate with urea exhibits morphology of large network of connected particles and this sorbent showed good performance for CO_2 sorption capacity of which 0.64 $gCO_2/gCaO$ at temperature 700ºC was obtained.

4.2 Introduction

CaO is important material used in calcium looping technology due to high CO_2 sorption ability at high-temperature; however, natural CaO sorbent or commercial sorbent was reported that having low capability for CO_2 adsorption due to effect of morphology structure and surface properties. Santos et al. (2012), Gupta and Fan (2002) Thus, synthetic CaO is an alternative way to improve properties of CaO sorbents.

It has been reported that morphology and surface properties of CaO depends upon synthesis method Olivares-Marín et al. (2013), calcium or carbonate precursors Kierzkowska et al. (2013), hydration Yin et al. (2012), and thermal pretreatment. Florin and Harris (2009) In this work, the effect of precursors on morphology and properties of synthetic $CaCO_3$ is of interest. We used precipitation technique with different precursors of calcium and carbonate to synthesize $CaCO_3$ prior to calcine to CaO sorbent for CO_2 capture at high temperature ranging from 600-700°C.

4.3 Literature review

Synthesis method is a factor that can control morphology, surface textural, and polymorph of $CaCO_3$. Several works have been reported the effect of either calcium or carbonate precursor on polymorph of $CaCO_3$, for example, Hadiko et al. (2005) divided precipitation into two groups from properties of precursors that 1) precipitation of calcium precursor with carbonate precursor, 2) precipitation of calcium precursor with CO_2 (carbonation process). Kammoe et al. (2012) used $Ca(NO_3)_2$ and Na_2CO_3 for the precipitation of $CaCO_3$ at 25ºC and the results showed cubic morphology. Yu et al. (2004) precipitated $CaCO_3$ from $CaCl_2$ and Na_2CO_3, the obtained $CaCO_3$ was aggregated particles of plate-like structure. Yu et al. (2006) synthesized needle-like $CaCO_3$ from precipitation of $Ca(CH_3COO)_2$ and $CO(NH_2)_2$ at 80ºC. Hadiko et al. (2005) synthesized hollow $CaCO_3$ by precipitation of $CaCl_2$ and CO_2 at pH 9.8 and 27ºC. Wen et al. (2003) obtained plate-like from precipitation of $Ca(OH)_2$ and CO_2 at 25ºC.

Effect of calcium precursor on CaO properties has also been investigated. Various calcium precursors has been used as CaO source, such as, calcium acetate ($Ca(CH_3COO)_2$) Chen et al. (2012), Grasa et al. (2007), Lui et al. (2010), calcium carbonate ($CaCO_3$) Florin et al. (2008) , Lui et al. (2010), calcium oxalate (CaC_2O_4) Grasa et al. (2007) , Lui et al. (2010), calcium hydroxide ($Ca(OH)_2$ Grasa et al. (2007) , Lui et al. (2010), calcium D-gluconate ($C_{12}H_{22}CaO_{14}$) Lui et al. (2010), calcium citrate ($Ca_3(C_6H_5O_7)_2$) Lui et al. (2010), calcium L-lactate ($C_6H_{10}CaO_6$) Lui et al. (2010), calcium formate ($Ca(HCOO)_2$) Lui et al. (2010). The use of CaO synthesized from different precursors and synthesis methods have been applied for CO_2 sorption test and some works are summarized in Table 4.1.

Table 4.1 Effect of synthesis method and calcium/carbonate precursor on CaO sorbent and CO_2 capture

Source	Methods	Carbonation	Regeneration	Reactor	Conversion 1st cycles	Conversion (n^{th}) cycles	Ref.
$Ca(OH)_2$	Precipitation	600ºC, 60%CO_2 (N_2), 20 min	700ºC, N_2, 10 min	TGA	95%	(10) 60%	Yang et al. (2009)
$Ca(OH)_2$	Precipitation	750ºC, 15%CO_2 (N_2), 60 min	750ºC, N_2, 60 min	Microbalance	82%	(25) 65%	López-Periago et al. (2013)
CaO					84%	(25) 50%	
$Ca(OH)_2$	Precipitation	600ºC, 15%CO_2 (N_2), 20 min	700ºC, N_2, 10 min	TGA	90%	-	Florin et al. (2008)
$CaCO_3$	Calcination				76%	(50) 14%	
$Ca(CH_3COO)_2$	Calcination	700ºC, 30%CO_2 (N_2), 100 min	700ºC, N_2	TGA	100%	(5) 95%	Grasa et al. (2007)
CaC_2O_4					97%	(8) 81%	
$Ca(OH)_2$					95%	(8) 80%	
$C_{12}H_{22}CaO_{14}$	Calcination	650ºC, 15%CO_2 (N_2), 30 min	900ºC, N_2, 10 min	TGA	88%	(9) 83%	Lui et al. (2010)
$Ca(CH_3COO)_2$					85%	(9) 52%	
$Ca_3(C_6H_5O_7)_2$					84%	(9) 57%	
$C_6H_{10}CaO_6$					80%	(9) 38%	
CaO (160 nm)					73%	(9) 59%	
$CaCO_3$					70%	(9) 30%	
$Ca(HCOO)_2$					66%	(9) 21%	
$Ca(OH)_2$					60%	(9) 45%	
$CaCO_3$ (70 nm)					51%	(9) 35%	
$Ca(CH_3COO)_2$	Calcination	700ºC, CO_2, 100 min	-	TGA	96%	-	Chen et al. (2012)
$CaCO_3$					70%	-	

4.4 Theory

Carbon dioxide capture and storage technology

Large amount of CO_2 emitted into the environment is found to be released from combustion process operated in power plants and industries. Such combustion process can be divided into three groups according to separation process: pre-combustion, post-combustion, and oxy-fuel (Fig. 4.1). CO_2 separation in pre-combustion is related to the separation of CO_2 from H_2 before H_2 is fed into the combustion process. In this process, CO_2 and H_2 are mostly produced from the reforming reaction and water-gas shift. High temperature CO_2 sorption under atmospheric pressure is involved in this separation system. For post-combustion, CO_2 is separated from N_2 by absorption after combustion process at 40-60^oC. Solvent mostly used to absorb is monoethanolamine (MEA). [Wang et al. (2011)] The oxy-fuel technologies separate N_2 from O_2, the O_2 is used in the combustion process. Therefore, gas after combustion is mainly CO_2. [Toftegaard et al. (2010)]

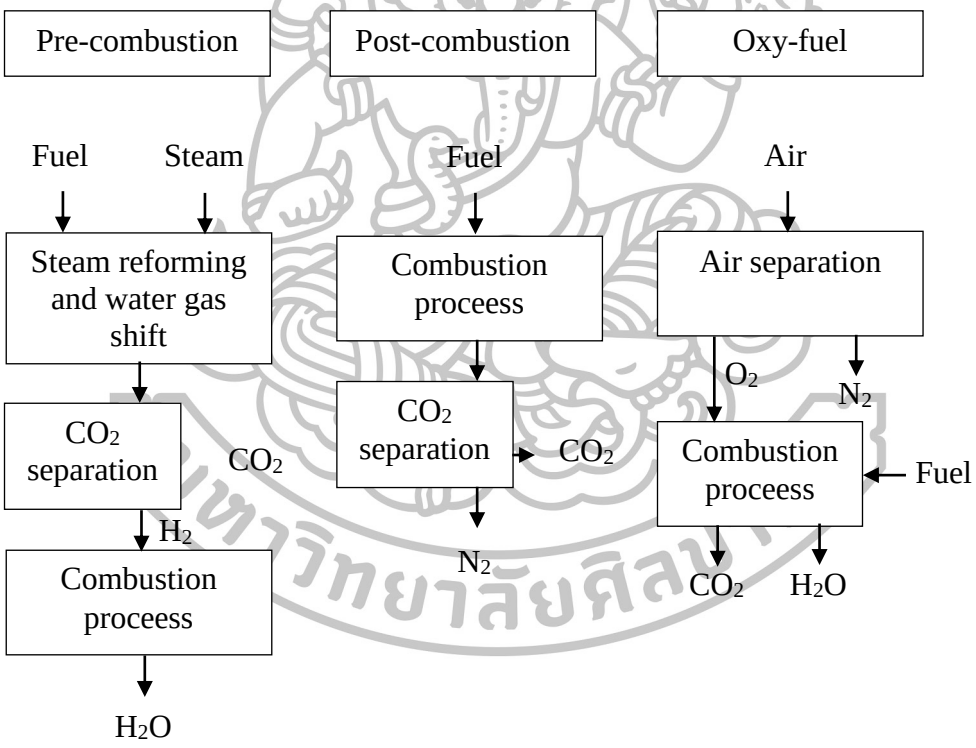

Fig. 4.1: Scheme of overall combustion process

Several techniques have been applied to separate CO_2 such as absorption by solvent i.e. Monoethanolamine (MEA), [Wang et al. (2011), Toftegaard et al. (2010)] Sterically hindered amine (KS-1), [Toftegaard et al. (2010)] or Diethanolamine (DEA) [Franchi et al. (2005)], physical adsorption by solid i.e. activated carbon, zeolite, or metal-organic

frameworks (MOFs), Samanta et al. (2012) and chemical adsorption by solid i.e. magnesium oxide, lithium zirconate, Ochoa-Fernandez at al. 2005 or calcium oxide.

Calcium looping technology is a process of which Ca-based sorbent is used to capture CO_2 separation at high temperature (Fig. 4.2). The reaction of adsorption called carbonation is exothermic reaction and the operating temperature is in the range of 600-700°C. The obtained product after carbonation is $CaCO_3$ which can be thermally regenerated by heat. $CaCO_3$ can be decomposed to CaO via the so-called calcination reaction, where the reaction could be occurred at high temperature above 800°C. The calcination is endothermic reaction.

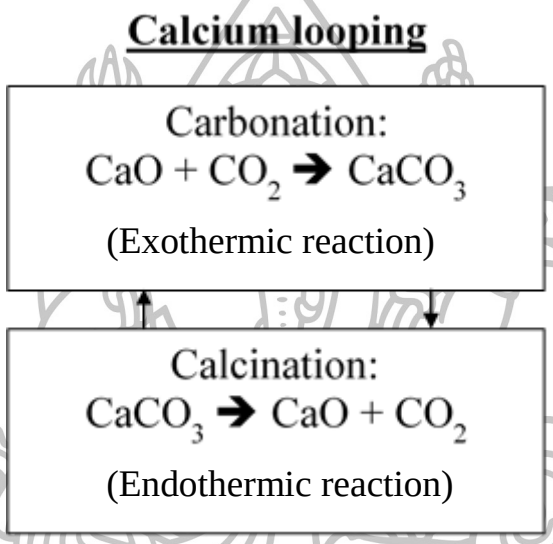

Fig. 4.2: Schematic diagram of calcium looping

Breakthrough curve

The fixed-bed adsorption is a system where a stationary phase is bed of the adsorbent and fluids (adsorbate) flow through the column of the bed. The concentration of adsorbate continuously increase because fluid is adsorbed on the adsorbent. The column adsorption includes used bed, mass transfer zone, and unused bed. The used bed is a section of adsorbent that cannot adsorb adsorbate (equilibrium), mass transfer zone (MTZ) is local of adsorbent that is remaining adsorption, and unused bed is a section of sorbent that is not used. Determination of adsorption in fixed-bed rector has two types: weight and length of adsorbent.

The ideal breakthrough curve has points of started breakthrough and ended breakthrough; these points are breakpoint and stoichiometric front.

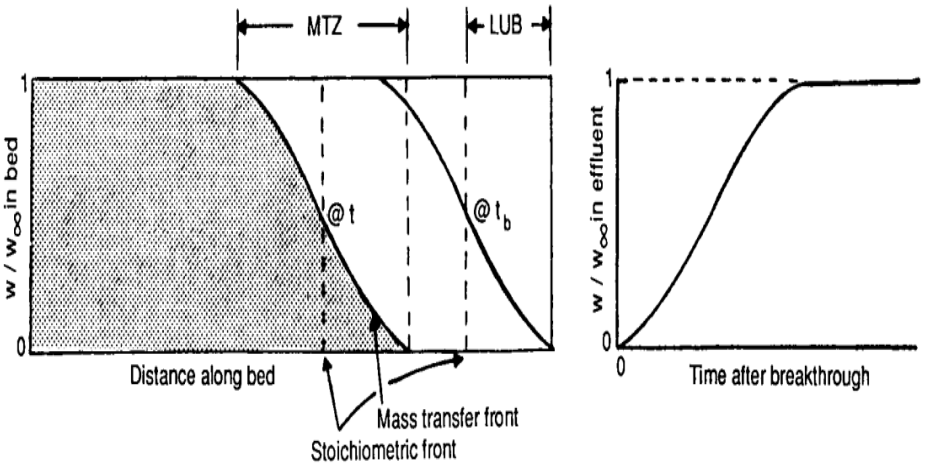

Fig. 4.3: Characteristic of adsorption in fixed-bed reactor

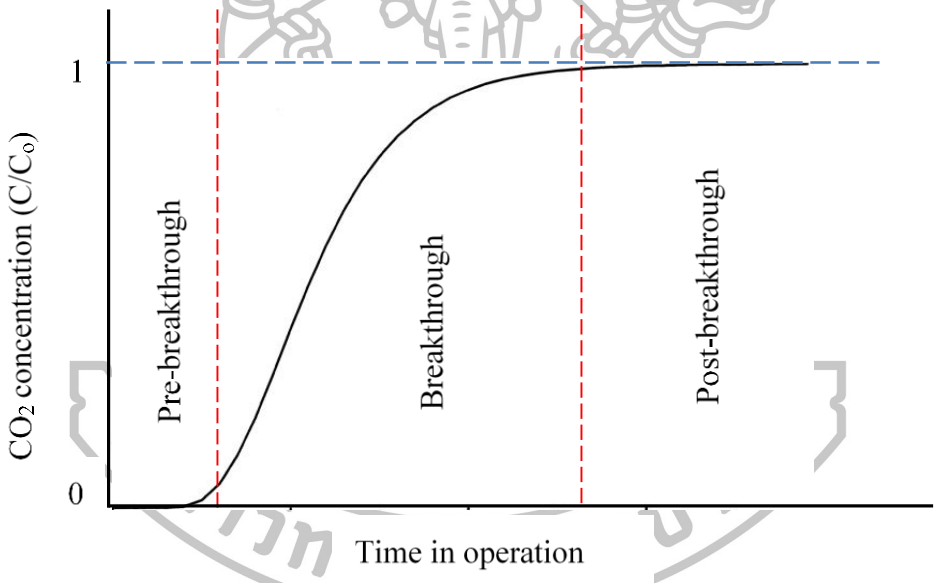

Fig. 4.4: Breakthrough curve of CO_2 adsorption

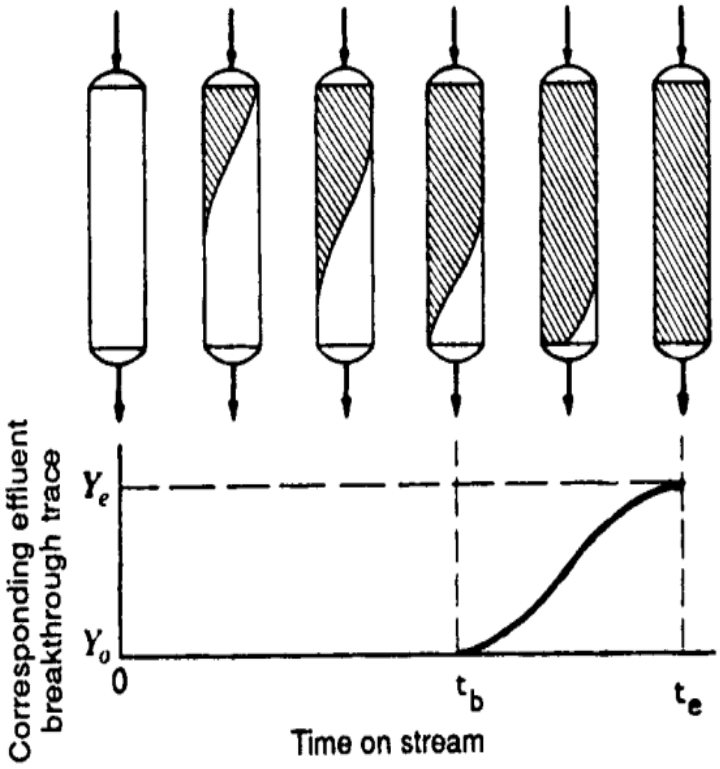

Fig. 4.5: Scheme of breakthrough curve and column of adsorption

The role of adsorbent is to capture fluid phase; when concentration of fluid nearly its initial concentration, it means that adsorbent is saturated in the bed. Mostly, the solid adsorbent has adsorption behavior as S-shaped as shown in Figs. 4.4 and 4.5.

4.5 Methodology

4.5.1 Material

Calcium chloride dihydrate ($CaCl_2.2H_2O$, 99%), purchased from Ajax finechem, and calcium acetate hydrate ($Ca(CH_3COO)_2.H_2O$, 99%), received from Lobachemie, were used as calcium precursors. Sodium carbonate anhydrous (Na_2CO_3, 99.8%), purchased from Ajax finechem, and urea ($(NH_2)_2$ CO, 99%) obtained from Carlo Erba, were used as carbonate sources. CaO commercial (powder) was received from Ajax finechem. All chemicals were used as received.

4.5.2 Preparation of $CaCO_3$

$CaCO_3$ samples were prepared via precipitation method using two different calcium precursors ($CaCl_2$ and $Ca(CH_3COO)_2$) and carbonate precursors (Na_2CO_3 and $(NH_2)_2CO$). In case of Na_2CO_3 precursor, 100-mL of 2.5 M $CaCl_2$/$Ca(CH_3COO)_2$ solution was mixed with equimolar concentration of 100-mL

Na_2CO_3. The mixture was stirred for 3 h at room temperature and the reaction was allowed to maintain for 5 h. The precipitate was filtered, washed with distilled water 3 times, and dried at 30°C. In case of using $CO(NH_2)_2$ as carbonate precursor, 100 mL of 2.5 M $CaCl_2$/$Ca(CH_3COO)_2$/$Ca(NO_3)_2$ solution was mixed with equimolar concentration of 100-mL $CO(NH_2)_2$ under vigorous stirring at 90°C for 24 h. The obtained precipitate was filtered, washed with distilled water, and dried at 30°C.

4.5.3 Preparation of CaO sorbents

To produce CaO sorbents for CO_2 capture, $CaCO_3$ samples were calcined under air at 850°C for 30 min.

4.5.4 Characterization

X-ray diffraction (XRD)

Technique of X-ray diffraction is used to characterize crystallinity of samples. The results can provide information about solid phase, structure, and a component of material.

X-rays are generated in a cathode X-ray tube (Fig. 4.6) by heating a filament to produce electrons. Then the electron, which is accelerated by voltage, bombard to target material such as Cu, Al, Mo, and Mg. The energy of electron is sufficient to dislocated inner shell electrons of the target material, the X-ray spectra, which is produced, include K_α and K_β (Figs. 4.7 and 4.8 show K_α and K_β of Cu). The K_α is used for XRD technique due to higher intensity than K_β (observed characteristic of Cu in Fig. 4.8), thus, K_β is separated by Ni filter or Carbon monochromator.

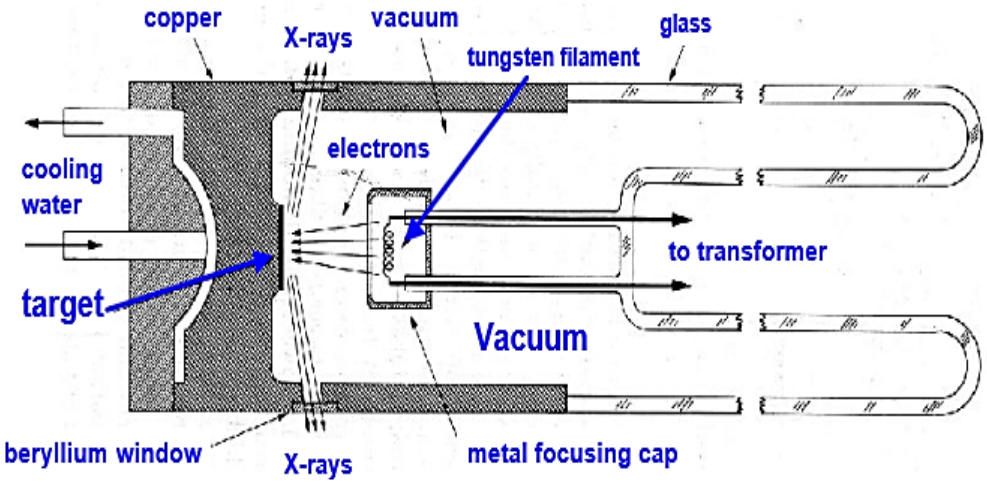

Fig. 4.6: Scheme of Cathod X-ray tube (http://web.pdx.edu/~pmoeck/phy381/Topic5a-XRD.pdf)

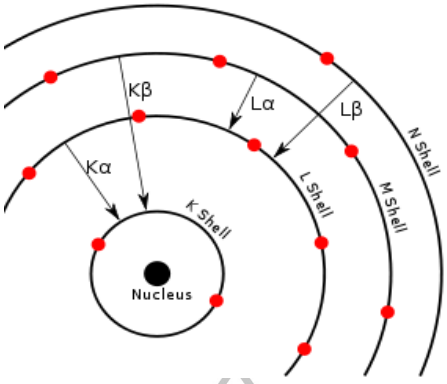

Fig. 4.7: Shell electron of target a material (https://en.wikipedia.org/wiki/User:Physmethpaper)

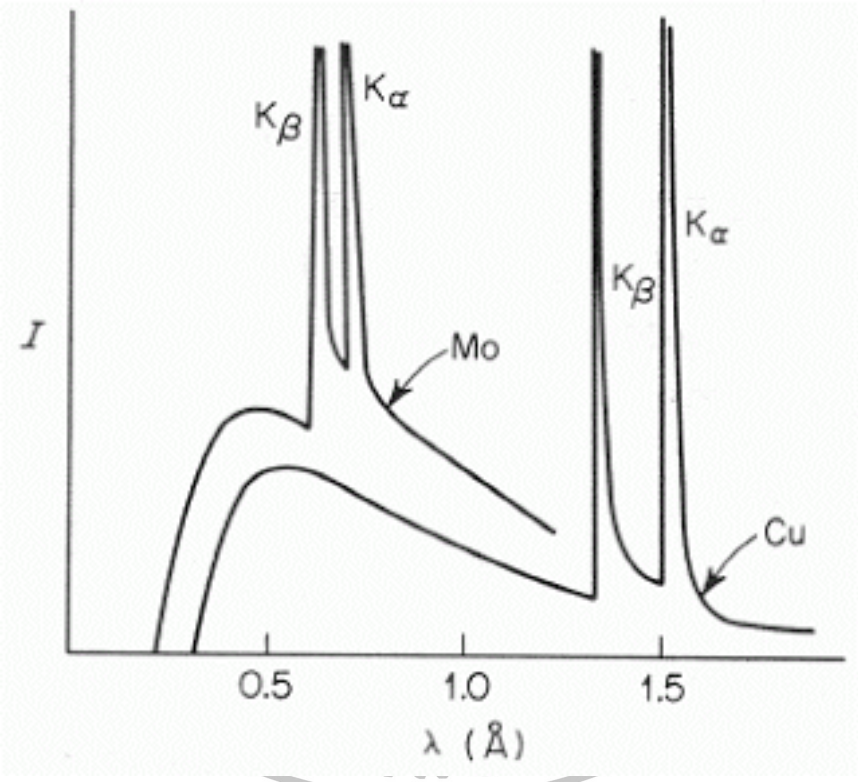

Fig. 4.8: Intensity of K_α and K_β of Cu (http://elarcoirisyeltiempo.blogspot.com/p/rayos-x.html)

The crystal structure of solid is a uniform arrangement of unit cells in 3-dimension, the unit cell is the smallest unit of volume that is symmetry information. The unit cell is considered edge length of three dimension as a, b, and c and three internal angle as α, β, and γ (Fig. 4.9) The properties of unit cell formation can be divided into 7 types from angles and edge lengths in each dimension as shown in Fig. 4.10 and Table 4.2.

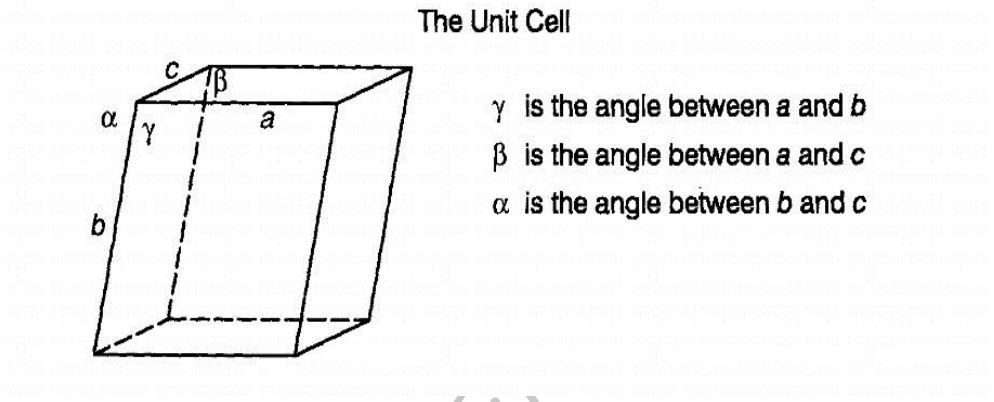

Fig. 4.9: Component of unit cell (http://ruby.colorado.edu/~smyth/G30102.html

Table 4.2 Properties of unit cell

Category	Edge lengths	Internal angle
Cubic	$a = b = c$	$\alpha = \beta = \gamma = 90^o$
Tetragonal	$a = b \neq c$	$\alpha = \beta = \gamma = 90^o$
Orthorhombic	$a \neq b \neq c$	$\alpha = \beta = \gamma = 90^o$
Hexagonal	$a = b \neq c$	$\alpha = \beta = 90^o, \gamma = 120^o$
Trigonal (a)	$a = b \neq c$	$\alpha = \beta = 90^o, \gamma = 120^o$
Trigonal (b)	$a = b = c$	$\alpha = \beta = \gamma \neq 90^o$
Monoclinic	$a \neq b \neq c$	$\alpha = \gamma = 90^o \beta \neq 90^o$
Triclinic	$a \neq b \neq c$	$\alpha \neq \beta \neq \gamma \neq 90^o$

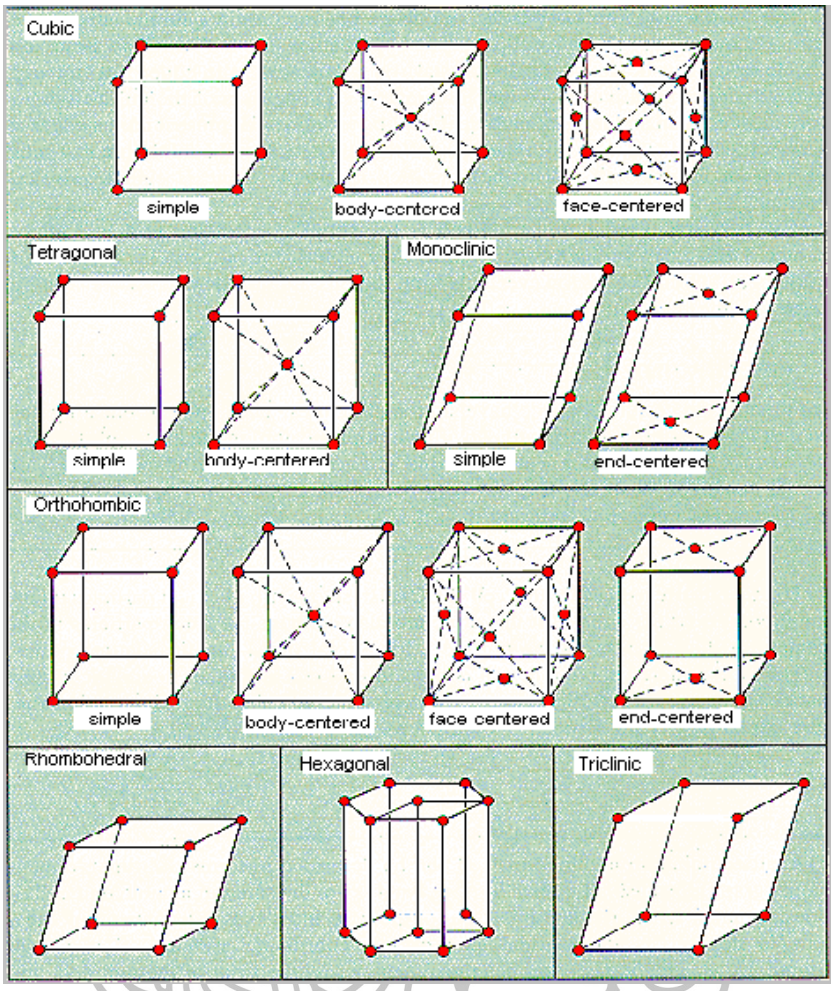

Fig. 4.10: Structure of unit cell (http://chemed.chem.purdue.edu/genchem/topicreview/bp/ch13/unitcell.php)

In this technique, the X-ray is diffracted when the beam is directed at a crystalline of material. The direction of diffraction depend on distance between atomic planes of crystal lattice (d or d-space) that is explained by Bragg's Law (Fig. 4.11), the Bragg exhibits the relationship between wavelengths of the X-ray beam (λ), the angle of diffraction (θ), order of diffraction (n), and the distance between atomic planes of the crystal lattice (d):

$$n\lambda = 2d \sin\theta \qquad (4.1)$$

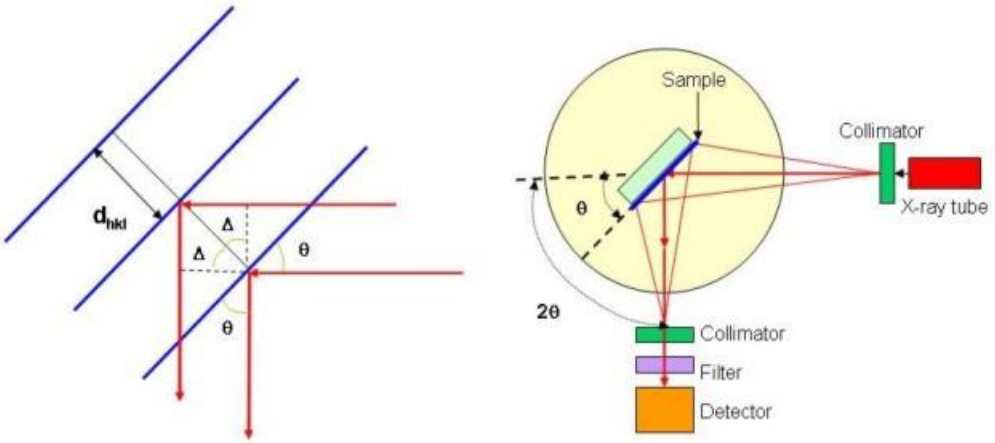

Fig. 4.11: Scheme of XRD analysis (http://nanoscience.skku.edu/index.php?cont=research&subcont=characterization)

In this work, Compositions and crystalline structure of either $CaCO_3$ or CaO were analyzed by X-ray powder diffractometer (XRD, Rigakuminiflex II) with Cu Kα radiation. Measurements were carried out with the scanning step of 2° per minute and the 2θ ranged from 10° to 80°. Crystallite size of each sample was approximated by the Scherrer Equation from the width at half-height of the highest intensity at 2θ of 37.4º for CaO:

$$d = \frac{0.89\lambda}{B\cos\theta} \times \frac{180°}{\pi} \qquad (4.2)$$

where d is the mean crystallite diameter, λ is the X-ray wave length of CuKα (1.542 Å), and B is the full width half maximum (FWHM) of the most intense ray of each phase.

Thermal gravimetric analysis (TGA)

Thermal gravimetric analysis (TGA) is a thermal analysis technique that used to characterize physical and chemical properties as a function of temperature change. The technique detects weight or weight loss with the change of temperature.

Thermal gravimetric analysis (TGA) is a technique to measure weight loss as a function of increasing temperature or time with constant heat rate. TGA consists of microbalance and electrically heated furnace (Fig. 4.12). The microbalance is used to measure weight change of the desired sample by comparing with reference sample. The furnace is used to heat sample by constant rate. The weight loss of sample is carried out in air or inert gas.

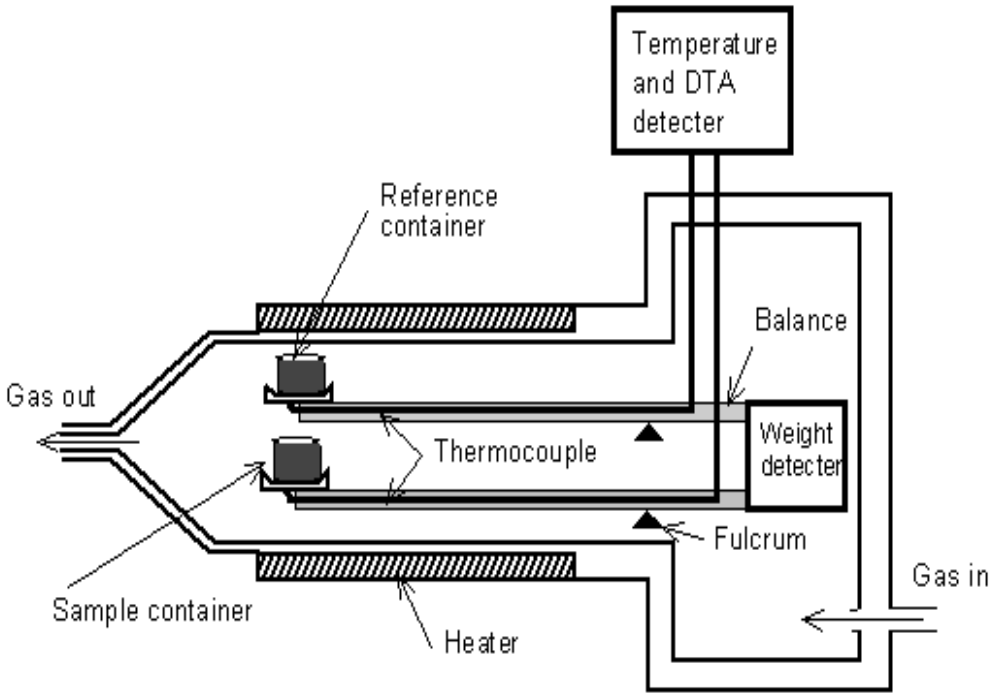

Fig. 4.12: Scheme of TGA instrument (http://article.sapub.org/10.5923.j.ijee.20120205.08.html)

Differential thermal analysis (DTA)

DTA technique is used to study the requirement or the release of thermal quantity for/from sample. Principle determination of DTA relies on measurement of temperature difference between the sample and the reference as shown in Fig. 4.13. When temperature of a sample has lower than that of the reference, it implies that the reaction between the sample and the flow gas is endothermic, whereas, the exothermic occurs when the temperature of the sample is higher than that of the reference.

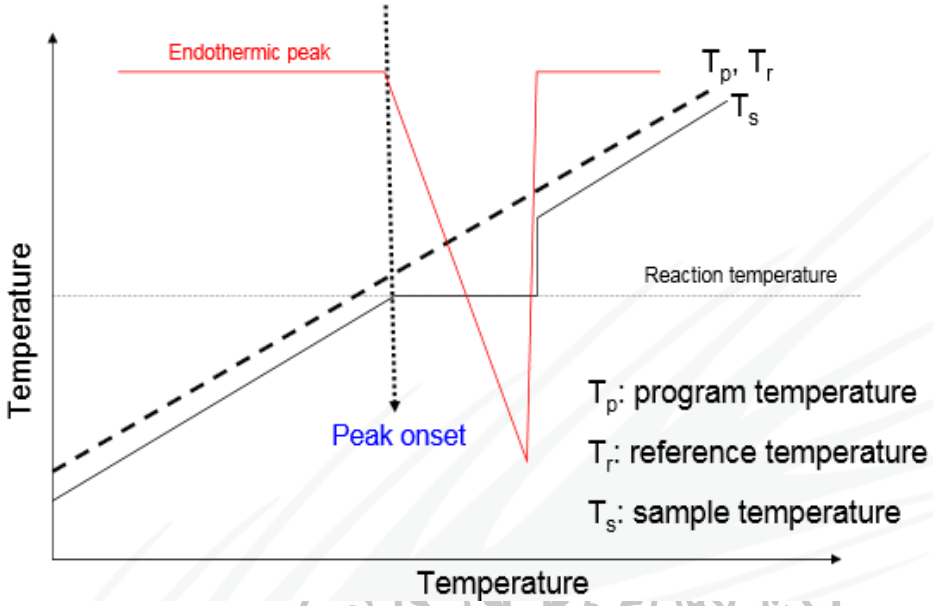

Fig. 4.13: Graph of Differential thermal analysis (http://web.abo.fi/instut/biofuelsGS-2/kursen/%C5A/lectures/Lectrure _Thermal %20Analysis.pdf)

Scanning electron microscopy (SEM)

Scanning electron microscopy (SEM) is used to study of surface and morphology of solid material. The image of SEM shows 3 dimensions by secondary electron and back scattered electron scanning.

Secondary electron is the electron that is released from atom due to the crashing of electron beam (Fig. 4.14). The released electron from surface of sample can give image of the sample.

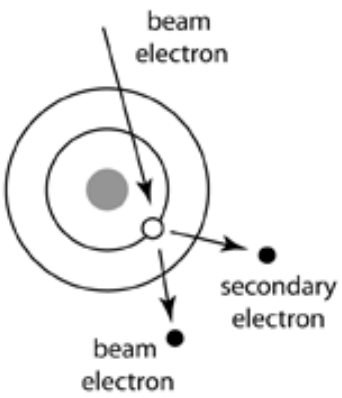

Fig. 4.14: Scheme of generation second electron (http://www.mcswiggen.com/FAQs/FAQ_EF-2.htm)

Back scattered electron occurs from crashing of electron beam with nucleus of sample, the electron beam is sent back to the same direction where the energy is not loss (Fig. 4.15). The amount of back scattered electron increases when size of atom is larger.

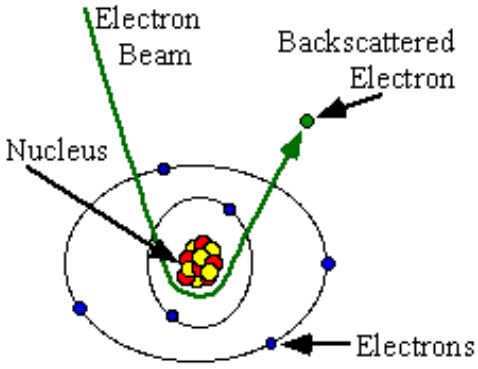

Fig. 4.15: Scheme of generation back scattered electron (http://www.mse.iastate.edu/research/laboratories/sem/microscopy/how-does-the-sem-work/high-school/how-the-sem-works/backscattered-electrons/)

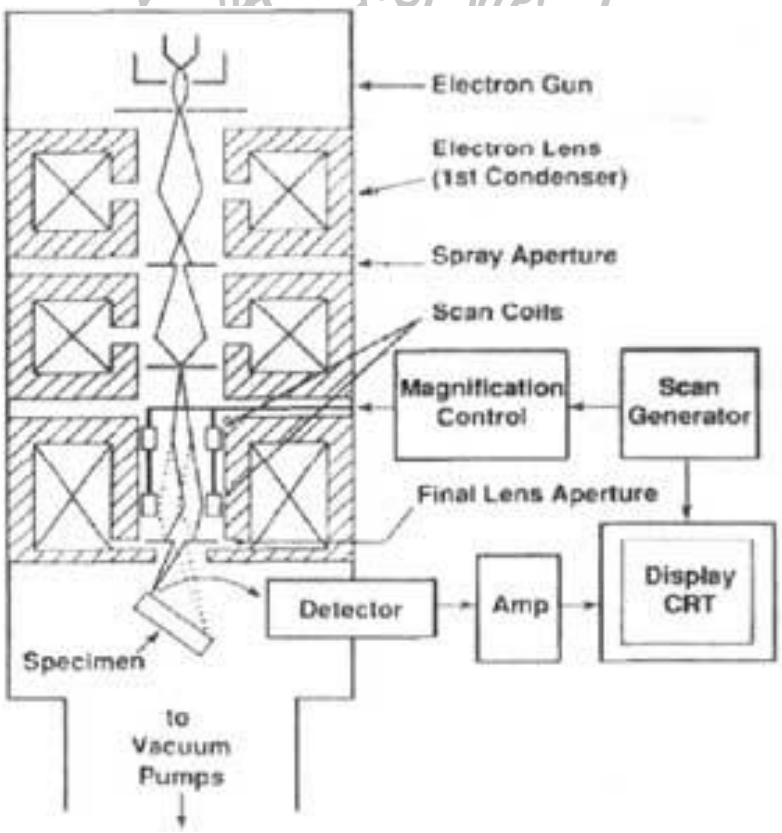

Fig. 4.16: Scheme of scanning electron microscopy instrument (http://www.rmutphysics.com/charud/oldnews/192/SEM.pdf)

Scanning electron microscopy (SEM) consists of electron gun, electromagnetic lens, aperture, and detector (Fig. 4.16). The electron gun is source of electrons and the electrons are accelerated by voltage in vacuum column (0-30 kV). The electromagnetic lens consist of condenser electron len and objective len, condenser len is used for controlling size of electron beam and amount of electron is set by aperture. The objective len is employed to focus the electron beam and scan coils distributing the electron beam to surface of sample. The detector detects the signal of reflected electron from sample. The signal from secondary electron exhibits morphology and surface of the sample in 3 dimensions and back scattered electron shows difference of composition on surface of particles.

Scanning electron microscopy (SEM) uses high resolution images that can observe morphologies and surface texture of small material size. The morphology of $CaCO_3$ and CaO are usually measured in the range of 5-500 μm.

N_2 adsorption/desorption

N_2 adsorption/desorption is used in this work to examine surface texture of sample such as surface area, pore size distribution, and pore volume. This technique operated based on the measurement of N_2 adsorption on surface of sample under liquid nitrogen system.

The physical adsorption is principle of condensation of gas on surface of a solid sample. The properties of adsorption can divide into 6 types of isotherms as shown in Fig. 4.17. Type I (Langmuir isotherm) represents monolayer adsorption of gases in Micropore that has average pore size less than 2 nm. Type II and III are multilayer gas adsorption on surface of solid, these types represent adsorption of macropore (> 50 nm). Isotherms type IV and V represent the adsorption of mesopore (2-50 nm). Type VI is specifically of homogeneous surface solid. The physical adsorption isotherm can be used to calculate surface area by Brunauer-Emmett-Teller (BET) method or Langmuir method.

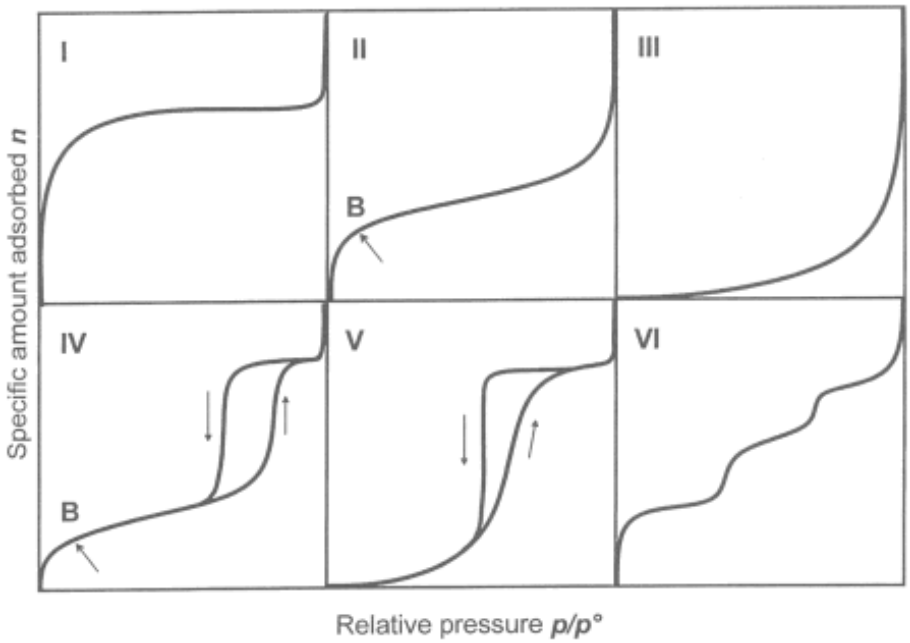

Fig. 4.17: Type of isotherm from N_2 adsorption/desorption (http://www.nippon-bel.co.jp/tech/seminar02_e.html)

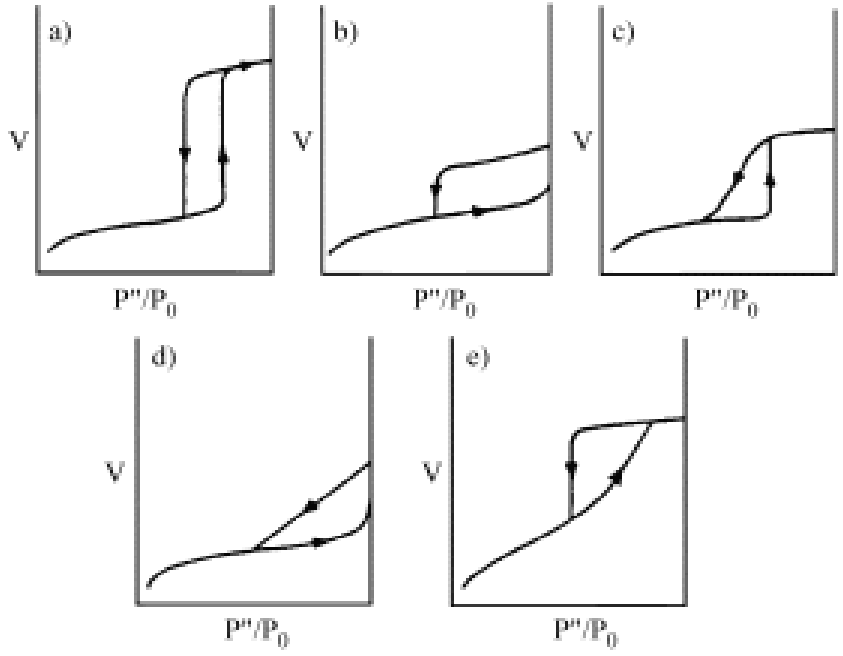

Fig. 4.18: Type of hysteresis loop from N_2 adsorption/desorption (http://www.scielo.br/scielo.php?script=sci_arttext&pid=S1516-1439 1999000300015)

N_2 adsorption and desorption can exhibit properties of adsorption by isotherm which shows the relationship between volume of gas adsorption and relative pressure (P/P_0). The isotherm can predict structure of porous by the aspect of Hysteresis loop as shown in Fig. 4.18.

Porous shape is estimated by the property of hysteresis as shown in Fig 4.18. Type I isotherm indicates that the porous of the sample possesses cylindrical shape and two sides of pore mouth is open. Slit shape is evaluated by hysteresis pattern of type 2 conical shape is presented when the hysteresis loop demonstrated as shown in type III. Type IV indicates slit shape pore and no parallel plates, and type V is shape of bottom neck.

The specific surface area of solid, which is determined by physical adsorption of a gas on the surface of the solid, is used to calculate the amount of gas at monomolecular layer on the surface as proposed by Brunauer–Emmett–Teller namced BET method. The equation of the isotherm is shown in the following equation:

$$\frac{1}{\left[V_a\left(\frac{P_0}{P}-1\right)\right]}=\frac{C-1}{V_mC}+\frac{1}{V_mC} \qquad (4.3)$$

where, P = partial vapor pressure of adsorbate gas in equilibrium with the surface at 77.4 K (b.p. of liquid nitrogen), (pa)

P_0 = saturated pressure of adsorbate gas, (pa)

V_a = volume of gas adsorbed at standard temperature and pressure (STP), (ml)

V_m = volume of gas adsorbed at STP to produce an apparent monolayer on the sample surface, (ml)

C = dimensionless constant that is related to the enthalpy of adsorption of the adsorbate gas on the powder sample

From Eq. 4.3, correlation of linear regression between P/P_0 (0.05-3) and V_a provides a linear plot where its slope is equal to $(C-1)/V_mC$, and the intercept is equal to $1/V_mC$. Thus, the value of V_m and C can be calculated. In monolayer adsorption, V_m is used to calculate specific surface area by equation (4.4):

$$S=\frac{V_mN_{AV}\alpha}{m\times 22400} \qquad (4.4)$$

where, S = Specific surface area, (m^2/g)

n_m = mole of gas adsorption

N_{AV} = Avogadro constant (6.022×10^{23} mol^{-1})

α = Effective cross-sectional area of one adsorbate molecule, m^2 (0.162 nm^2 for nitrogen)

m = mass of solid sample, (g)

22400 = volume occupied by 1 mole of the adsorbate gas at STP, (ml)

A sample is prepared in tube of sample cell by approximately 0.3-0.5 g. Then contaminate such as water is removed by degassing at temperature higher than 150°C under inert carrier flow, the sample cell is loaded into instrument for analysis by N_2 adsorption/desorption at -196°C.

In this research, to determine surface area, pore volume, pore diameter, and pore size distribution of the samples, N_2 adsorption/desorption isotherms were examined using BEL Japan, INC Belsorp mini II. The samples were degassed at 200 °C for 3 h prior to conducting the measurement at -196°C. From the results of N_2 isotherms, the appearances of hysteresis loops of N_2 isotherm at P/P_0 ~1 was used to characterize the possible structure of pore of the samples (IUPAC). Specific surface area was estimated by applying the BET (Brunauer-Emmett-Teller) method at $0.05<P/P_0<0.30$. Total pore volume was estimated from the amount of N_2 adsorbed at relative pressure of 0.95. Pore diameter and pore size distribution of the sample was examined by the BJH (Barrett-Joyner-Hallenda) method.

4.6 CO_2 sorption performance tests

The CO_2 uptake capacity of the synthetic CaO was tested via packed-bed reactor. For each experiment, the sample of 0.8 g was placed in a quartz tube and heated from ambient temperature to 850°C under N_2 flow and held for 30 min before taking measurement to refresh the material. CO_2 sorption (carbonation reaction) was carried out at 750 °C under 15 mL min^{-1} gas flow containing 15% CO_2 (balanced N_2). For desorption test (calcination reaction), the sample was heated to 850°C under 100% N_2 for 30 min (or until no CO_2 was observed).

4.7 Results and discussion

4.7.1 Characterization

Phase compositions of the synthesized $CaCO_3$ with different calcium precursors examined by XRD are shown in Fig. 4.19. The results show that calcite is observed with the sorbent synthesized from calcium chloride precursors, $CaCO_{3,Cl\text{-}Na}$ and $CaCO_{3,Cl\text{-}Urea}$. Mixed phases of calcite (30%) and vaterite (70%) is found with $CaCO_{3,Ac\text{-}Na}$, and aragonite is observed with $CaCO_{3,Ac\text{-}Urea}$.

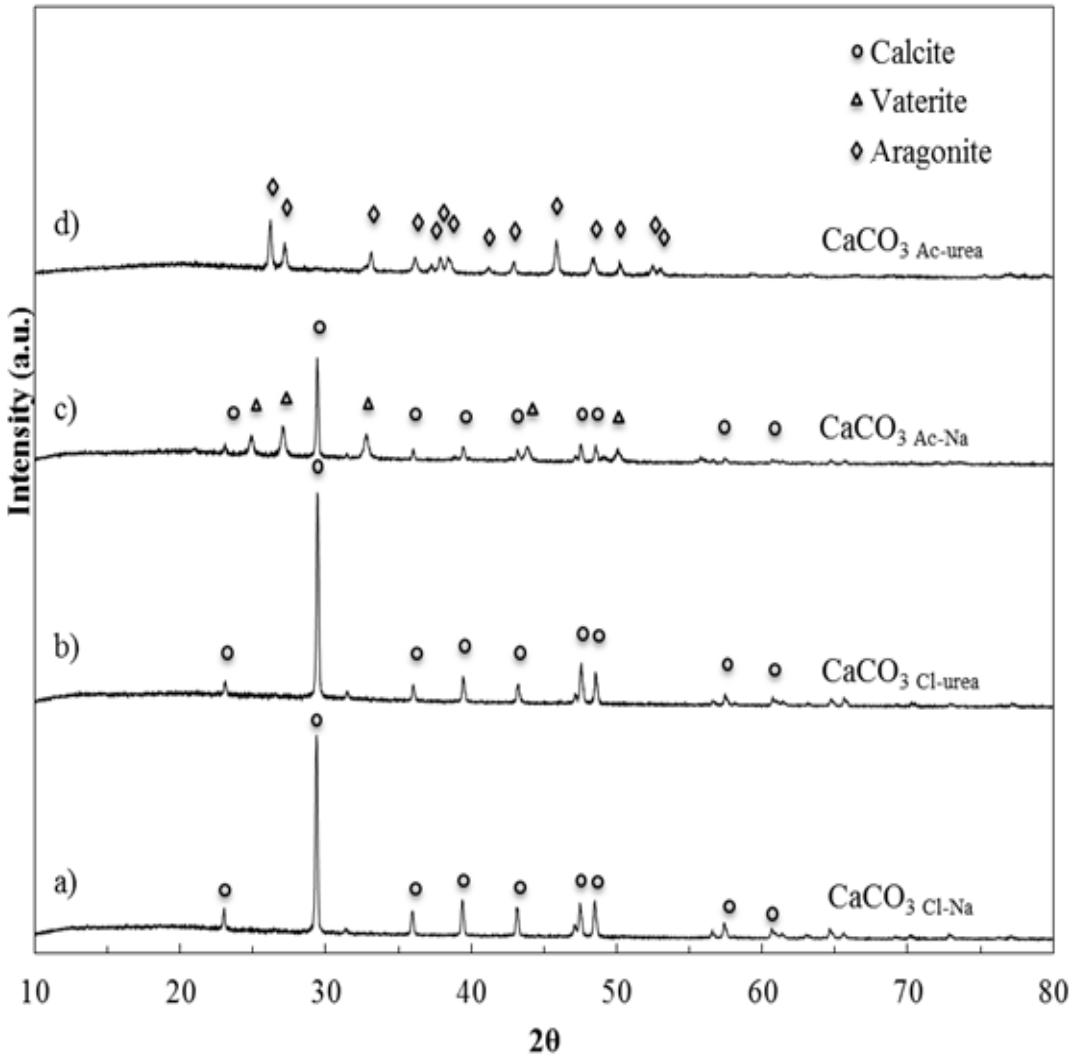

Fig. 4.19: XRD patterns of $CaCO_3$ synthesized from different calcium and carbonate precursors a) $CaCO_{3,Cl\text{-}Na}$, b) $CaCO_{3,Cl\text{-}urea}$, c) $CaCO_{3,Ac\text{-}Na}$, and d) $CaCO_{3,Ac\text{-}urea}$.

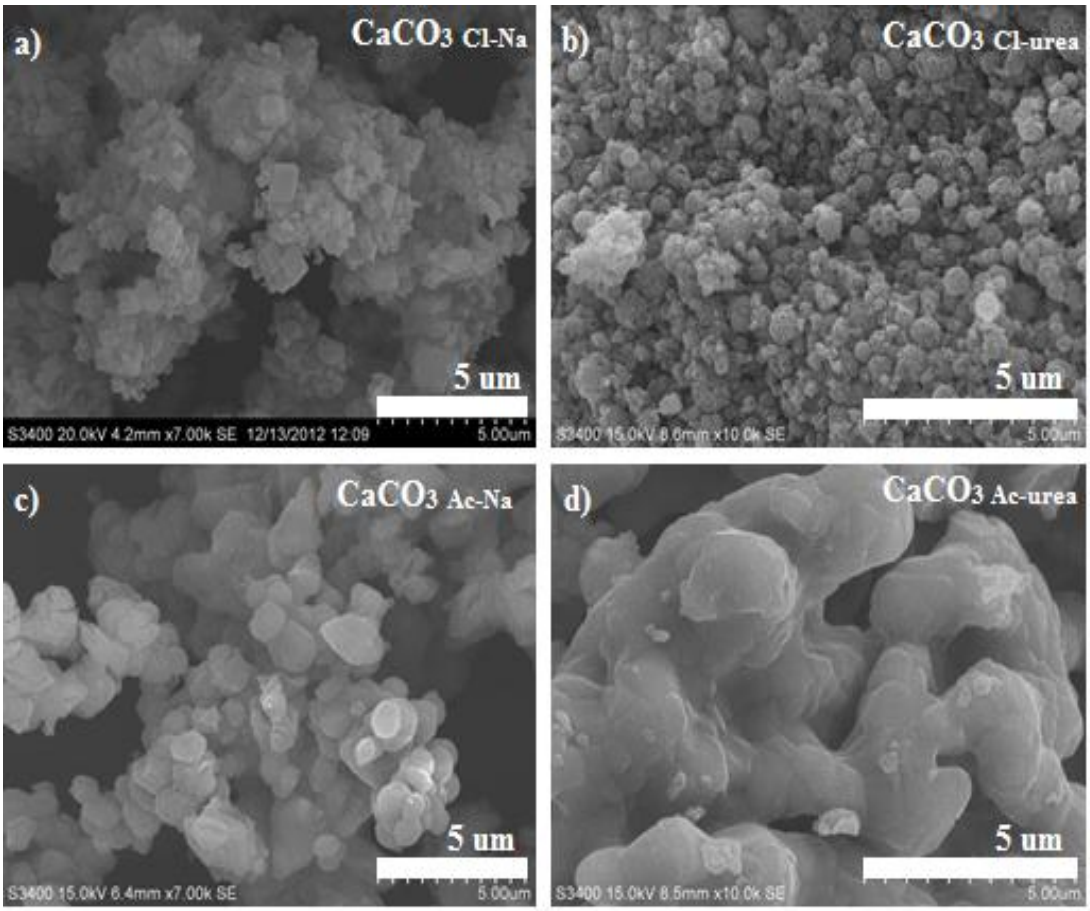

Fig. 4.20: SEM images of $CaCO_3$ synthesized from different calcium and carbonate precursors: a) $CaCO_{3,Cl\text{-}Na}$, b) $CaCO_{3,Cl\text{-}urea}$, c) $CaCO_{3,Ac\text{-}Na}$, and d) $CaCO_{3,Ac\text{-}urea}$.

SEM images of $CaCO_3$ samples are presented in Fig. 4.20. The results of precipitation by different precursors show morphology of the samples differ significantly; $CaCO_{3,Cl\text{-}Na}$ exhibits agglomeration of small cubic (rhombohedral) particle with particle size ranging in between 0.5 and 2 μm. $CaCO_{3,Cl\text{-}Urea}$ possesses spherical particle with rough surface with an average size of approximately 1 μm, $CaCO_{3,Ac\text{-}Na}$ has spherical-liked morphology with smooth surface and an average particle size of 0.5 to 2 μm. $CaCO_{3,Ac\text{-}Urea}$ shows aggregated form of $CaCO_3$ particle with large particle.

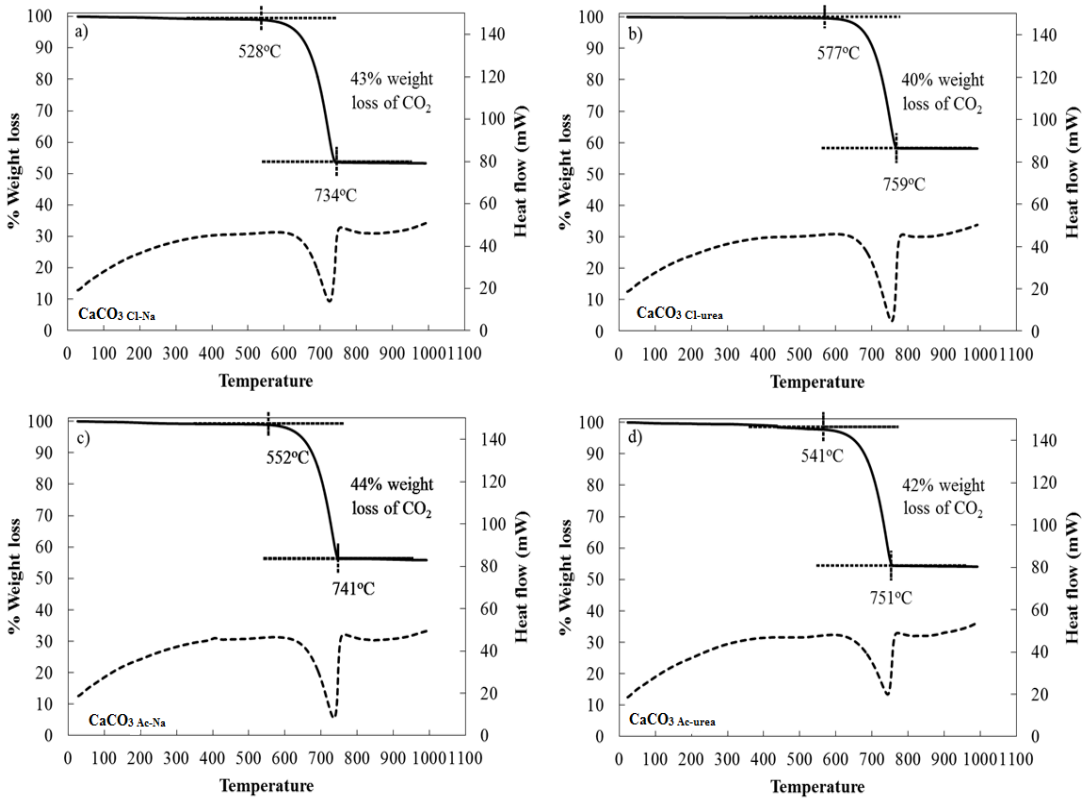

Fig. 4.21: TGA results of weight decomposing: a) $CaCO_{3,Cl\text{-}Na}$, b) $CaCO_{3,Cl\text{-}urea}$, c) $CaCO_{3,Ac\text{-}Na}$, and d) $CaCO_{3,Ac\text{-}urea}$.

In order to obtain CaO for CO_2 sorption test, synthetic $CaCO_3$ has to be calcined to decompose into CaO. We firstly checked the temperature requirement for the complete decomposition of $CaCO_3$ into CaO by TGA analysis. The results of TGA measurements presented in Fig. 4.21 show that all $CaCO_3$ sorbents has approximately 44 %wt loss of CO_2 which indicates the decomposition of $CaCO_3$ to CaO when $CaCO_3$ was heated to high temperature. $CaCO_{3,Cl\text{-}Na}$ shows the weight loss at 528°C, $CaCO_{3,Cl\text{-}urea}$ at 577°C, $CaCO_{3,Ac\text{-}Na}$ decomposes CO_2 at 552°C, and decomposition of $CaCO_{3,Ac\text{-}urea}$ is observed from the weight loss at 541°C. For all samples, complete weight loss of $CaCO_3$ to CaO is shown in the temperature range of 700-800°C so it could be concluded here that in order to ensure the obtained pure CaO, the $CaCO_3$ sample should be calcined at temperature higher than 850°C. Note that the decomposition of $CaCO_3$ to CaO exhibits endothermic reaction.

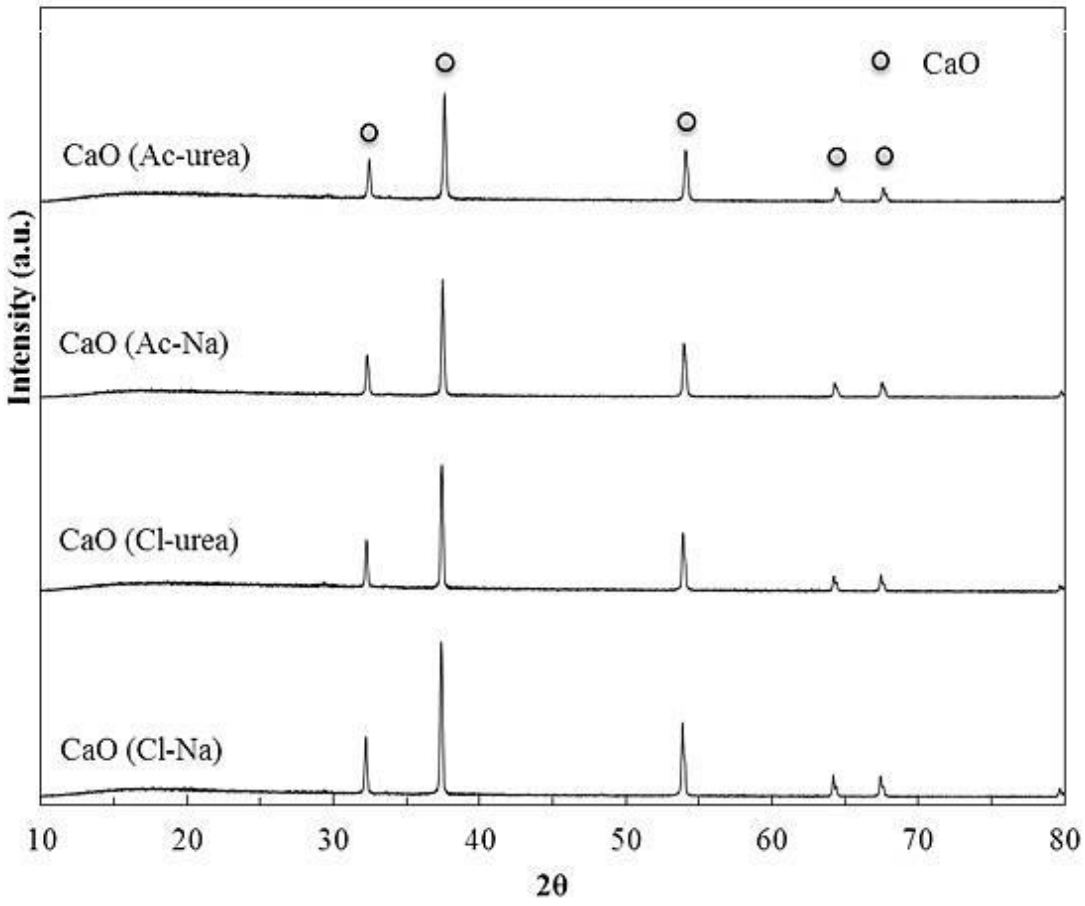

Fig. 4.22: XRD patterns of CaO derived from different calcium carbonate precursors a) $CaO_{Cl\text{-}Na}$, b) $CaO_{Cl\text{-}urea}$, c) $CaO_{Ac\text{-}Na}$, and d) $CaO_{Ac\text{-}urea}$.

XRD pattern of CaO sorbents derived from different $CaCO_3$ precursors are shown in Fig. 4.22. All samples exhibit major peaks at *2θ* of 32.2, 37.4, 53.9, 64.2, and 67.4, corresponding to CaO phase [Akgsornpeak et al. (2014), Cho et al. (2009), Lu et al. (2008)]. This result indicates complete decomposition of $CaCO_3$ can be obtained at 850°C regardless of $CaCO_3$ precursors, which is in agreement with TGA results demonstrated in Fig. 4.21.

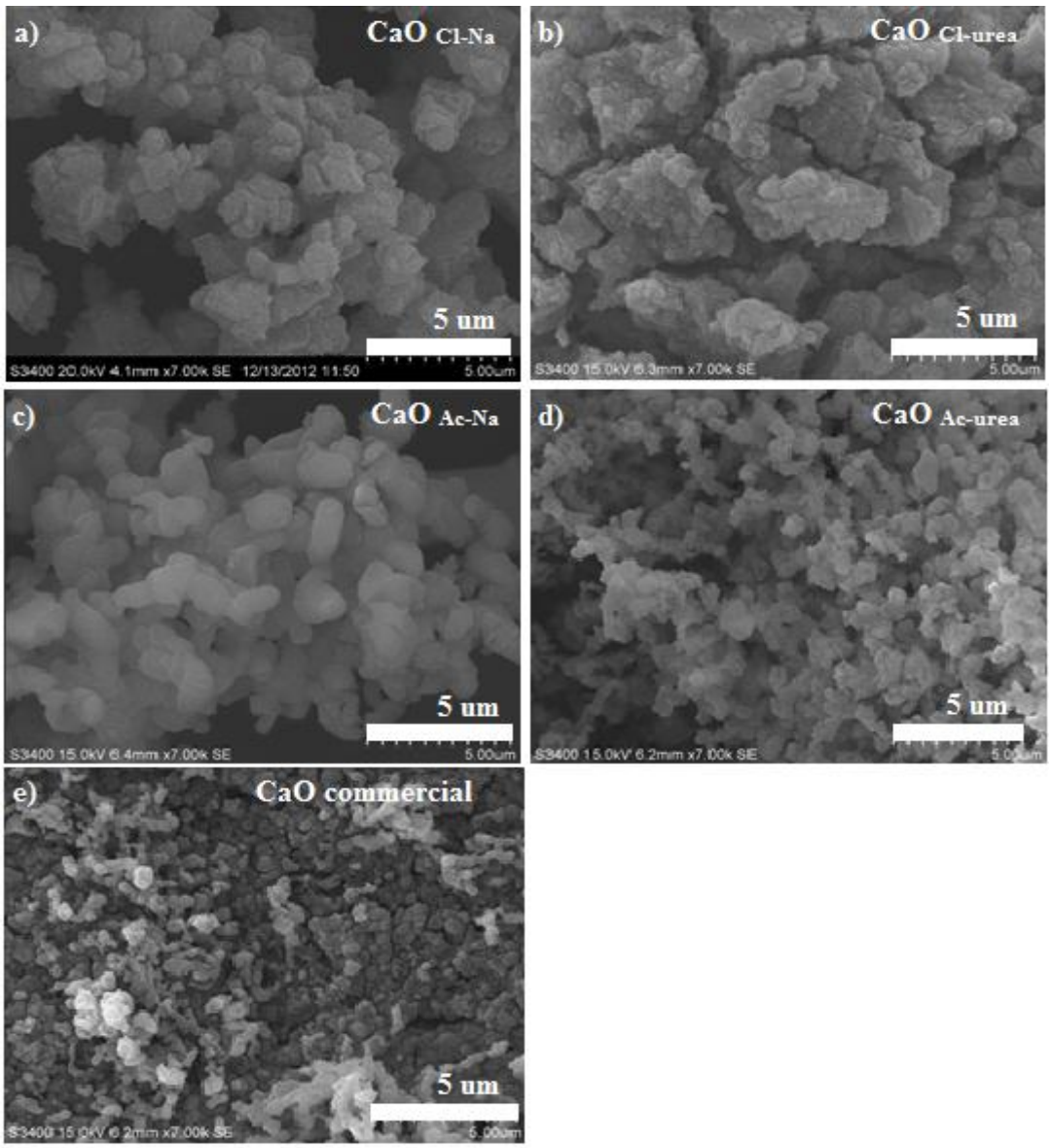

Fig. 4.23: SEM images of CaO synthesized from different calcium and carbonate precursors a) $CaO_{Cl\text{-}Na}$, b) $CaO_{Cl\text{-}urea}$, c) $CaO_{Ac\text{-}Na}$, d) $CaO_{Ac\text{-}urea}$, and e) $CaO_{commercial}$.

SEM images of CaO samples are depicted in Fig. 4.23. The results of all CaO sorbents obtained from precipitation of $CaCO_3$ show aggregated particles after calcination. $CaO_{Cl\text{-}Na}$ exhibits agglomeration of small particles. $CaO_{Ac\text{-}Na}$ has oval-like particle with smooth surface morphology having average size of approximately 2 μm. $CaO_{Ac\text{-}urea}$ has large network of connected particles with particle size ranging from 0.5 μm to 2 μm.

Table 4.3. Textural properties of CaO sorbents

Sample	Surface area (m^2/g)	Pore volume (cm^3/g)	Pore size diameter (nm)	Crystal size
$CaO_{Cl\text{-}Na}$	4.8	0.012	12.2	52.01
$CaO_{Cl\text{-}urea}$	8.4	0.033	14.6	54.37
$CaO_{Ac\text{-}Na}$	8.0	0.024	10.7	45.8
$CaO_{Ac\text{-}urea}$	9.8	0.063	27.5	44.27
$CaO_{commercial}$	4.8	0.012	9.7	-

Crystallized size of CaO calculated from Scherrer equation at the highest peak of CaO of 37.4° is in the order: $CaO_{Cl\text{-}urea} > CaO_{Cl\text{-}Na} > CaO_{Ac\text{-}Na} > CaO_{Ac\text{-}urea}$ as shown in Table 4.3. In Table 4.3 also presents textural properties of CaO sorbents derived from different $CaCO_3$ sources. Large surface area, pore volume, and pore size diameter are observed with $CaO_{Ac\text{-}urea}$ and these values are significant deviated from other sorbents. Note that the synthetic CaO sorbents possess higher BET surface area double in magnitude than that of commercial CaO, implying that the synthetic CaO samples have higher CO_2 sorption capability.

4.7.2 CO_2 sorption tests

Effect of carbonation temperature on CO_2 sorption performances

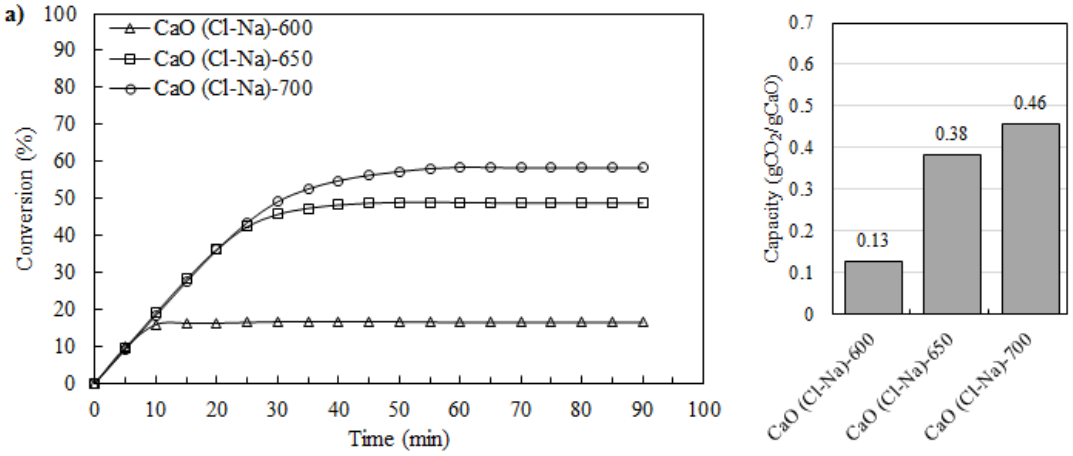

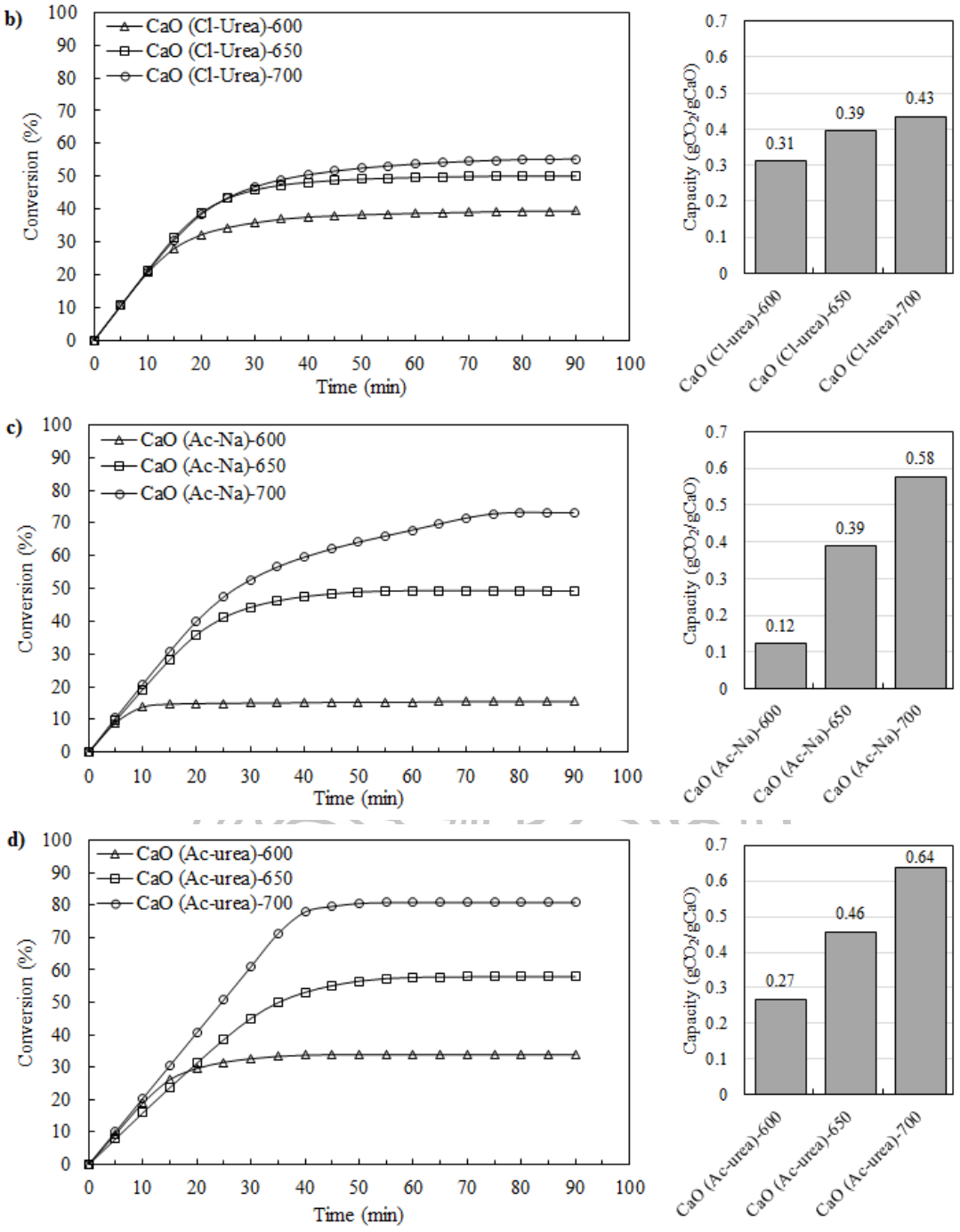
b)
CaO (Cl-Urea)-600
CaO (Cl-Urea)-650
CaO (Cl-Urea)-700
Conversion (%)
Time (min)
Capacity (gCO2/gCaO)
0.31
0.39
0.43
CaO (Cl-urea)-600
CaO (Cl-urea)-650
CaO (Cl-urea)-700
c)
CaO (Ac-Na)-600
CaO (Ac-Na)-650
CaO (Ac-Na)-700
Conversion (%)
Time (min)
Capacity (gCO2/gCaO)
0.12
0.39
0.58
CaO (Ac-Na)-600
CaO (Ac-Na)-650
CaO (Ac-Na)-700
d)
CaO (Ac-urea)-600
CaO (Ac-urea)-650
CaO (Ac-urea)-700
Conversion (%)
Time (min)
Capacity (gCO2/gCaO)
0.27
0.46
0.64
CaO (Ac-urea)-600
CaO (Ac-urea)-650
CaO (Ac-urea)-700

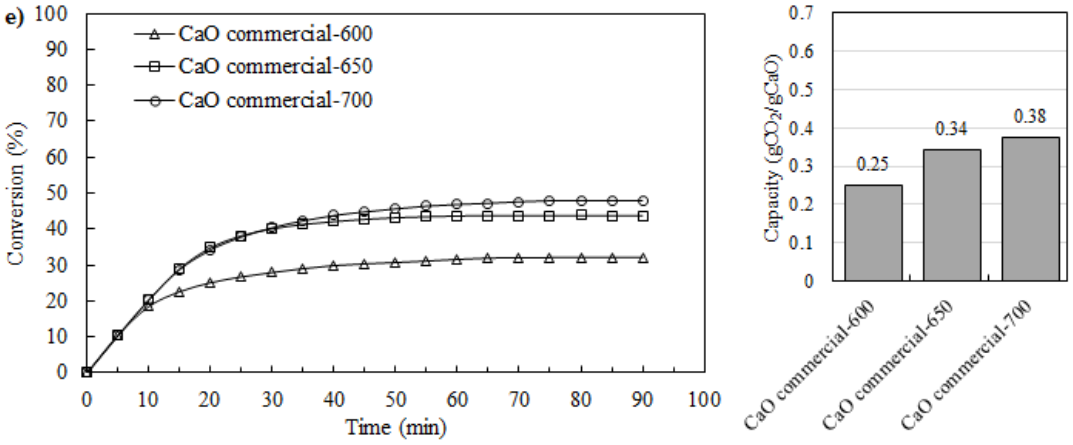

Fig. 4.24: Conversion of CaO synthesized from different calcium and carbonate precursors a) $CaO_{Cl\text{-}Na}$, b) $CaO_{Cl\text{-}urea}$, c) $CaO_{Ac\text{-}Na}$, d) $CaO_{Ac\text{-}urea}$, and f) $CaO_{commercial}$.

Fig. 4.24 presents conversion of CaO applying to capture CO_2 at high temperature for different CaO sorbents at temperature ranging from 600-700 ^oC. The results in Fig. 24a show that conversion of $CaO_{Cl\text{-}Na}$ increases with increasing carbonation temperature, indicating higher sorption is preferable at elevated temperature. This might be due to an increase of sorption rate at elevated temperature where CO_2 molecules can access to the available active CaO easier than that at low temperature. Our results are in good agreement with those reported by Florin and Harris (2008) of which their thermodynamic data showed equilibrium partial pressure of CO_2 increases with increasing carbonation temperature: equilibrium CO_2 partial pressure at 600^oC, 650^oC and 700^oC showed 0.006, 0.01 and 0.04 atm, respectively. Florin and Harris (2008) By comparison of CO_2 uptake capacity at the same sorption temperature, it is found that $CaO_{Ac\text{-}urea}$ offers comparatively high sorption capacity than others. This might be due to $CaO_{Ac\text{-}urea}$ possesses high surface area and small particle, which enhances the accessibility of CO_2 molecules to adsorb on CaO. In addition, $CaO_{Cl\text{-}urea}$ also show a good performance on CO_2 sorption as a fair sorption capacity is observed when compared with the sorbents synthesized using sodium as carbonate precursors. It could be concluded here that using urea as carbonate precursor offers higher sorption capacity than the use of sodium.

Reaction kinetics of CO_2 on CaO particle was examined using shrinking-core model as the reaction is likely to be governed by both chemical reaction at the surface and the product layer diffusion. The particle of CaO sorbent was assumed to be spherical grain and the sorption process was isothermal system. A model of the reaction core considers the change in radius of particle, which is given by Dou et al. (2010):

$$\frac{r^3}{r_0^3} = 1 - \alpha x , \qquad (4.5)$$

where r_0 is the initial particle radius. The shringkage factor, α , is defined as:

$$\alpha = \frac{\Delta v_i}{\Delta v_i^{t=0}} , \qquad (4.6)$$

where i represents single volume element, Δv_i is the volumetric shrinkage rate at time t , and $\Delta v_i^{t=0}$ is the volumetric shrinkage rate at time t =0.

It was proposed that if the reaction is controlled by chemical reaction at the surface, the shrinking-core model is expressed as:

$$\frac{t_g}{\tau_g} = 1 - (1 - \alpha x)^{1/3} = g(x), \qquad (4.7)$$

where t_g is the reaction time and is defined as:

$$t_g = \frac{\rho_s r_0 (1 - (r/r_0))}{b k_s c_0} , \qquad (4.8)$$

ρ_s is density of the particle, k_s rate constant of surface chemical reaction, b is stoichiometric coefficient.

The parameter τ_g is the time required for complete conversion $(x = 1)$ of the sorbent and can be calculated from

$$\tau_g = \frac{\rho_s r_0}{b k_s c_0} , \qquad (4.9)$$

If the reaction is controlled by mass transfer diffusion through the product layer, the model is expressed as:

$$\frac{t_g}{\tau_p} = 1 - 3(1 - \alpha x)^{2/3} + 2(1 - \alpha x) = p(x), \qquad (4.10)$$

where

$$\tau_p = \frac{\rho_s r_0^2}{6 b D_e c_0} , \qquad (4.11)$$

D_e is the effective diffusion coefficient.

If the reaction is controlled by both surface reaction and mass transfer diffusion, the model can be rationale as:

$$\frac{t - t_b}{\tau_g} = g(x) + \delta^2 p(x), \qquad (4.12)$$

where t_b is breakthrough time, and

$$\delta^2 = \frac{\tau_P}{\tau_g} = \frac{k_s r_0}{6 D_e}. \qquad (4.13)$$

The parameter δ^2 is the shrinking core reaction modulus defined as the ratio of product layer diffusion resistance to surface reaction resistance. The reaction is suggested to be surface reaction control when $\delta^2 << 1$ whereas product layer diffusion control is reliably assumed when $\delta^2 > 10$. Intermediate values of δ^2 are suggested to be controlled by both surface reaction and layer diffusion.

The kinetic of high-temperature CO_2 sorption was calculated through mass balance on fluid and solid phase. This model was calculated based on the assumption of isothermal system, constant gas velocity, one dimension of reactor (axis z), and ideal gas. The results of kinetic are presented in term of the ratio of diffusion resistance to chemical reaction resistance (δ^2) that could be used to predict the controlled adsorption behavior at surface reaction or the diffusion through product layer. The value lower than 1 implies surface reaction is controlled the adsorption process whereas the δ^2 values that higher than 10 indicate diffusion through product layer control the adsorption. The intermediate values exhibit that the system are controlled by both surface reaction and diffusion through product layer. Dou et al. (2010)

The calculation of kinetic shown in Fig. 4.25 reveal that diffusion control is observed at 600ºC for all sorbents as indicated by the values of δ^2 higher than 10. This might be due to low kinetic rate of CO_2 molecules leading to low possibility in diffusing through the layer of $CaCO_3$. When temperature was increased to 650ºC and 700ºC, surface reaction tend to become predominant as shown by a decrease of δ^2 value for all sorbents except for $CaO_{Cl\text{-}Na}$ and commercial. This possibly be because increasing temperature could increase acceleration of CO_2 molecules. No sorbent sample has δ^2 less than 1, indicating the sorption system is controlled by both surface and diffusion through the layer of $CaCO_3$, which is the nature of CaO sorbent as reported by Cazorla-Amoros et al. (1991).

$CaO_{Cl\text{-}Na}$ and $CaO_{Ac\text{-}Na}$ are found to adsorb low CO_2 capacity (0.14 $gCO_2/gCaO$) at 600ºC due to low kinetic rate. With increasing temperature to650ºC and 700ºC, capacity of $CaO_{Cl\text{-}Na}$ and $CaO_{Ac\text{-}Na}$ largely increase. On the other hand, rate of increasing capacity of $CaO_{Cl\text{-}urea}$ is too low at elevated temperature of carbonation because CO_2 might diffuse through layer of $CaCO_3$ of the small aggregated particle of $CaO_{Cl\text{-}Na}$ and $CaO_{Ac\text{-}Na}$ easier than the larger particle of $CaO_{Cl\text{-}urea}$. $CaO_{Ac\text{-}urea}$ shows good performance for CO_2 sorption because the morphology of CaO exhibits large network of connected small particles. The channels of porous on surface of CaO, which observed from SEM image (Fig. 4.23), would favor mass transfer Florin and Harris (2009) and hence promotes the ease accessibility of CO_2 to available surface active of CaO.

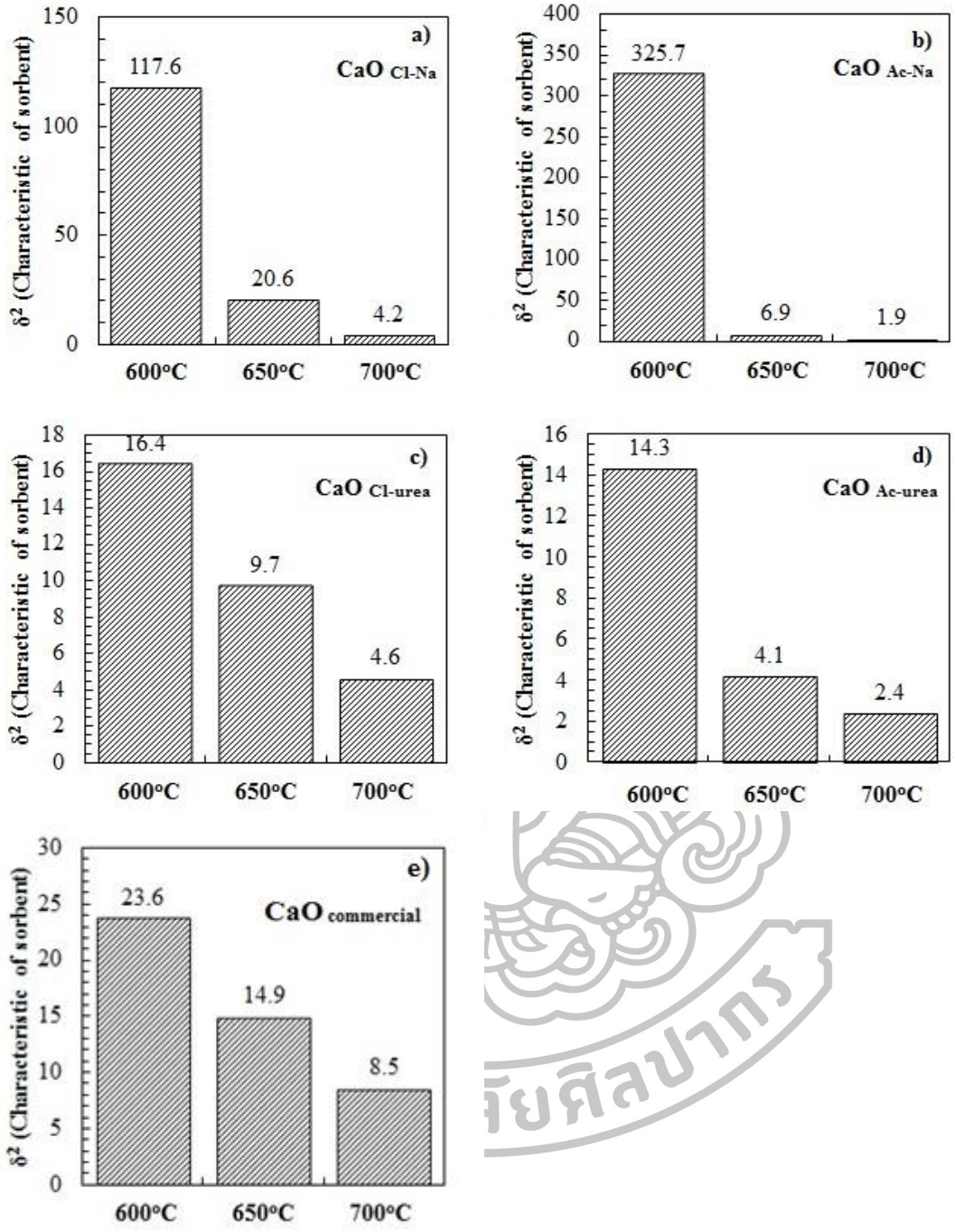

Fig. 4.25: The characteristic of CaO synthesized from different calcium and carbonate precursors a) $CaO_{Cl\text{-}Na}$, b) $CaO_{Cl\text{-}urea}$, c) $CaO_{Ac\text{-}Na}$, d) $CaO_{Ac\text{-}urea}$, and e) $CaO_{commercial}$.

From our results, different polymorphs of $CaCO_3$ were obtained from different calcium or carbonate precursors. Carbonate source seems to have a greater effect of polymorph of $CaCO_3$ than calcium source. In the system of $CaCl_2$ and Na_2CO_3, $CaCO_3$ is precipitated due to the formation of Ca^{2+} and CO_3^{2-} dissociated in the solution as shown in the following equations:

$$CaCl_2 \rightarrow Ca^{2+} + 2Cl^- \quad (4.14)$$

$$Na_2CO_3 \rightarrow 2Na^+ + CO_3^{2-} \quad (4.15)$$

Due to the high solubility and small molecular size of Ca^{2+} and CO_3^{2-}, the interaction between Ca^{2+} and CO_3^{2-} would be favorable and formed compact particle and stable phase of calcite. For the case of $Ca(CH_3COO)_2$ and Na_2CO_3, negatively charge of CH_3COO^- could competitively interact with Ca^{2+} during the formation with CO_3^{2-}, which would lead to the weak interaction between Ca^{2+} and CO_3^{2-}, resulting in the growth of polymorph to metastable phase (vaterite). Liang et al. (2004), Coenen et al. (2011)

$$Ca(CH_3COO)_2 \rightarrow Ca^{2+} + 2(CH_3COO^-) \quad (4.16)$$

$$Na_2CO_3 \rightarrow 2Na^+ + CO_3^{2-} \quad (4.17)$$

For the precipitation of $CaCO_3$ by using $Ca(CH_3COO)_2$ and $CO(NH_2)_2$, metastable of aragonite phase and morphology of agglomeration large particle was formed. This might be due to CH_3COO^- group interacted with Ca^{2+} during reaction of precipitation and this interaction leaded to the formation of void between large particles (see Fig. 4.20)

$$Ca(CH_3COO)_2 \rightarrow Ca^{2+} + 2(CH_3COO^-) \quad (4.18)$$

$$CO(NH_2)_2 \rightarrow NH_3 + HNCO \rightarrow NH_4^+ + NCO^- \quad (4.19)$$

$$NCO^- + OH^- + H_2O \rightarrow NH_3 + CO_3^{2-} \quad (4.20)$$

4.8 Conclusion

Different $CaCO_3$ precursors provide different morphologies of CaO and hence affect to CO_2 sorption capacity. $CaO_{Ac\text{-}urea}$ yields large network of connected small particles, $CaO_{Cl\text{-}urea}$ shows large aggregated particle, and $CaO_{Cl\text{-}Na}$ and $CaO_{Ac\text{-}Na}$ shows agglomeration of small particles. The different morphologies of CaO have a direct effect on CO_2 sorption capacity. $CaO_{Ac\text{-}urea}$ shows good performance for CO_2 sorption of 0.74 $gCO_2/gCaO$ at temperature 700°C. The kinetic model reveals that the sorption systems are controlled by both surface and diffusion through the layer.

CHAPTER V

EFFECT OF ADDITIVE ADDITION ON PROPERTIES OF CaO-DERIVED $CaCO_3$ AND CO_2 SORPTION CAPACITY

5.1 Abstract

Anionic surfactants, sodium dodecyl sulfate (SDS) and Gemini surfactant (12-3-12, GS), are used as structure directing agents in the synthesis of $CaCO_3$. The $CaCO_3$ was obtained by precipitation of calcium acetate and urea with several concentrations of the adding surfactants. The properties of $CaCO_3$ and CaO sorbent were characterized by X-ray diffraction, scanning electron microscopy, thermal gravimetric analysis, and N_2 adsorption/desorption. The results showed that the addition of surfactant can affect morphology and surface properties of CaO which also have influence on CO_2 sorption capacity of CaO sorbent. The sorbent synthesized with the use of Gemini surfactant at 2 mM showed connected of rod-like with rough surface and large surface area of 16.3 m^2/g. This sorbent provides good adsorption capacity of 0.29 $gCO_2/gCaO$ under the operating condition of 600^oC, atmospheric pressure, CO_2 15%v/v (balanced N_2).

5.2 Introduction

Calcium looping technology is a typical process used for CO_2 capture. One of its applications relating CO_2 capture process is a combination in hydrogen production technology named sorption enhanced steam reforming (SESR). The implementation of calcium looping in SESR leads to an improvement in hydrogen purity in a single step, resulting in a reduction of investment and operating costs.

CaO-based sorbents are widely used in pre-combustion process as they are abundant in nature and it can be operated under severe operating conditions of steam reforming process. However, CaO from natural resources such as natural lime, egg shell, seashells, or snail shells have uncertain morphologies, which would be difficult to control their applications. Chen et al. (2010) As a consequence, synthetic CaO becomes an interesting material for CO_2 capture. One technique to control morphology of CaO is the use of additive or structure directing agent in the synthesis step of $CaCO_3$. Additives that are used to enforce structure of $CaCO_3$ include polymer, surfactant, or organic compounds.

In this section, the effect of adding additive on properties of synthetic $CaCO_3$ and CaO-derived $CaCO_3$ is a subject of interest. Anionic surfactant and anionic Gemini surfactant are used to modify/improve properties of CaO sorbent. The synthetic sorbents are tested for the application of CO_2 capture under the operating conditions relating sorption enhanced steam methane reforming process.

5.3 Literature review

Surfactant additive is one of techniques used to control particle size, morphology and textural surface of $CaCO_3$. The effect of surfactant on precipitation of $CaCO_3$ is summarized in Table 5.1. Zhang et al. (2008) studied the effect of addition of anionic surfactant sodium dodecyl sulfate (SDS) and cationic surfactant hexadecyltrimethylammonium bromide (CTAB) on morphology of $CaCO_3$. The results showed adding cationic surfactant CTAB provided no different in morphology of rhombohedral with smooth surface when compared with that prepared without surfactant. The $CaCO_3$ precipitation with SDS surfactant showed rhombohedral with rough surface.[Yu et al. (2005)] Chen et al. (2011) enhanced structure of CaO sorbent by adding calcium lignosulfonate (CLS) as additive that could provide capacity of 85% conversion of CaO at 700^{o}C in 15%CO_2 (balanced N_2). Coenen et al. (2012) improved CaO by adding P123 (or PEG) during synthesis step, the results exhibited conversion of 90% of CaO with P123 and 74% of CaO with PEG at 600^{o}C for 30 min under 60%CO_2 (balanced N_2). Florin and Harris (2008) precipitated $CaCO_3$ with the addition of Dispex N400 as an anionic surfactant for controlling textural structure and increasing surface area, the results showed conversion of 90% at 600^{o}C in 15%CO_2 (Balanced N_2). Works relating to the use of additives on the synthesis of $CaCO_3$ are summarized in Table 5.1.

Table 5.1 Examples of the effect of adding additives on polymorph of $CaCO_3$

Precursors	Additive	Concentration of additive	Polymorph	Morphology	Ref.
$Ca(OH_2) + CO_2$	-	-	Calcite	Rhombohedral	Zhang et al. (2008)
	Sodium dodecyl sulfate (SDS)	2 g/L	Calcite	Cubic with rough surface	
	Hexadecyltrimethylammonium bromide (CTAB)	2 g/L	Calcite	Rhombohedral	
$CaCl_2 + Na_2CO_3$	-	-	n/a	Rhombohedral	Yu et al. (2005)
	Hexadecyltrimethylammonium bromide (CTAB)	1 mM	n/a	Rhombohedral	
$CaCl_2 + Na_2CO_3$	Sodium dodecyl sulfate (SDS)	5 mM	Calcite	Monodispersed hollow-sphere particles	Wei et al. (2005)
	Sodium dodecylbenzenesulfonate (SDBS)	5 mM	Vaterite	Spherical particles	
	Sodium dodecyl sulfonate (DDS)	5 mM	Calcite	Rhombohedral with smooth surface	
$Ca(CH_3COO)_2$ + urea	Sodium dodecyl sulfate (SDS)	0.5 mM	Aragonite	Rod-shaped	Chen et al. (2010)
		1 mM	Vaterite	Flower-shaped	
		2.5 mM	Calcite and Vaterite	Tube, Rhombohedral, Hexagonal-shaped	

5.4 Theory

Surfactant

Surfactants are used in many applications such as detergents, wetting agents, emulsifiers, or foaming agents. Surfactants usually are organic compounds that consist of hydrophobic part (tail) and hydrophilic part (head). Hydrophobic of surfactant is mostly hydrocarbon chain whereas hydrophilic of surfactant can be anionic, cationic, zwitterionic, or nonionic (Fig. 5.1).

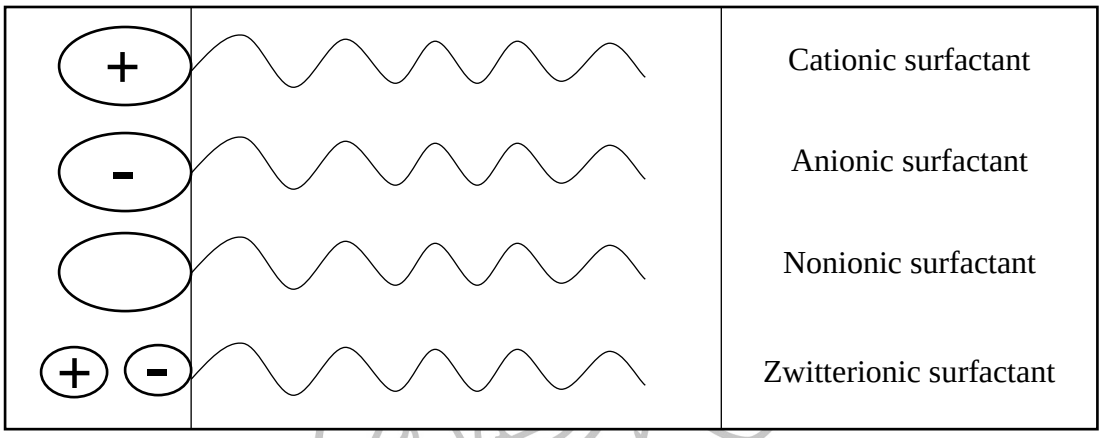

Fig. 5.1: Hydrophilic types of surfactant

When surfactants are dissolved in solvent, the addition of surfactants can lead to the reduction of surface tension at low concentration (Fig. 5.2). When concentration is increased to a certain value, the surfactants will form into a specified structure. This concentration is called critical micelle concentration or CMC value and the specified structure is named as micelle.

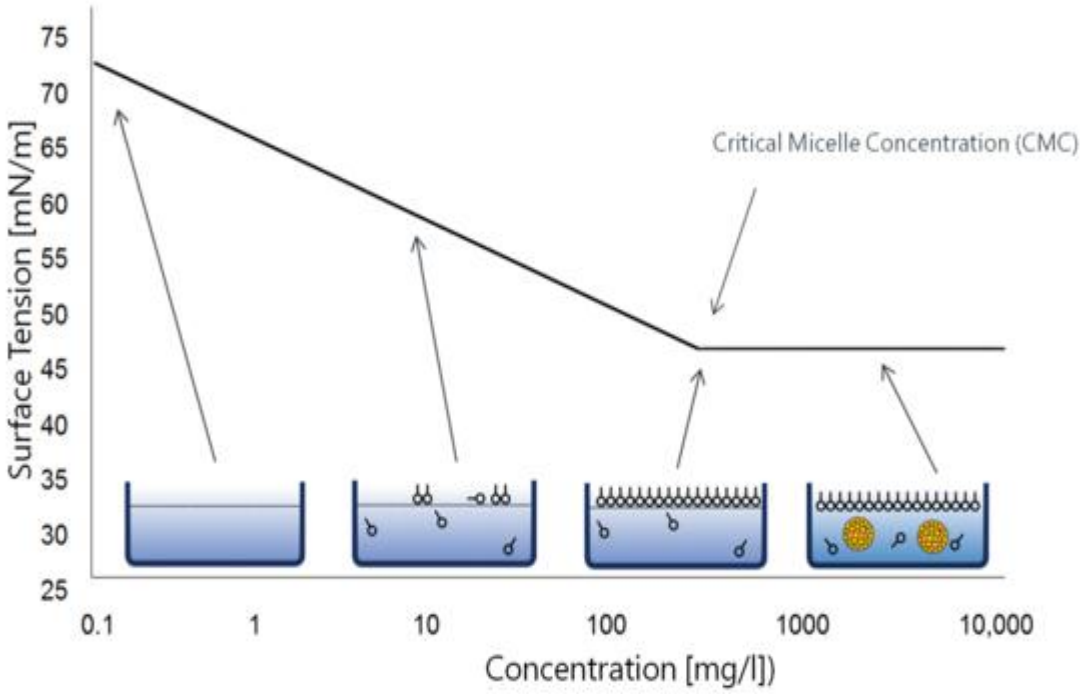

Fig. 5.2: Relationship between surfactant concentration and surface tension properites
(http://www.kruss.de/services/education-theory/glossary/cmc/)

5.5 Methodology

5.5.1 Materials

Calcium acetate hydrate ($Ca(CH_3COO)_2.H_2O$, 99%), received from Lobachemie, was used as calcium precursor. Urea ($(NH_2)_2CO$, 99%) obtained from Carlo Erba, was used as carbonate source. CaO commercial (powder) was received from Ajax finechem. Sodium dodecyl sulfate (SDS, 97%), received from Carlo Erba and Gemini surfactants synthesized followed Wang et al. (2008), were used as additives. All chemicals were used as received.

5.5.2 Preparation of Gemini surfactant

Gemini surfactant was synthesized followed Wang et al. (2008) by firstly connecting hydrophobic part to a spacer and then the hydrophilic part was added. To synthesize tail group, a 20-mL of 2.5 M of 1,3-dibromopropane in ethanol solution and 50-mL of 3 M dodecylamine in ethanol solution were mixed in a 4-neck round bottom. The mixture solution was stirred under reflux at 78^{o}C for 48 h. The solvent was removed by evaporation at 78^{o}C. The wet residue was extracted by diethyl ether, and was filtrated for 3 times. The solid was recrystallized for 3 times by 1:1 of petroleum ether and acetone. At this step, two tails of hydrophobic (dodecylamine)

were connected by the spacer (1,3-dibromopropane). To connect the head group, 1,3-propanesultone was reacted with the tail group obtained from the first step (n,n-didodecylpropane-1,3-diamine) in methanol. The 20-mL solution of 2.5 M 1,3-propanesultone and 50-mL of 0.5 M n,n-didodecylpropane-1,3-diamine were stirred under reflux at 64^{o}C for 24 h. The solution was neutralized by 0.05 mol of Na_2CO_3 for 1 h, then the solvent was removed by heating at 64^{o}C. The solid was separated by filtration. Finally, the Gemini surfactant was recrystallized by 1:3 of methanol and acetone mixture for 3 times.

5.5.3 Preparation of $CaCO_3$

$CaCO_3$ was prepared by dissolving 100 mL of 2.5 M of $Ca(CH_3COO)_2$ with a desired concentration of SDS or Gemini surfactant. Then $CO(NH_2)_2$ (carbonate precursor) solution was added into the mixture solution under vigorous stirring at 90^{o}C for 24 h. The obtained precipitate was filtered, washed with distilled water, and dried at 30^{o}C. The concentrations of surfactant were used at, 10, 20, 40 mM for SDS, and 0.045, 0.08, 0.12, 2, and 4 mM for Gemini surfactant. Similarly, the products were denoted as $CaCO_3$-SDS xx mM, and $CaCO_3$-GS xx mM, where xx stands for concentration of surfactant.

5.5.4 Preparation of CaO sorbents

To produce CaO sorbents for CO_2 capture, $CaCO_3$ samples were calcined under air at 850^{o}C for 30 min.

5.6 Characterization

Nuclear Magnetic Resonance Spectroscopy (NMR)

This technique involves the absorption of electromagnetic wave in radio wavelength. This technique is used to analyze structure of organic, inorganic, and biological compounds; however, the compounds of sample must contain nucleus that spin is not zero such as ^{1}H and ^{13}C.

Chemical shift is parameter that related resonance frequency of sample and reference, thus, the chemical shift value does not directly proportional to the magnetic field. The chemical shift is calculated by the following equation:

$$chemical\ shift\ (\delta) = \frac{frequency\ of\ signal - frequency\ of\ refference}{frequency\ of\ refference} \times 10^{6} \quad (5.1)$$

Generally, the nucleus of an element, which contains charge, can spin around nucleus axis. The spinning of nucleus generates magnetic moment, when external magnetic field (B_0) is presented, the nucleus will arrange direction to align

with or align against the magnetic field. The spinning aligns (α-spin stage) with magnetic field is lower energy than that aligns against the field (β-spin stage) as shown in Fig. 5.3. The nucleus that has low energy is excited by radio frequency, the direction of spinning can flip to against magnetic field. In the same way, the high energy can flip to align with magnetic field. This phenomena of flip is called resonance. The difference of energy shows relation with magnetic field by the following equation:

$$\Delta E = \frac{h\gamma}{2\pi} B_0 \qquad (5.2)$$

$h = Plank's constant$

$\gamma = Gyromagnetic\ ratio\ (Proton(H) = 2.675 \times 10^8,\ T^{-1} \cdot S^{-1})$

$B_0 = Magnetic\ force,\quad T$

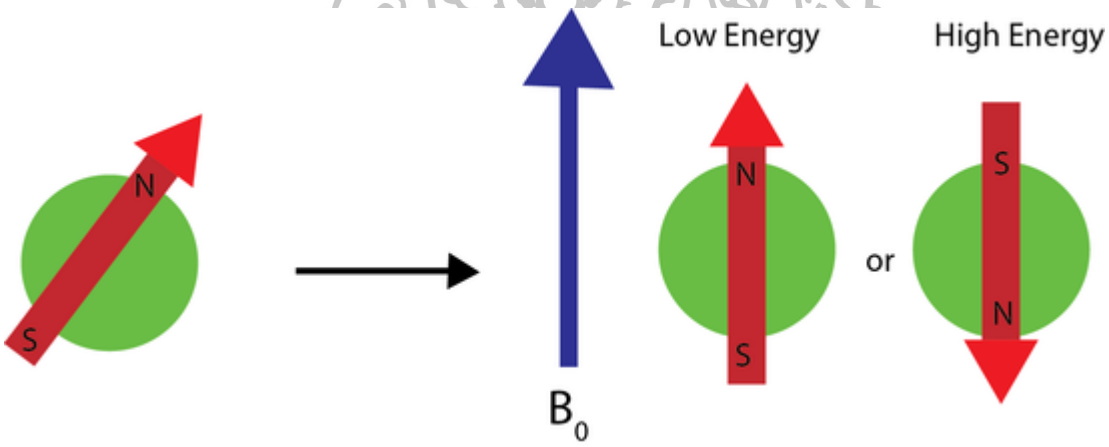

Fig. 5.3: Spinning of nucleus when magnetic field is presented (http://chemwiki.ucdavis.edu/Physical_Chemistry/Spectroscopy/Magnetic_Resonance_Spectroscopies/Nuclear_Magnetic_Resonance/Nuclear_Magnetic_Resonance_II)

NMR composes of tube sample, magnetic field, source of radio frequency, and detector. A sample is contained in sample tube and place in the magnetic field. The radio frequency excites the nucleus of sample by absorbing signal. After the nucleus come to ground stage and release the energy in radiofrequency signal. The intensity of signals at each frequency is detected and the frequency is converted into chemical shift. In this work, the H-NMR was used to investigate structure of Gemini surfactant.

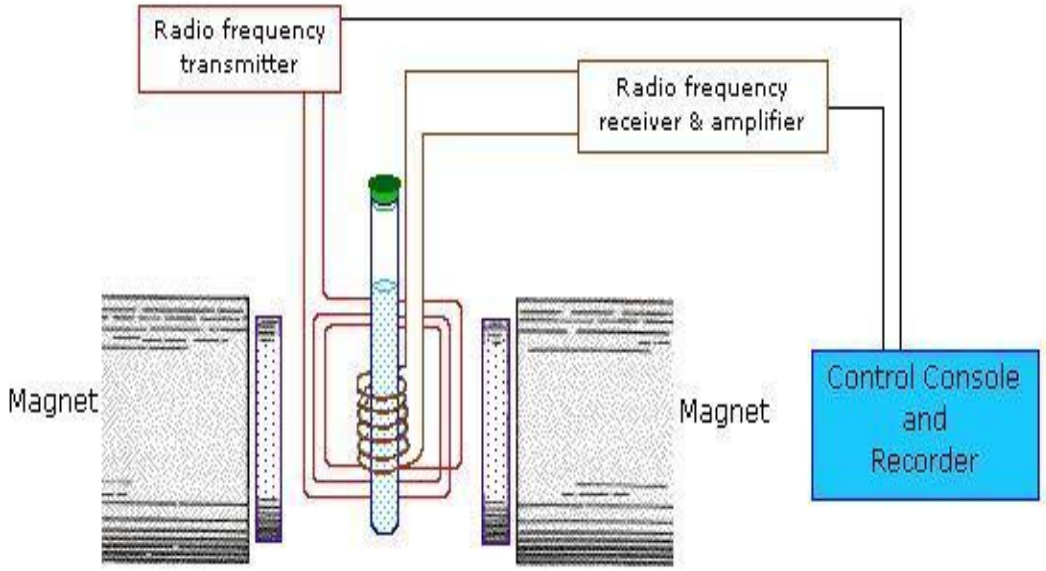

Fig. 5.4: Scheme of NMR instrument (http://share.psu.ac.th/blog/secpin/5348)

5.7 CO_2 sorption performance tests

CO_2 uptake capacity of the synthetic CaO was tested via packed bed reactor. For each experiment, the sample of 0.8 g was placed in a quartz tube and heated from ambient temperature to 850ºC under N_2 flow and held for 30 min before taking measurement to refresh the material. CO_2 sorption (carbonation reaction) was carried out at 600 °C under 15 mL/min gas flow containing 15% CO_2 (balanced N_2). For desorption test (calcination reaction), the sample was heated to 850ºC under 100% N_2 for 30 min (or until no CO_2 was observed).

5.8 Results and discussion

5.8.1 Characterization of Gemini surfactant

The structure of Gemini surfactant was examined by H-NMR, of which the position of chemical peak shift can identify bond of hydrogen in molecule. The results of H-NMR shown in Table 5.2 reveal chemical peak shift of hydrophobic group is presented at 0.818 ppm, 1.236-1.249 ppm, 2.184-2.241 ppm and 2.181-2.237 ppm, and the peak of spacer shows at 2.184-2.241 ppm. The connected of hydrophilic group can be found at 1.903-1.960 ppm and 2.859-2.890 ppm. Note that NMR peaks observed with our results show similar results to those reported by Wang et al. (2008).

Table 5.2: H-NMR of Gemini surfactant

Proton position	Chemical Peak Shift (δ), ppm (Wang et al. 2008)	Chemical Peak Shift (δ), ppm (Our synthesis)
(t, 3H, $\boldsymbol{CH_3}$)	0.78	0.818
(m, 18H, CH_3–$\boldsymbol{(CH_2)_9}$–CH_2–CH_2)	1.18-1.21	1.236-1.249
(m, 2H, CH_3–$(CH_2)_9$–$\boldsymbol{CH_2}$–CH_2)	1.40	
(m, 1H, N–CH_2–$\boldsymbol{CH_2}$–CH_2–N)	2.10	2.184-2.241
(m, 2H, N–CH_2–$\boldsymbol{CH_2}$–CH_2–SO_3^-)	1.84	1.903-1.960
(m, 4H, CH_3–$(CH_2)_9$–CH_2–$\boldsymbol{CH_2}$–N–$\boldsymbol{CH_2}$)	2.47–2.53	2.181-2.237
(t, 2H, N–CH_2–CH_2–$\boldsymbol{CH_2}$–SO_3^-)	2.77	2.859-2.890

Surface properties of surfactant plotted as a function of surfactant concentration are shown in Fig. 5.5. The results show that surface tension reduces dramatically when concentration of Gemini surfactant was increases to 0.045 mM. After that, its surface tension was not changed as a function of surfactant concentration. Critical micelle concentration was found to be 0.045 mM.

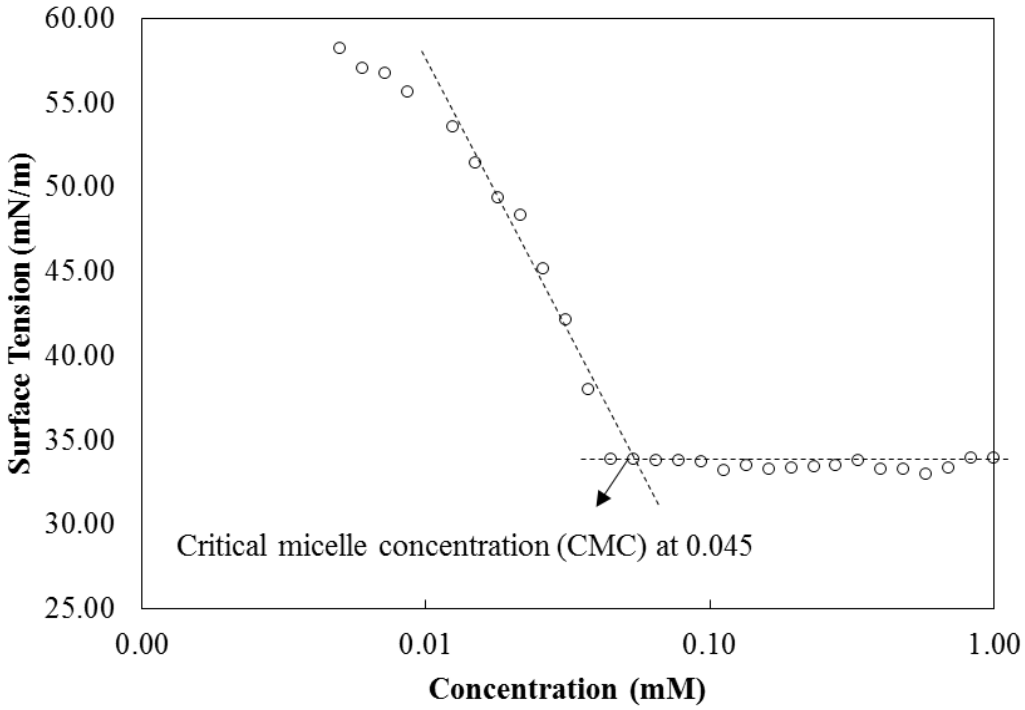

Fig. 5.5: Surface tension plot as a function Gemini concentration measured at temperature of 30°C

5.8.2 Characterization of $CaCO_3$ sorbent

XRD patterns of $CaCO_3$ synthesized with the use of different concentrations of SDS surfactant are shown in Fig. 5.6. $CaCO_3$ synthesized with SDS surfactant at 10 mM and 20 mM, show aragonite phase, which is similar to the synthesized $CaCO_3$ without surfactant. $CaCO_3$ with the addition of 40 mM SDS surfactant occurs phase transfer from pure aragonite to the mixed phases of calcite (24%) and aragonite (76%).

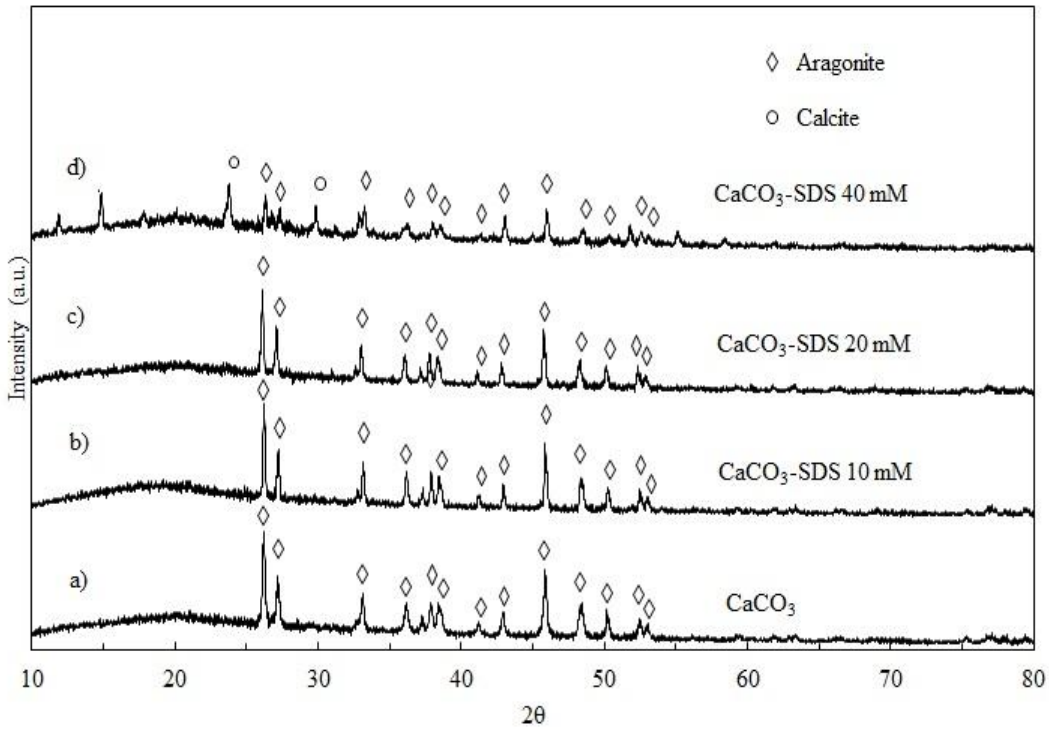

Fig. 5.6: XRD patterns of $CaCO_3$ synthesized with the addition of SDS surfactant at concentration of a) without SDS, b) 10 mM, c) 20 mM, d) 40 mM.

For $CaCO_3$ synthesized with the addition of Gemini surfactant, XRD patterns indicate aragonite phase of $CaCO_3$ at 0.045 mM, which is similar to the synthetic $CaCO_3$ without surfactant. Adding Gemini surfactant at concentration of 0.08 mM, 0.12 mM, and 2 mM during precipitation show phase of aragonite whereas 4 mM of Gemini surfactant induces the mixture of calcite (3%) and vaterite (97%) phase to form.

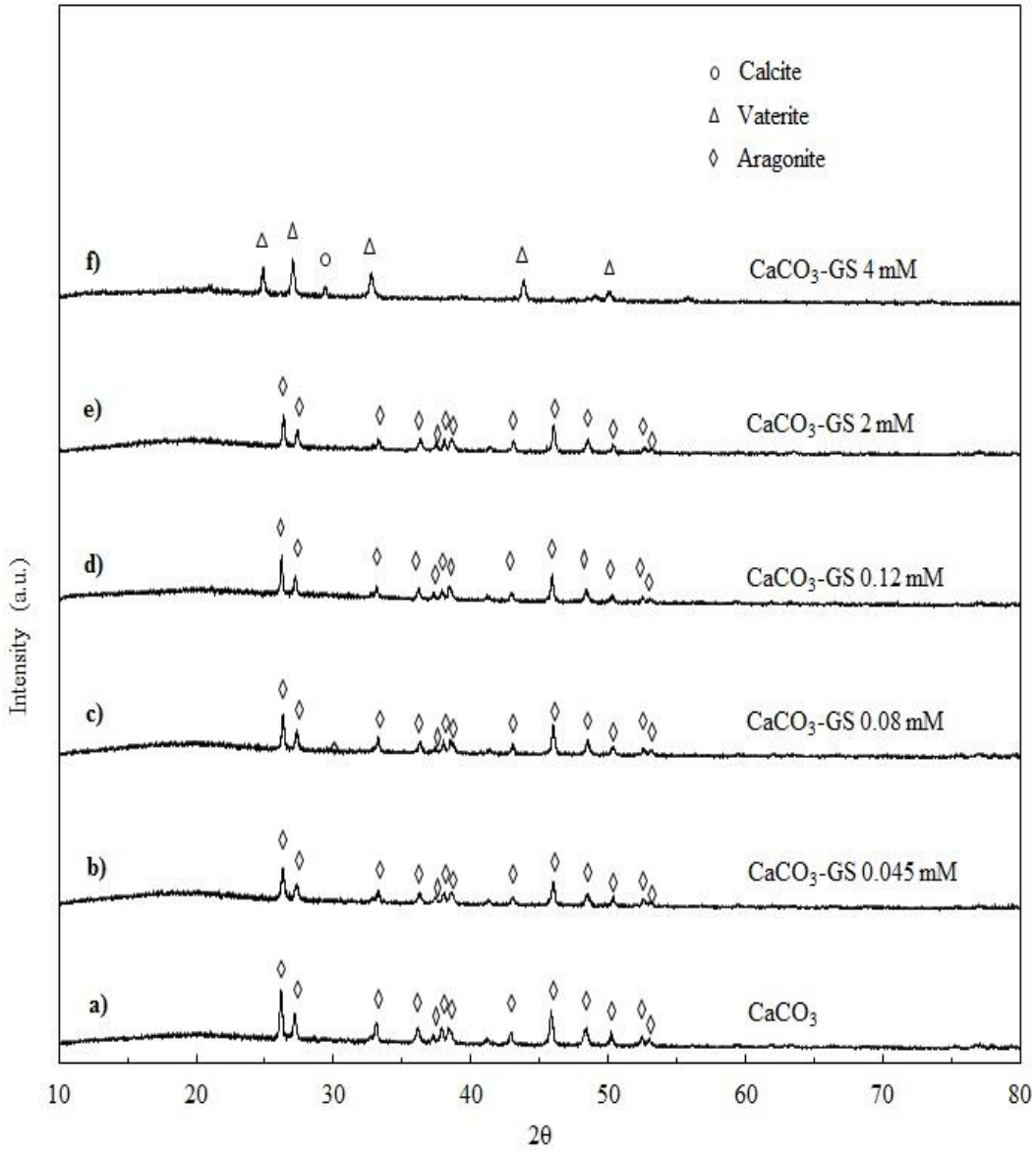

Fig. 5.7: XRD patterns of $CaCO_3$ with Gemini surfactant at concentration of a) without Gemini surfactant, b) 0.045 mM, c) 0.08 mM, d) 0.12 mM, e) 2 mM, f) 4 mM.

Morphology of $CaCO_3$ sorbents observed by SEM are shown in Fig. 5.8. $CaCO_3$ without surfactant shows morphology of aggregated particles whereas $CaCO_3$ with surfactant presents rod-like structure with different particle sizes depending upon surfactant concentration used. Concentration of 10 and 20 mM of adding Gemini surfactants resulted in rod-like structure with average particle size of 3-5 µm. The rod shape of $CaCO_3$ is shorter than 1 µm when concentration of surfactant was increased to 40 mM together with the aggregation of particles as shown in Fig. 5.8d.

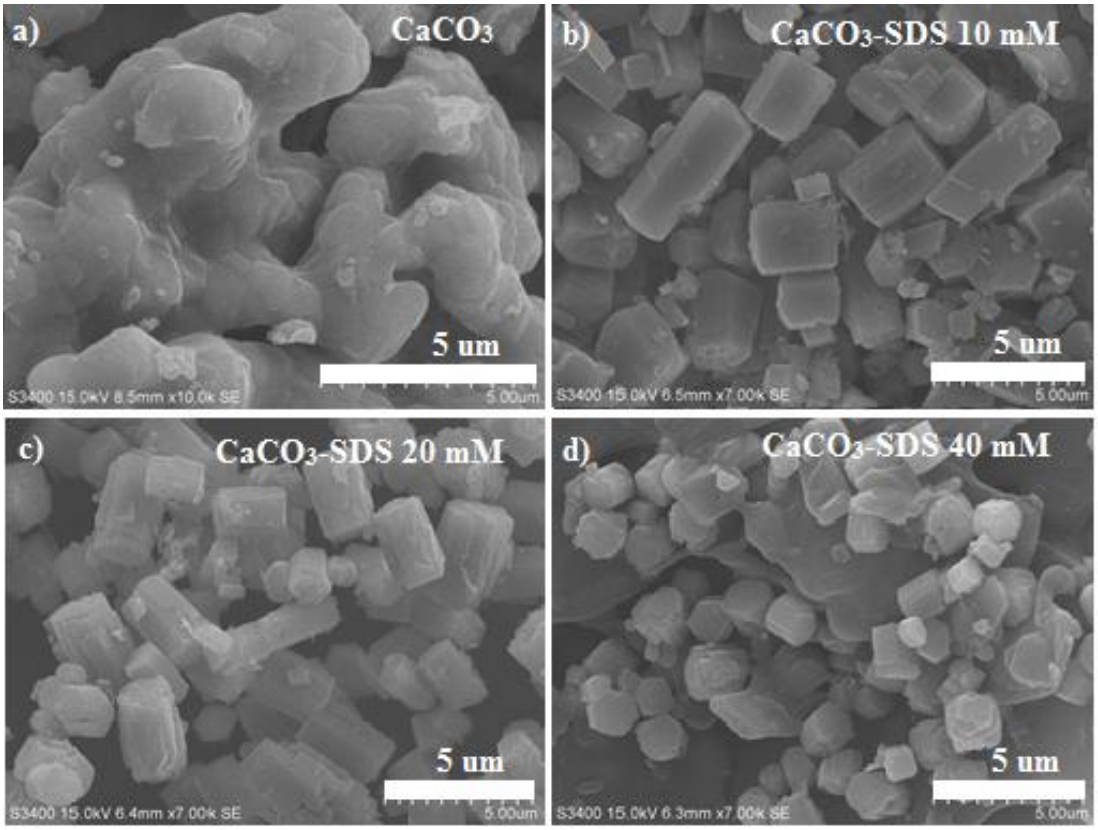

Fig. 5.8: SEM image of $CaCO_3$ at various concentration of SDS, a) without surfactant, b) 10 mM, c) 20 mM, and d) 40 mM

SEM images of $CaCO_3$ synthesized with the addition of Gemini surfactant are shown in Fig. 5.9. The results of adding Gemini surfactant at 0.045 mM, 0.08 mM, and 0.12 mM show uniform needle-like structure. $CaCO_3$-GS 2 mM provides large needle-like, whereas, 4 mM concentration of Gemini surfactant exhibits small aggregated particles.

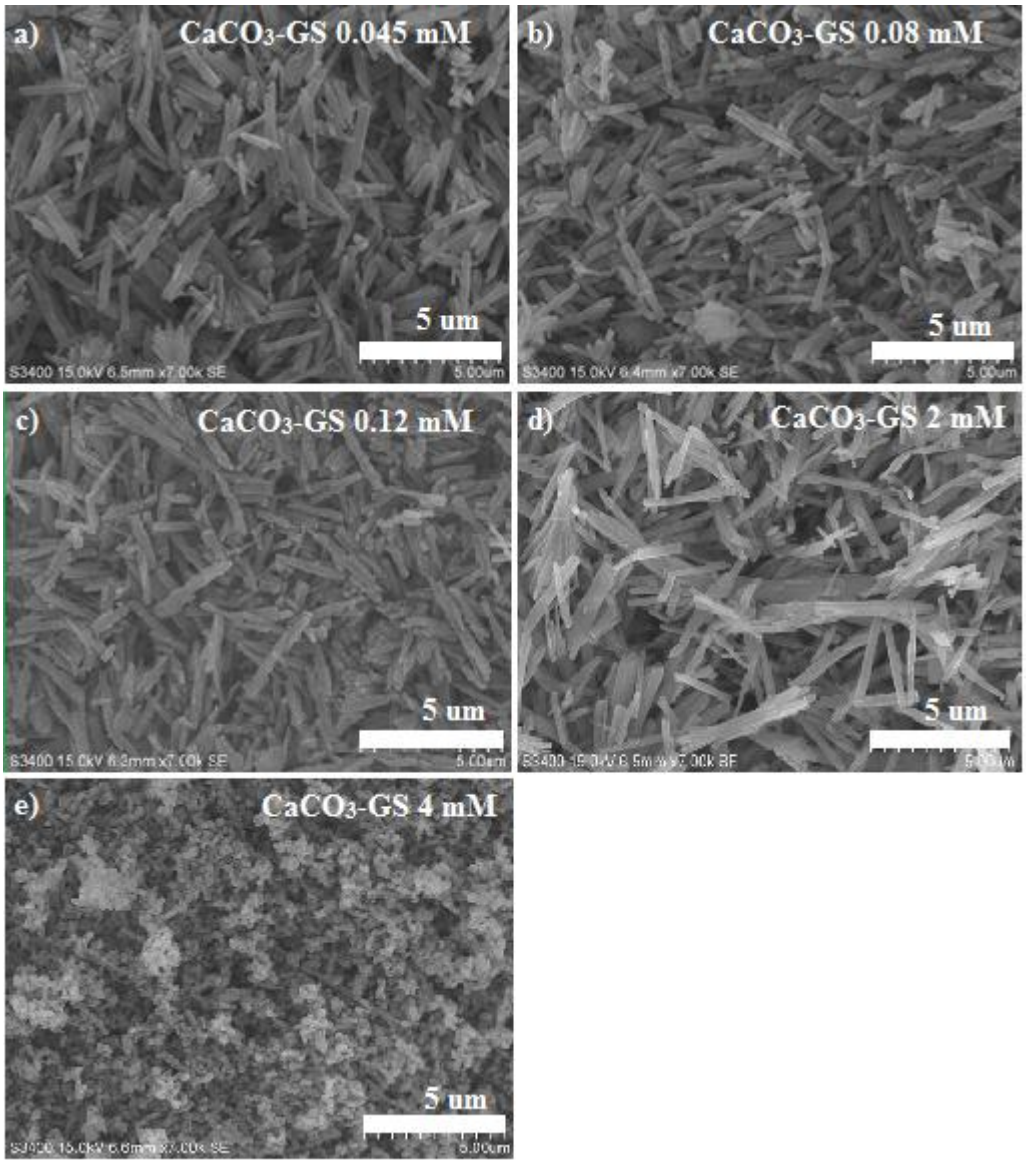

Fig. 5.9: SEM images of $CaCO_3$ synthesized by adding different concentrations of Gemini surfactant a) 0.045 mM, b) 0.08 mM, c) 0.12 mM, d) 2 mM, e) 4 mM.

Fig. 5.10 shows decompositions of $CaCO_3$ synthesized with the use of different SDS concentrations analyzed by TGA. The 10-mM $CaCO_3$-SDS and the 20-mM $CaCO_3$-SDS show one step decomposition of the $CaCO_3$ at approximately 600-800^oC, indicating the release of CO_2 as 40% weight loss of CO_2 is observed. The 40-mM $CaCO_3$-SDS exhibits weight loss at 220-450^oC and 630-740^oC, indicating decomposition of SDS surfactant and CO_2 from $CaCO_3$, respectively. The presence of two decomposition temperature implies that surfactant can adsorb on surface of $CaCO_3$. The decomposition of $CaCO_3$ and SDS at all concentrations observed from DTA exhibits endothermic reaction of decomposition.

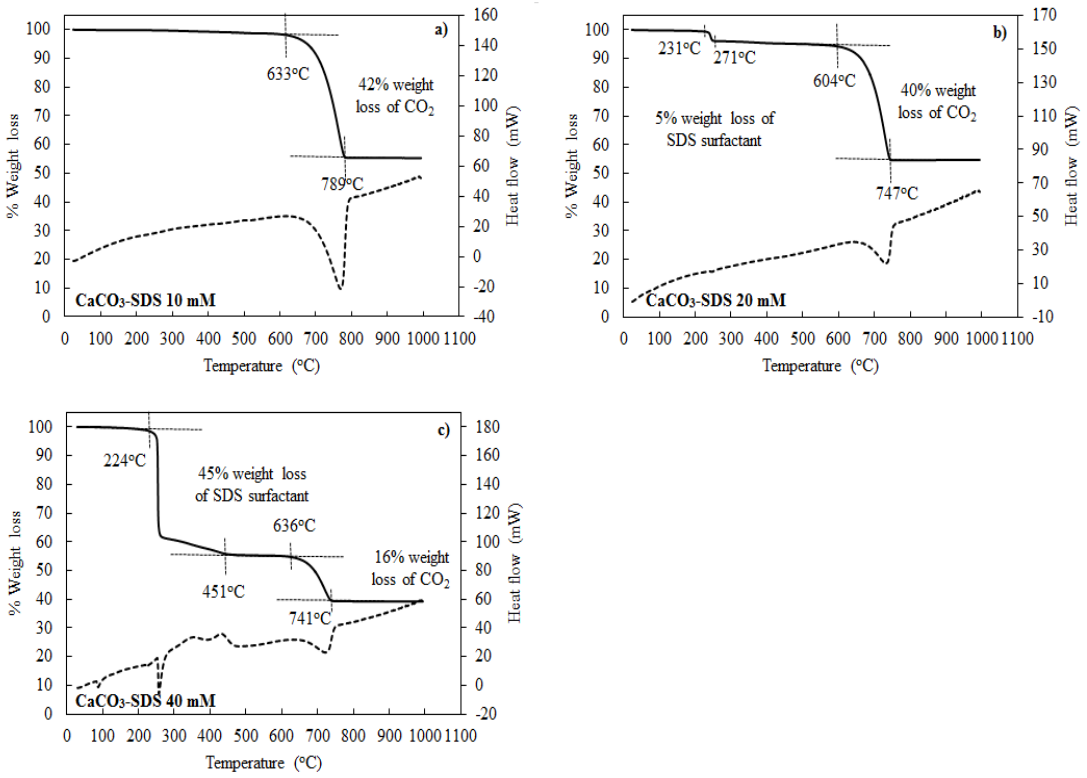

Fig. 5.10: TGA results of $CaCO_3$ with SDS surfactant at a) 10 mM, b) 20 mM , c) 40 mM.

TGA results of $CaCO_3$ with Gemini surfactants using concentrations of 0.045 mM, 0.08 mM, 0.12 mM, 2 mM, and 4 mM are shown in Fig. 5.11. $CaCO_3$-GS 0.045 consists of two steps of decomposition, which are the weight loss of Gemini surfactant at 343-428°C and CO_2 from $CaCO_3$ at 571-702°C. For the other $CaCO_3$ sorbents: $CaCO_3$-GS 0.08 mM, 0.12 mM, 2 mM, and 4 mM, 44% weight loss were found at 600-800°C, which indicates the release of CO_2. DTA results show endothermic reaction of decomposition of Gemini surfactant and $CaCO_3$ in both range of 350-450°C and 500-700°C, respectively. The $CaCO_3$ is completely decomposed to CaO at temperature higher than 800°C.

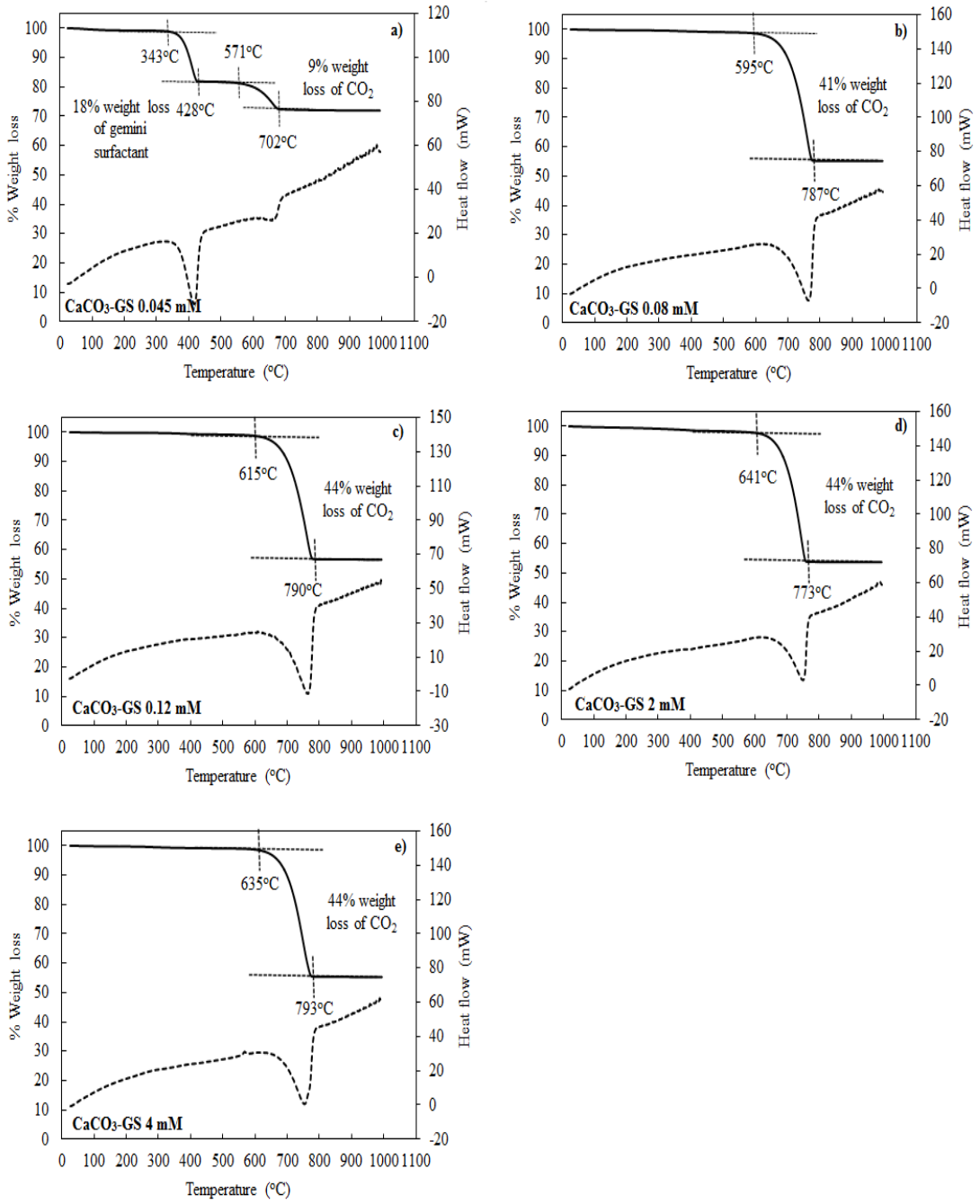

Fig. 5.11: TGA results of $CaCO_3$ with Gemini surfactant at a) 0.045 mM, b) 0.08 mM, c) 0.12 mM, d) 2 mM, e) 4 mM.

Fig. 5.12 and Fig. 5.13 show XRD patterns of CaO obtained from the calcination of $CaCO_3$ synthesized with the use of SDS surfactant and Gemini surfactant. The pattern of all CaO samples exhibit major peaks at 2θ of 32.2, 37.4, 53.9, 64.2, and 67.4°, indicating the complete decomposition of $CaCO_3$ to CaO.

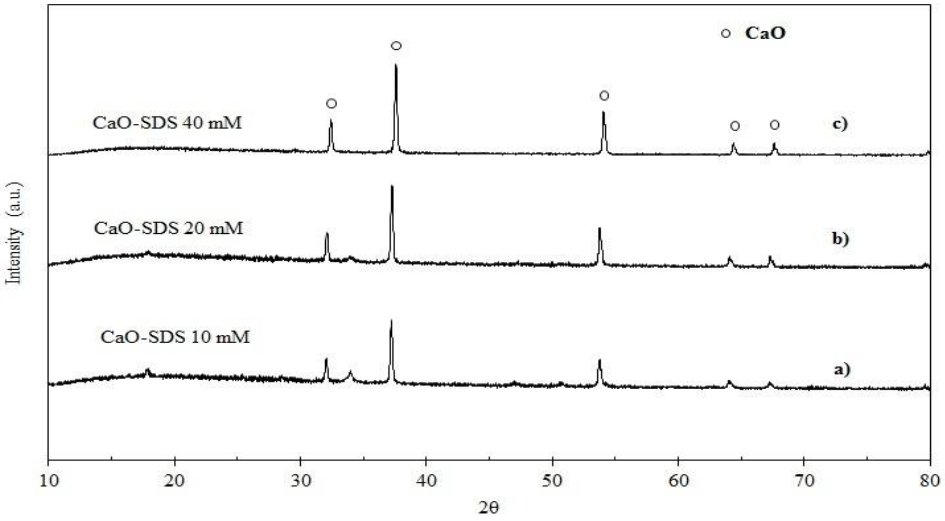

Fig. 5.12: XRD patterns of CaO with SDS surfactant at concentration a) 10 mM, b) 20 mM, d) 40 mM.

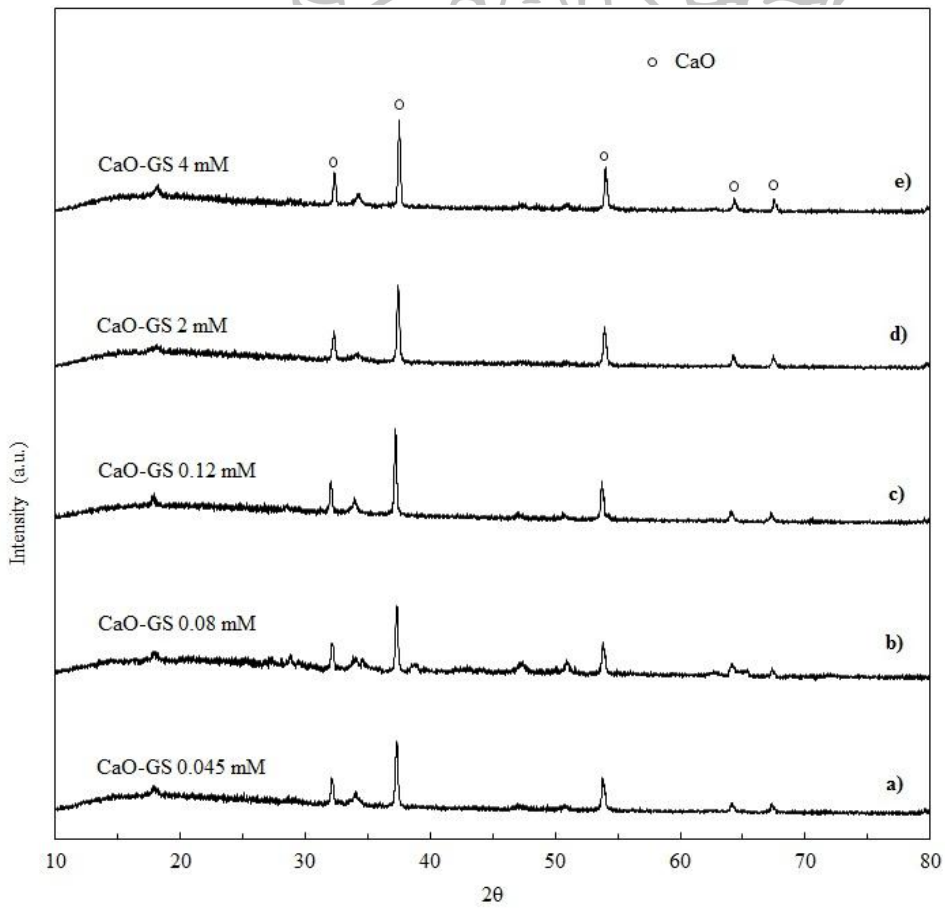

Fig. 5.13: XRD patterns of CaO with Gemini surfactant at concentration a) 0.045 mM, b) 0.08 mM, c) 0.12 mM, d) 2 mM, e) 4 mM.

Morphology of CaO derived from $CaCO_3$ synthesized with the use of SDS obtained by SEM photographs are shown in Fig 5.14. CaO with 10 mM of SDS surfactant has oval-like morphology with rough surface and average particle size of 2-5 μm, whereas, CaO with 20 mM and 40 mM of SDS show agglomeration of small particles.

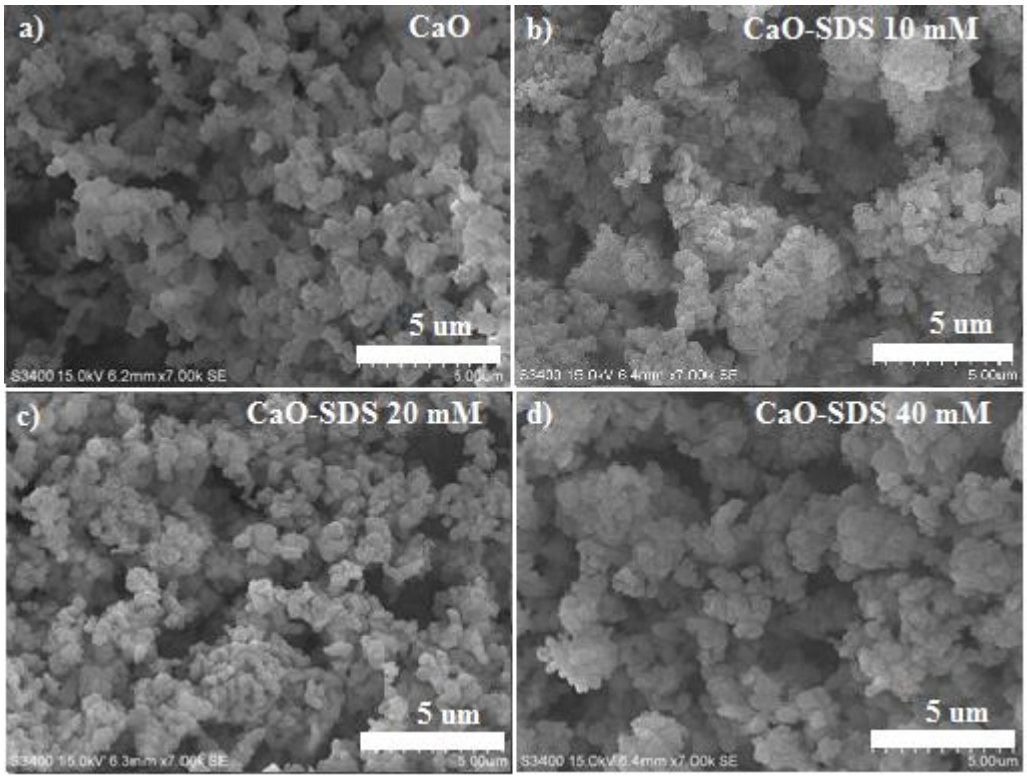

Fig. 5.14: SEM images of CaO at various concentrations of SDS: a) without surfactant, b) 10 mM, c) 20 mM, d) 40 mM.

Fig. 5.15 exhibits morphology of CaO obtained from $CaCO_3$ synthesized with the addition of Gemini surfactant. CaO with Gemini surfactant adding at 0.045 mM has aggregation of smooth particle. Increasing concentration of Gemini surfactant leads to small aggregated particles.

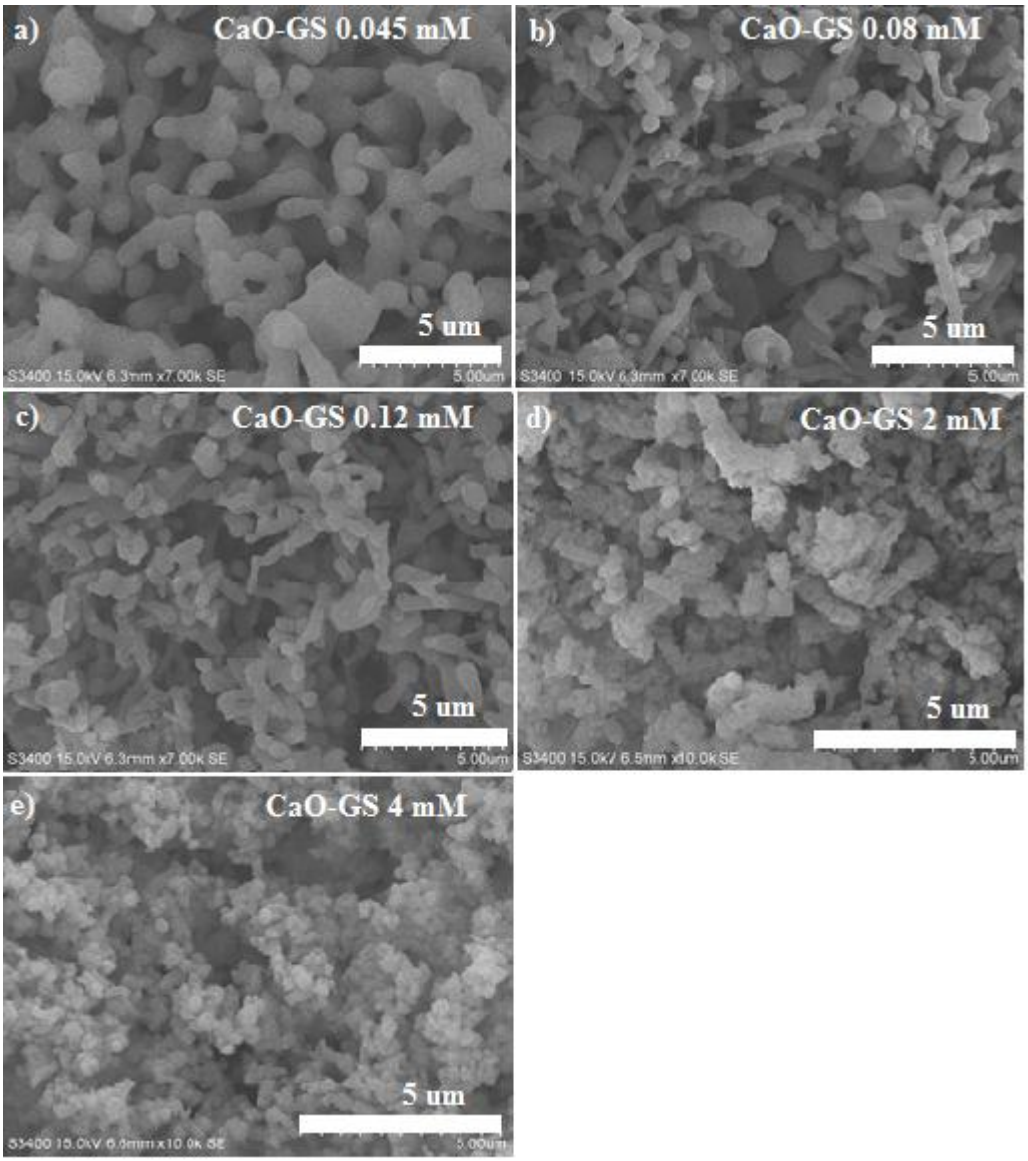

Fig. 5.15: SEM images of CaO at various concentrations of Gemini surfactant a) 0.045 mM, b) 0.08 mM, c) 0.12 mM, d) 2 mM, e) 4 mM.

Textural properties such as surface area, pore volume, and pore diameter of CaO synthesized with the addition of surfactant at different concentrations are shown in Table 5.3. The BET surface area of CaO synthesized with the use of SDS surfactant is lower than that without surfactant whereas CaO synthesized with adding Gemini surfactant possess higher BET surface area than others systems. In addition, crystallite size of CaO is calculated by Scherrer equation at the highest peak of CaO of 37.4^{o}. CaO synthesized with SDS surfactant has similar crystallite size to CaO synthesized without surfactant; however, the Gemini surfactant offers smaller crystallite size of CaO when compared to those without using surfactants and those with adding SDS surfactant.

Table 5.3 Textural properties of CaO sorbents

Sample	Surface area (m^2/g)	Pore volume (cm^3/g)	Pore size diameter (nm)	Crystallite size (nm)
CaO	9.8	0.063	27.5	44.3
CaO-SDS 10 mM	7.6	0.026	14.1	45.0
CaO-SDS 20 mM	9.4	0.036	15.0	44.0
CaO-SDS 40 mM	1.7	0.004	9.9	40.4
CaO-GS 0.045 mM	12.1	0.138	45.6	37.8
CaO-GS 0.08 mM	14.9	0.084	22.6	37.9
CaO-GS 0.12 mM	14.6	0.063	17.4	37.7
CaO-GS 2 mM	16.3	0.059	14.5	37.6
CaO-GS 4 mM	12.9	0.097	30.2	41.1

5.8.3 CO_2 sorption test

CaO sorbents, which improved by adding SDS surfactant at different concentrations, were tested for CO_2 adsorption at 600ºC. The results in Fig. 5.16 show that adding SDS surfactant during synthesis of $CaCO_3$ have an effect on CO_2 sorption capacity and the ability of the adsorption also depends upon concentration of surfactant used. The CaO synthesized without SDS shows 20% conversion, whereas, adding 10 mM and 20mM of SDS leads to an increase of CaO conversion to 32% and 34%, respectively. In contrast, conversion of CaO decreases to 19% when concentration of SDS was further increased to 40 mM. Lower CaO conversion observed with the 40 mM-SDS might be due to aggregated of particles, resulting in low surface area (1.7 m^2/g). Maximum CaO conversion of 34% is observed with CaO-SDS 20 mM.

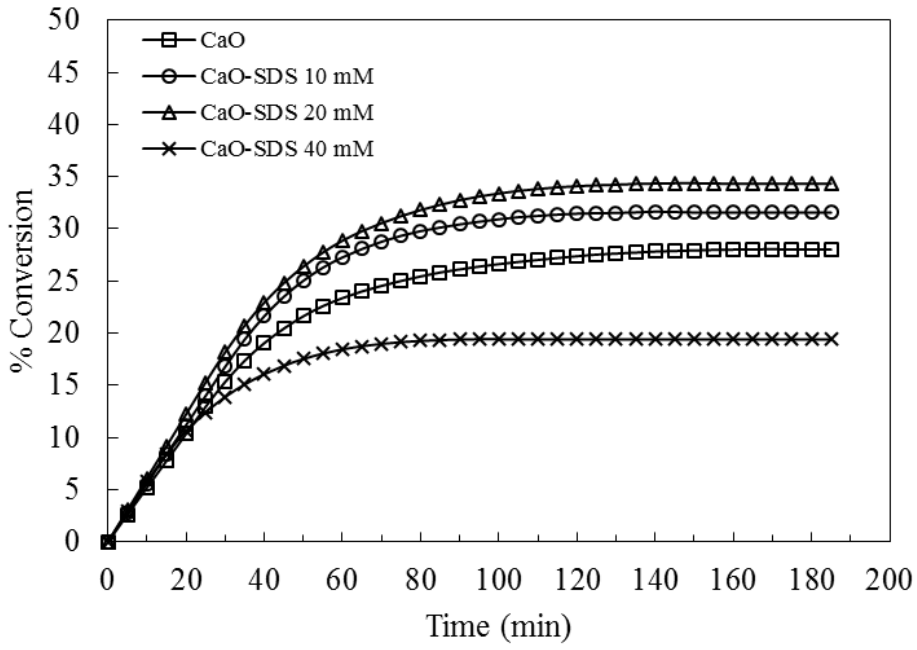

Fig. 5.16: Conversion of CaO synthesized without and with SDS surfactant at concentration 10 mM, 20 mM, and 40 mM.

Fig. 5.17 shows conversion of CaO synthesized with the use of Gemini surfactant at various concentrations. The CaO with small amount of Gemini surfactant, 0.045 mM, 0.08 mM, 0.12 mM, obtained closely conversion of 30% and the conversion increases to 37% when Gemini surfactant was increased to 2 mM. Conversely, CaO-GS 4 mM exhibits low conversion of 20%.

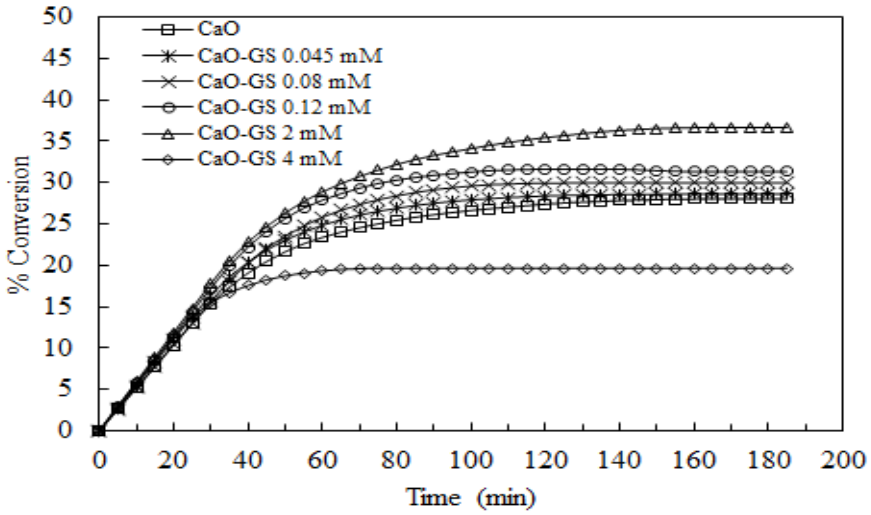

Fig. 5.17: Conversion of CaO synthesized without and with Gemini surfactant at concentration 0.045 mM, 0.08 mM, 0.12 mM, 2 mM, and 4 mM.

Fig. 5.18 shows CO_2 sorption capacity adsorbed by different CaO sorbents synthesized with the use of different concentrations of surfactant additive. CaO-SDS 10 mM and CaO-SDS 20 mM exhibit capacity of 0.25 and 0.27 $gCO_2/gCaO$, respectively, the value of which is closed to CO_2 sorption capacity of CaO without surfactant. In contrast, CO_2 sorption capacity of CaO-SDS 40 mM has the lowest sorption capacity of 0.18 $gCO_2/gCaO$ because the sorbent has low surface area (1.7 m^2/g) and dense structure as shown in Table 5.3 and Fig 5.14, respectively.

CaO sorbents with Gemini surfactant with concentrations of 0.045 mM, 0.08 mM, and 0.12 mM show sorption capacity of 0.22, 0.24, and 0.25 $gCO_2/gCaO$, respectively. Maximum sorption capacity is observed with 2 mM of adding Gemini surfactant due to the highest BET surface area of 16.3 m^2/g. CaO-GS 2 mM shows capacity of 0.29 $gCO_2/gCaO$, whereas, CaO-GS 4 mM has capacity of 0.15 $gCO_2/gCaO$ because high concentration of Gemini surfactant (4 mM) promotes agglomeration of particles.

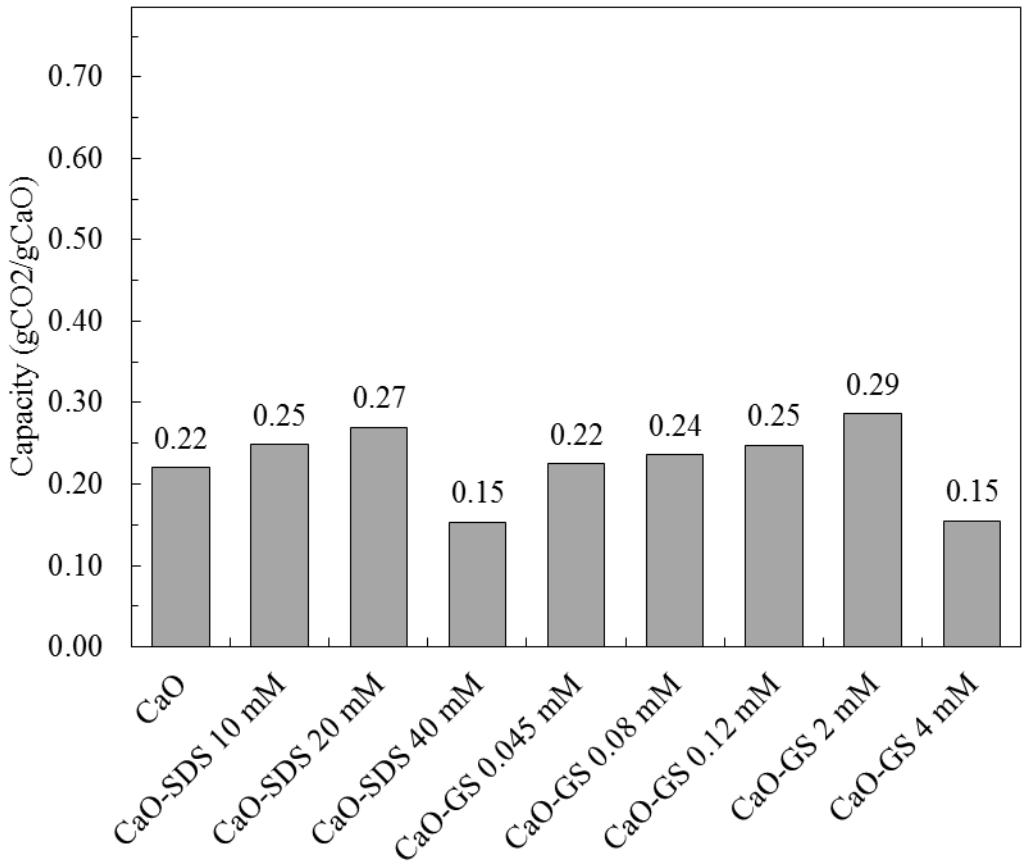

Fig. 5.18: Capacity of CaO with the addition of surfactant

5.8.4 Proposed mechanism of surfactant on structure of $CaCO_3$

Surfactant additives, SDS and Gemini surfactants, are consisted of anionic head group $–SO_3^-$ group. At critical micelle concentration (CMC), SDS forms rod-like micellar structure whereas needle-like is formed in case of Gemini surfactant.

$CaCO_3$ without surfactant shows agglomeration of particles that observe from Fig. 5.8, when SDS surfactant was added into the system, the particles was separated and the $CaCO_3$ morphology was controlled to shaped rod-like structure by SDS surfactant. The results of TGA (Fig. 5.10) can indicate adsorption of SDS surfactant on $CaCO_3$. The SDS micelle at 10 mM and 20 mM might adsorb on surface of $CaCO_3$ as shown in Fig 5.19. $CaCO_3$ with 40 mM shows small cubic and agglomeration that might be due to the large amount of SDS surfactant is sufficient for coverage to small cubic particles and induces particles to aggregate. Proposed mechanism of the role of SDS surfactant to act as structure directing agent is shown in Fig. 5.19.

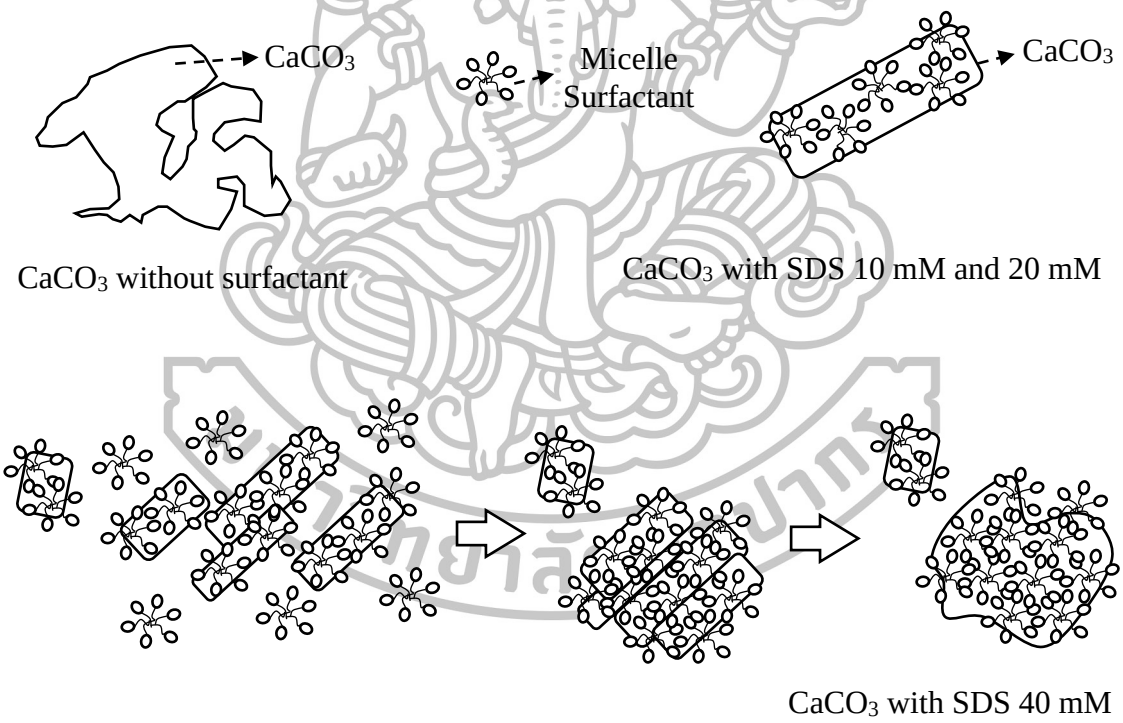

Fig. 5.19: Proposed mechanism of SDS at 10 mM 20 mM and 40 mM on $CaCO_3$ structure

$CaCO_3$ sorbents with Gemini surfactant show different structures depending upon the concentration of Gemini surfactant added as shown in Fig. 5.9. The needle-like morphology observed with adding low concentration of Gemini

surfactant (0.045 mM) might occur from rod-like formation of Gemini surfactant. When concentration was increased in the range of 0.08-2 mM, larger particle of $CaCO_3$ is observed. This might be due to the result of self-interaction among Gemini surfactant molecules, leading to the lowering interaction between Gemini surfactant and $CaCO_3$ (Fig. 5.20). At 4 mM of Gemini surfactant, morphology of ellipse small particles is observed, which could be due to the control by admicelles.

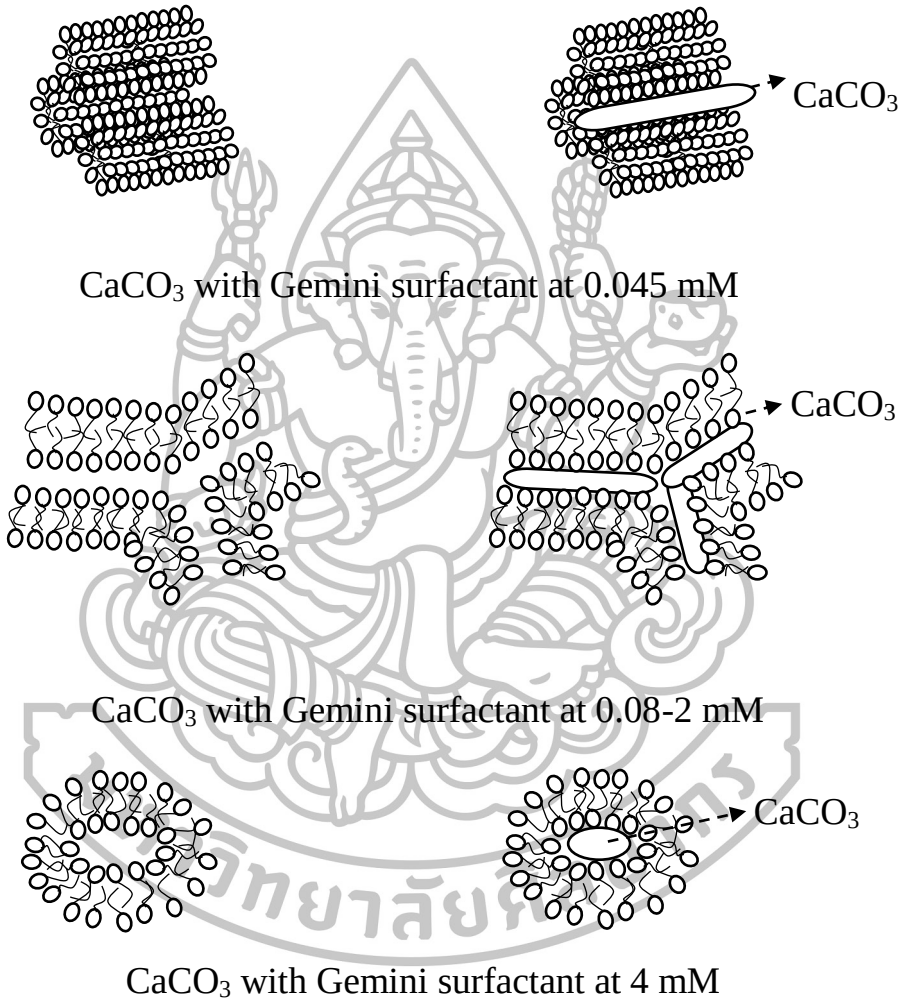

Fig. 5.20: Proposed mechanism of Gemini surfactant at 0.045 mM, 0.08 mM, 0.12 mM, 2 mM, and 4 mM on $CaCO_3$ structure

5.9 Conclusion

The anionic surfactants: SDS and Gemini surfactants have shown that affect on morphology of $CaCO_3$. The results of rod-like structure obtained from the addition of SDS and needle-like structure obtained from adding Gemini surfactant are observed in this work. The concentration of surfactant can change morphology

structure and polymorph of $CaCO_3$ due to the different interactions between anionic head group $-SO_3^{2-}$ and $CaCO_3$. Wei et al. (2005) The concentration of surfactant on CaO-based sorbent exhibits both positive and negative impacts on CO_2 sorption when compared with CaO without surfactant. For the positive effect of surfactant concentration, the CaO-SDS 20 mM and CaO-GS 2 mM can increase CO_2 sorption capacity to 0.27 and 0.29 $gCO_2/gCaO$, respectively, at carbonation 600°C due to connected small particles of CaO-SDS 20 mM and high surface area (16.3 m^2/g) of CaO-GS 2 mM. In contrast, high concentration of surfactant, CaO-SDS 40 mM and CaO-GS 4 mM show negative effect because the interaction of surfactant on $CaCO_3$ promoted aggregation of small particles to large compact particle.

CHAPTER VI

SYNTHESIS OF CaO-BASED ALUMINA SORBENTS FOR HIGH-TEMPERATURE CO_2 CAPTURE

6.1 Abstract

CaO-based alumina sorbents were synthesized by different incorporating techniques to improve thermal stability of the sorbents for multiple-cycle used in CO_2 capture process. Properties of the as-synthesized sorbents were examined by X-ray diffraction, scanning electron microscopy, thermal gravimetric analysis, and N_2 adsorption/desorption. The results showed that different morphologies of the adsorbents are obtained according to the synthesis method. Further, such difference is also effect to CO_2 sorption performance. The sorbent synthesized by sol-gel method provides the best performance of CO_2 capture at 0.63 $gCO_2/gCaO$ and stability of the sorbent show capacity of 0.41 $gCO_2/gCaO$ at 10^{th} cycles.

6.2 Introduction

CaO is widely used to capture CO_2 in calcium looping technologies; however, the major problem of CaO sorbent is the loss in capacity upon multicycle uses. The expose of CaO to high temperature of carbonation and calcination leads to shape decay, CaO agglomeration, or pore collapse. As a consequence, the problem of capacity loss has been attempted to resolve by incorporating inert material to act as a support.

In this work, CaO-based sorbent with/without adding additive was incorporated with aluminum to enhance stability of adsorbent upon multicycle tests of high temperature CO_2 capture. Different preparation methods including wet mixing, sol mixing, co-precipitation, and sol-gel were applied to investigate the effect on properties of sorbent.

6.3 Literature reviews

Using CaO sorbent in calcium looping technologies has faced loss-in-capacity problem upon multicycle uses due to sintering effect. Most researches have been attempted to improve stability of CaO by incorporating with materials that can act as/form into inert materials such as MgO Filitz et al. (2012), SiO_2 Lu et al. (2009), Al_2O_3 Kierzkowska et al. (2013), etc.

Techniques to prepare CaO-based sorbent have been investigated such as wet mixing Zhou et al. (2012), sol mixing Martavaltzi and Lemonidou (2008), Qin et al. (2012) , co-precipitation Kierzkowska et al. (2013), Florin et al. (2010) , or sol-gel combustion Luo et al. (2011), etc.

Wet mixing method is the mix of calcium and aluminum precursors that can soluble in solution. The soluble of both calcium and aluminate precursors was used to prepare CaO-based sorbent such as calcium formate Z. Zhou et al. (2012), calcium acetate Z. Zhou et al. (2012), calcium propionate Z. Zhou et al. (2012), calcium citrate Z. Zhou et al. (2012), calcium lactate Z. Zhou et al. (2012), calcium gluconate Z. Zhou et al. (2012), aluminum nitrate Z. Zhou et al. (2012), aluminum acetate Z. Zhou et al. (2012), and aluminum chloride Z. Zhou et al. (2012).

Sol mixing is a method that is used the mix of soluble precursor with insoluble precursor. Martavaltzi and Lemonidou (2008) used CaO derived from calcination of calcium hydroxide and calcium acetate to mix with soluble precursor of aluminum nitrate and used it as sorbent for CO_2 capture. The results showed that CaO derived from calcium acetate provided higher % conversion than that derived from calcium hydroxide as shown in Table 1. Qin et al. (2012) prepared CaO-based sorbent by sol mixing technique with the use of calcium acetate, calcium gluconate, calcium formate, and calcium lactate as soluble source and calcium aluminate cement as insoluble source. The results CO_2 sorption capacity of each precursor showed 80% conversion of calcium acetate, 73% conversion of calcium gluconate, 71% conversion of calcium formate, and 82% conversion of calcium lactate at 650^{o}C in 15%v/v CO_2 (Balanced N_2). Florin et al. (2010) incorporated CaO into calcium alumina complex ($Ca_{12}Al_{14}O_{33}$) by co-precipitation of $Ca(OH)_2$, $Al(NO_3)_3$ and CO_2, the CaO-based sorbent consists of 85%wt CaO and 15%wt $Ca_{12}Al_{14}O_{33}$. Experimental results showed %conversion of 50 could be obtained in the 1st cycle and the conversion reduced to 23% in the 30th cycle. Broda et al. (2012) prepared Cao-based sorbent by sol-gel method that showed 49% conversion of 90% CaO in $Ca_{12}Al_{14}O_{33}$ and 41% conversion 80% CaO in $Ca_{12}Al_{14}O_{33}$ at 650^{o}C in 20%v/v CO_2 (Balanced N_2).

In addition, the CaO-based sorbents have been improved by addition additive during synthesis method. Liu et al. (2013) synthesized CaO-$Ca_{12}Al_{14}O_{33}$ that used sulfonated polystyrene as template of spherical. The sorbent of 85%wt CaO with 15%wt $Ca_{12}Al_{14}O_{33}$, which morphology is hollow spherical structure showed constant conversion of 96% conversion over 30 cycles. Zhao et al. (2014) synthesized CaO-based sorbent by sol-gel method, which consists of $Ca(NO_3)_2$ as calcium precursor, $Al(NO_3)_3$ as aluminum precursor, and PEG (m_w=300 g/mol) as additive. The results of CO_2 sorption exhibited approximately 82% conversion for 15 cycles.

Table 6.1 Examples of the effect of synthesis methods on CO_2 sorption performance

Method (Ref.)	Precursors	Supported precursors	Inert supports	%CaO	Carbonation	Calcination	Reactor	Conversion 1st cycle	Conversion (n^{th}) cycle
Wet mixing (Zhou et al. (2012))	Calcium formate	Al(NO3)3	$Ca_9Al_6O_{18}$	80	650°C, 15%CO_2 (N_2), 30 min	800°C, N_2, 10 min	TGA	66%	(7) 58%
	Calcium acetate		$Ca_9Al_6O_{18}$					100%	(28) 79%
	Calcium propionate		Absence					39%	(7) 25%
	Calcium citrate		$Ca_9Al_6O_{18}$					93%	(28) 81%
	Calcium lactate		Absence					79%	(7) 73%
	Calcium gluconate		$Ca_9Al_6O_{18}$					84%	(28) 68%
	Calcium lactate	AlCl3	$Ca_{12}Al_{14}O_{33}$					58%	(7) 18%
	Calcium lactate	$Al(CH_3COO)_3$	Absence					49%	(7) 37%
Sol mixing (Martavaltzi and Lemonidou (2008))	$Ca(OH)_2$	$Al(NO_3)_3$	$Ca_{12}Al_{14}O_{33}$	75	650°C, 15%CO_2 (N_2), 30 min	850°C, N_2, 10 min	TGA	21%	(45) 21%
	$Ca(CH_3COO)_2$							35%	(45) 29%
Sol mixing (Qin et al. (2012))	Calcium acetate	Calcium aluminate cement	Calcium aluminate cement	75	650°C, 15%CO_2, 30 min	900°C, N_2, 10 min	TGA	80%	(18) 61%
	Calcium gluconate							73%	(18) 66%
	Calcium formate							71%	(18) 47%
	Calcium lactate							82%	(18) 67%
Co-precipitation (Florin et al. (2010))	$Ca(OH)_2$ and CO_2	$Al(NO_3)_3$	$Ca_{12}Al_{14}O_{33}$	85	650°C, 15%CO_2 (He), 10 min	900°C, N_2, 5 min	TGA	50%	(30) 23%
Sol-gel (Broda et al. (2012))	$Ca(OH)_2$	Aluminium isopropoxide	$Ca_{12}Al_{14}O_{33}$	90	650°C, 20%CO_2, 10 min	900°C, CO_2, 10 min	TGA	49%	(10) 38%
				80				41%	(10) 29%

6.4 Experimental

6.4.1 Chemicals

Calcium acetate hydrate ($Ca(CH_3COO)_2.H_2O$, 99%), received from Lobachemie, and calcium nitrate tetrahydrate ($Ca(NO_3)_2.4H_2O$, 99%) purchased from Carlo Erba, were used as calcium precursors. urea ($(NH_2)_2CO$, 99%) obtained from Carlo Erba, was used as carbonate source. aluminium nitrate ($Al(NO_3)_3$, 99%) obtained from Carlo Erba, was used as aluminum source. Citric acid ($C_6H_8O_7$, 99%) was purchased from Carlo Erba. Gemini surfactants synthesized followed Wang et al. (2008) were used as additives. All chemicals were used as received.

6.4.2 Preparation of CaO-based alumina sorbent

In this section, CaO-based alumina sorbents were prepared by different methods including co-precipitation, wet mixing, sol-gel, and sol mixing. Each method is summarized as follows:

Co-precipitation

For co-precipitation method, CaO-based alumina sorbent was prepared by mixing metal solution of $Ca(CH_3COO)_2$ with the solution of $Al(NO_3)_3$, and then urea solution was added in mixture solution. The ratio of calcium and alumina was set at 70:30 by weight, where equimolar of metal and urea of 2.5 M (100 ml) was mixed. For the sample with the addition of Gemini surfactant, 0.35 g of Gemini surfactant was added to obtain 2 mM concentration in metal solution (calcium and aluminum). Then the solution of urea was added into the mixture solution under vigorous stirring at 90^{o}C for 24 h. The obtained precipitate was filtered, washed with distilled water, and dried at 30^{o}C. The powder was calcined at 850^{o}C for 2 h. The products were denoted as Co-precipitation and Co-precipitation-GS 2 mM.

Wet mixing

$Ca(CH_3COO)_2$ (6.60 g) and $Al(NO_3)_3$ (3.76 g) were mixed in DI-water to obtain calcium to alumina ratio of 70:30%wt. The mixture solution of metal and 2 mM of Gemini surfactant was allowed to stir at 75^{o}C for 1 h and then the solution was dried in an oven at 110^{o}C for 12 h. The white powder was calcined at 900^{o}C for 1.5 h. The products were denoted as Wet mixing and Wet mixing-GS 2 mM.

Sol-gel combustion synthesis

The sol-gel combustion was synthesized with the use of $Ca(NO_3)_2$ and $Al(NO_3)_3$ as precursors. To obtain calcium to alumina ratio of 70:30%wt, 4.22 g of calcium was mixed with 2.31 g of alumina in DI water. Then citric acid 5.02 g was added into the solution to be an ignitor during calcination. The solution was continuously stirred at 80^{o}C for 7 h. After that, the mixture solution was placed at ambient temperature for 18 h. The solution, which obtained as wet gel, was dried at

80°C for 5 h and at 110°C for 12 h, respectively. The dried gel was quickly calcined at 850°C for 2 h and white powder was obtained. For the case of adding Gemini surfactant, 0.024 g of Gemini surfactant was added in the solution containing citric acid, $Ca(NO_3)_2$, and $Al(NO_3)_3$. The rest of the method was followed as same as those without adding surfactants. The sorbents were denoted as Sol-gel and Sol-gel-GS 2 mM.

Sol mixing

$Ca(CH_3COO)_2$ (6.60 g) and $Al(NO_3)_3$ (3.76 g) were mixed in DI-water to obtain calcium to alumina ratio of 70:30%wt. In sol mixing technique, 2.68 g of $Al(NO_3)_3$ and 1.5 g of CaO, which synthesized with Gemini surfactant 2 mM, was dissolved in DI-water to obtain calcium to alumina ratio of 70:30%wt. The solution of CaO was added into the solution of $Al(NO_3)_3$ and then allowed to stir at 75°C for 1 h. The mixture solution was placed at room temperature for 24 h and dried at 110°C for 24 h. The solid was then calcined at 850°C for 1.5 h. The sorbents were denoted as Sol mixing and Sol mixing-GS 2 mM.

6.4.3 Examination of CaO and alumina composition of synthetic materials

The excess CaO in alumina complex support was investigated through hydration and dehydration of CaO sorbent. The amount of CaO was based on dehydration of $Ca(OH)_2$ that indicated by weight loss from TGA analysis.

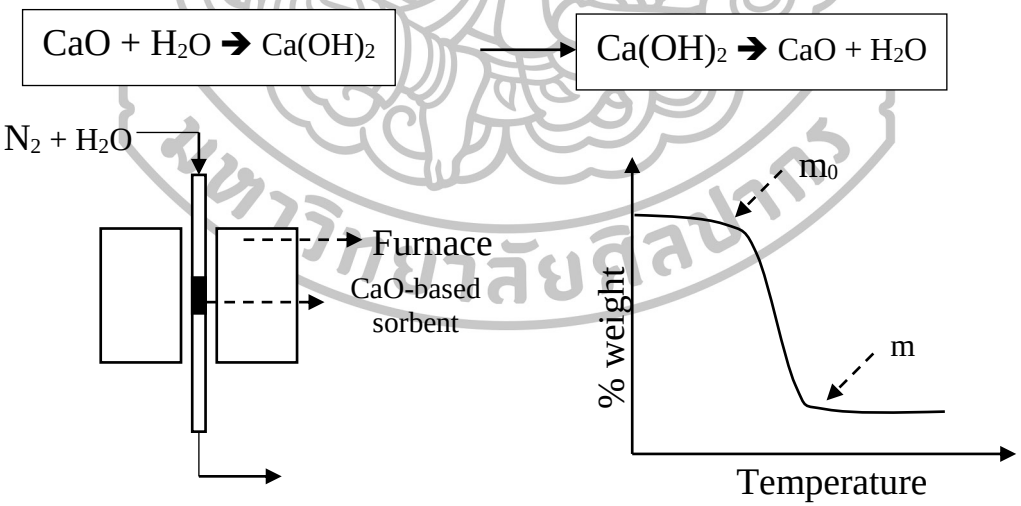

Fig. 6.1: Scheme of hydration test of CaO-based alumina sorbent for composition of determination

The component of CaO is calculated by the following equation

$$x_{CaO} = \frac{m_0 - m}{m} \times \frac{m_{w,CaO}}{m_{w,H_2O}} \qquad (6.1)$$

x_{CaO} = fraction of CaO

m_0 = % weight loss of CaO at start of $Ca(OH)_2$ decomposition

m = % weight loss of CaO at final of $Ca(OH)_2$ decomposition

$m_{w,\,CaO}$ = molecular weight of CaO

$m_{w,\,H2O}$ = molecular weight of H_2O

6.4.4 CO_2 sorption performance tests

The CO_2 uptake capacity of the synthetic CaO was tested via packed bed reactor. For each experiment, the length bed of sorbent was fixed at 7.5 cm and heated from ambient temperature to 850°C under N_2 flow and hold for 30 min before taking measurement to refresh the material. CO_2 sorption (carbonation reaction) was carried out at 600°C under 15 mL/min gas flow containing 15%v/v CO_2 (balanced N_2). For desorption test (calcination reaction), the sample was heated to 850°C under 100% N_2 for 30 min (or until no CO_2 was observed).

6.5 Results and discussion

6.5.1 Characteristic of the synthetic CaO-based alumina sorbents

CaO-based alumina sorbents synthesized by different methods including wet mixing, co-precipitation, sol-gel, and sol mixing, were characterized by XRD as shown in Fig. 6.2. All sorbents show major peaks of CaO at 2θ of 32.2, 37.4, 53.9, 64.2, and 67.4. The CaO-based alumina sorbent, which was synthesized by sol mixing, wet mixing-GS 2 mM, co-precipitation, and co-precipitation-GS 2 mM, showed the mixture of CaO and $Ca_{12}Al_{14}O_{33}$, where the pattern of $Ca_{12}Al_{14}O_{33}$ exhibited at 2θ of 18.0, 29.8, 33.2, 36.4, 40.9, 46.4, 54.9, and 57.2. The sol-gel and sol-gel-GS 2 mM sorbents show XRD pattern of CaO and $Ca_9Al_6O_{18}$, as the pattern of $Ca_9Al_6O_{18}$ peak of 2θ at 33.2, 47.7, and 60.0 was observed. Formation of calcium alumina complex occurred from diffusion of CaO into Al_2O_3 and the complex substance of $Ca_{12}Al_{14}O_{33}$ can be occurred from reaction of CaO with Al_2O_3 at high temperature (more than 800°C). Zhou et al. (2012) The presence $Ca_9Al_6O_{18}$ in sol-gel method occurred due to Ca^{2+} can continue to diffuse into $Ca_{12}Al_{14}O_{33}$, which might be due to the release of high energy from combustion reaction. Zhou et al. (2012) Formation of In addition, the absence calcium aluminate complex might be occurred from diffusion resistant of CaO into Al_2O_3 preventing conversion of calcium aluminate complex, that resulted in CaO and Al_2O_3. Zhou et al. (2012)

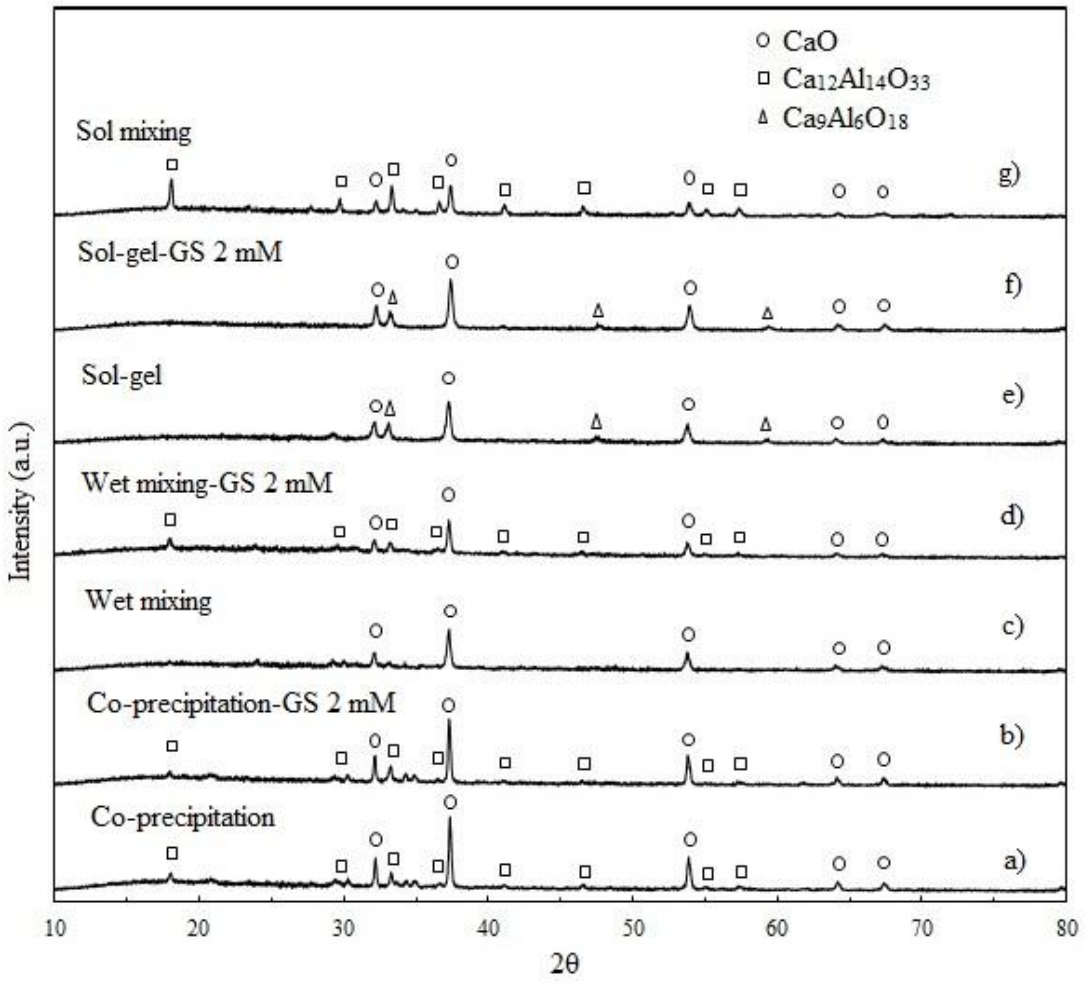

Fig. 6.2: XRD patterns of CaO-based alumina sorbent synthesized by different methods.

Morphologies of CaO-based alumina sorbent observed from SEM images are shown in Fig. 6.3. The sol mixing sorbent has large particle with rough surface; however, when sol mixing GS 2 mM shows an agglomeration of particles with rough surface. Aggregation of particles and rough surface are also found with the sorbents synthesized by co-precipitation: rough surface is observed with co-precipitation sorbent whereas slit on surface is observed with co-precipitation-GS 2 mM. The sol-gel sorbent formed uniform small particles with particle size of 1-2 um whereas sol-gel-Gemini-2 mM formed agglomerated particle. Structure of sol-mixing sorbent shows aggregation of un-uniform large particles (4-5 um) and small particles (1-2 um).

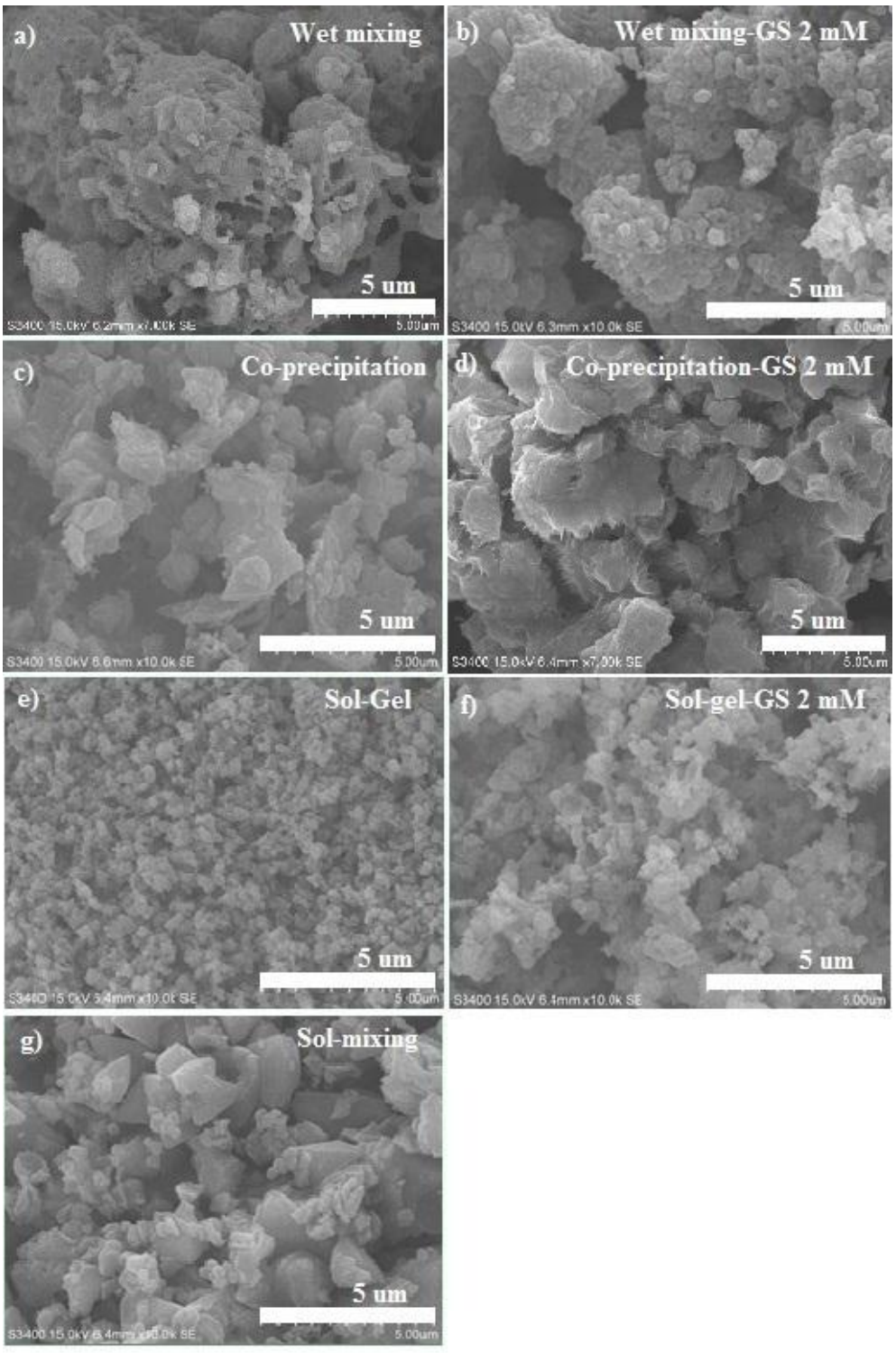

Fig. 6.3: SEM images of CaO-based alumina sorbents synthesized from different methods: a) wet mixing, c) co-precipitation, e) sol-gel, and g) sol-mixing, and CaO-based sorbent from addition additive: b) wet mixing-GS 2 mM, d) co-precipitation-GS 2 mM, and f) sol-gel-GS 2 mM.

Distribution of calcium and aluminum on CaO-based alumina sorbents were observed by SEM-EDX as shown in Fig. 6.4. All of sorbents exhibit uniform dispersion of calcium an aluminum. The ratio of calcium and aluminum of each sorbent determined by EDX is exhibited in Table. 6.2. In addition, Table 6.2 is also shown percent amount of CaO examined by TGA technique.

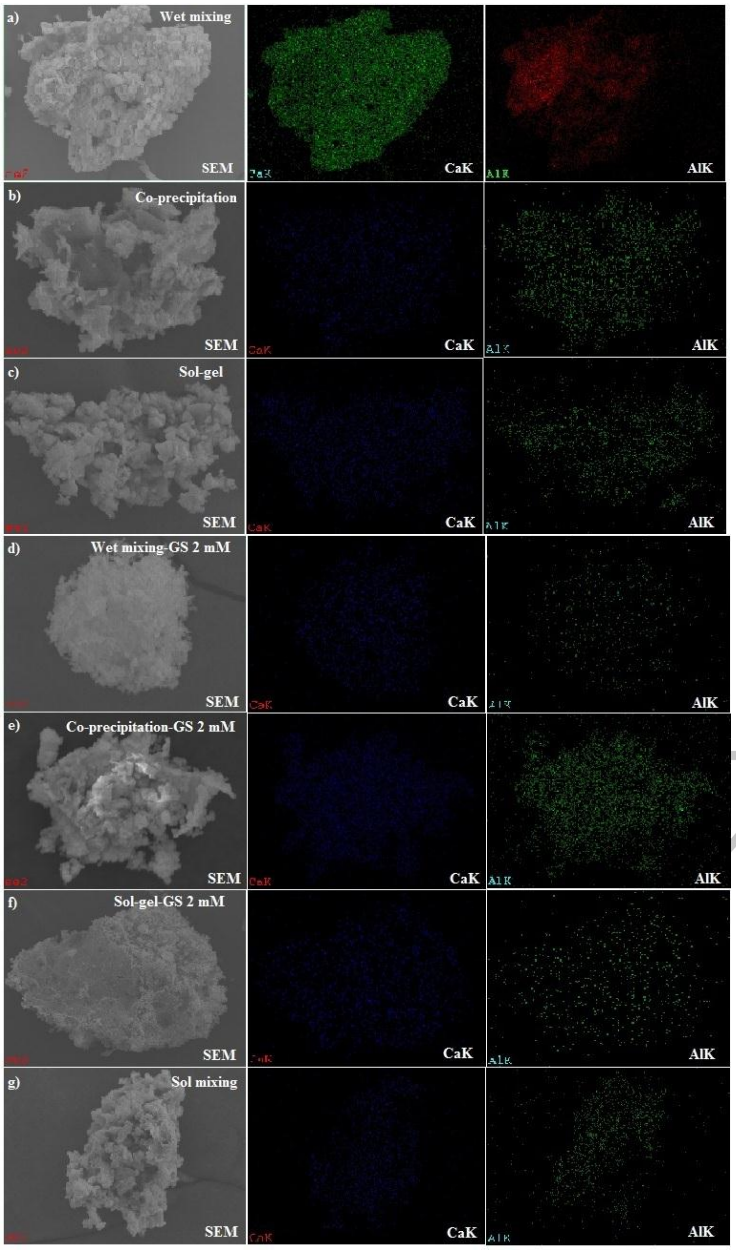

Fig. 6.4: SEM-EDX of calcium and aluminum composition in sorbents a) wet mixing, b) co-precipitation, c) sol-gel, d) wet mixing-GS 2 mM, e) co-precipitation-GS 2 mM, f) sol-gel-GS 2 mM and g) sol mixing

Table. 6.2 Composition at surface of sorbent by SEM-EDX

Samples	%Ca (EDX)	%Al (EDX)	%CaO ($TGA_{Decomposition}$)
Wet mixing	78	22	73
Co-precipitation	55	45	47
Sol-gel	70	30	65
Wet mixing-GS 2 mM	85	15	80
Co-precipitation-GS 2 mM	68	32	64
Sol-gel-GS 2 mM	86	14	77
Sol-mixing (GS 2 mM)	70	30	64

Table 6.3 presents textural properties including surface area, pore volume, and pore size distribution of CaO-based alumina synthesized from different synthesis methods. CaO-based sorbents, which were synthesized with Gemini surfactant, obtained low surface area than those without surfactant. These results indicating that addition of Gemini surfactant promoted agglomeration of particles, leading to a decrease in surface area. The sorbent prepared by wet mixing and sol-gel show surface area of 8 m^2/g and precipitated sorbent obtained small surface area at 2 m^2/g.

Table 6.3 Textural properties of CaO-based alumina sorbents

Sample	Surface area (m^2/g)	Pore volume (cm^3/g)	Pore size diameter (nm)
Wet mixing	8.8	0.040	18.1
Co-precipitation	2.2	0.033	58.6
Sol-gel	8.4	0.067	31.5
Wet mixing-GS 2 mM	4.3	0.108	100.7
Co-precipitation-GS 2 mM	1.7	0.0035	8.42
Sol-gel-GS 2 mM	8.0	0.060	29.7
Sol-mixing (GS 2 mM)	0.9	0.003	10.7

6.5.2 CO_2 sorption tests

Ability of CaO-based alumina sorbents to CO_2 sorption was shown as conversion depicted in Fig. 6.5.

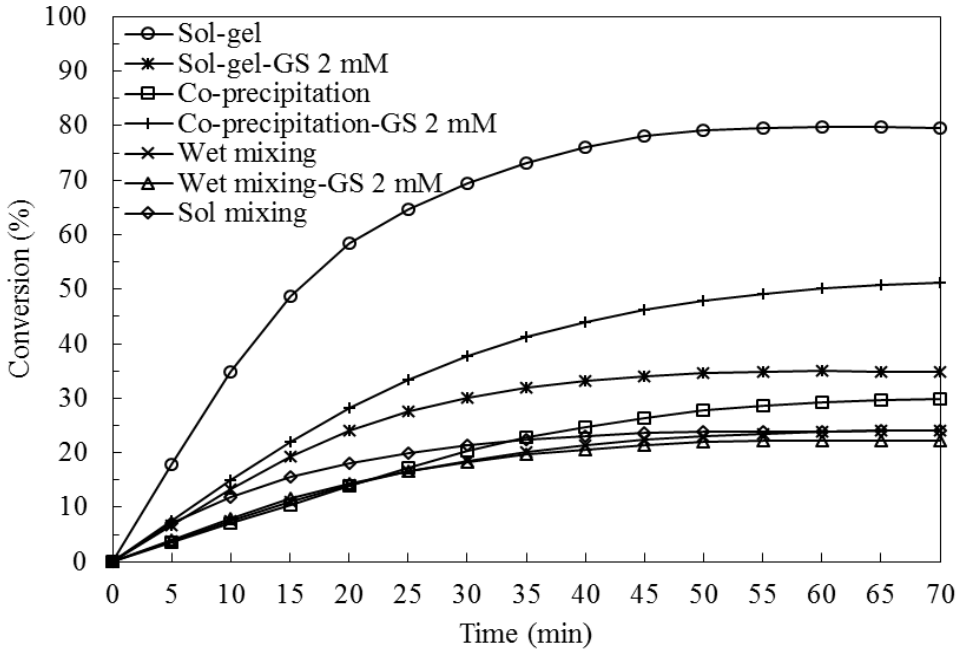

Fig. 6.5: Conversion of CaO-based alumina sorbents synthesized from different methods

Magnitude of CaO conversion is in the order: sol-gel > wet mixing > co-precipitation. The different in CO_2 sorption ability found with different methods could be due to the different structures; small particles from sol-gel method provides good performance than large particles with rough surface obtained from co-precipitation or wet mixing. Large compact particles obtained from co-precipitation offers the lowest sorption capacity.

Adding Gemini surfactant does not affect conversion of the sorbent synthesized by wet mixing method as 18% conversion is maintained. However, when surfactant was added, conversion of Co-precipitation-GS 2 mM increases to 33%. This result might be due to the slit on surface of the sorbent. In contrast, conversion of the sol-gel-GS 2 mM decreases from 52% to 27% when compared with sol-gel. This might be because Gemini surfactant induced particle to agglomerate as shown by SEM results. Sol mixing method shows the lowest conversion of 15%, which is due to the lowest surface area (0.9 m^2/g) and dense aggregated particles. The capacity of CO_2 sorption compared in unit of gram of CO_2 per gram of CaO content are shown in

Fig. 6.5. The capacity is in the order: sol-gel > co-precipitation-GS 2 mM > sol-gel-GS 2 mM > co-precipitation > wet mixing ~ sol mixing.

Comparison between the sorbents with/without 2 mM of Gemini surfactant, wet mixing and sol mixing techniques show similar morphology between both sorbents and comparative sorption capacity of 0.20 $gCO_2/gCaO$, implying that the Gemini surfactant does not affect properties of CaO-based alumina sorbent. This might be due to Gemini surfactant does not interact to calcium and aluminate as that obtained similar morphology. For co-precipitation technique, the sorbent with the addition of Gemini surfactant possess slit on surface. This could be a reason to enhance CO_2 sorption capacity due to an increase of an accessible active surface. CaO-based alumina with Gemini surfactant prepared by sol-gel shows agglomeration of particles that influenced on a decrease of sorption capacity.

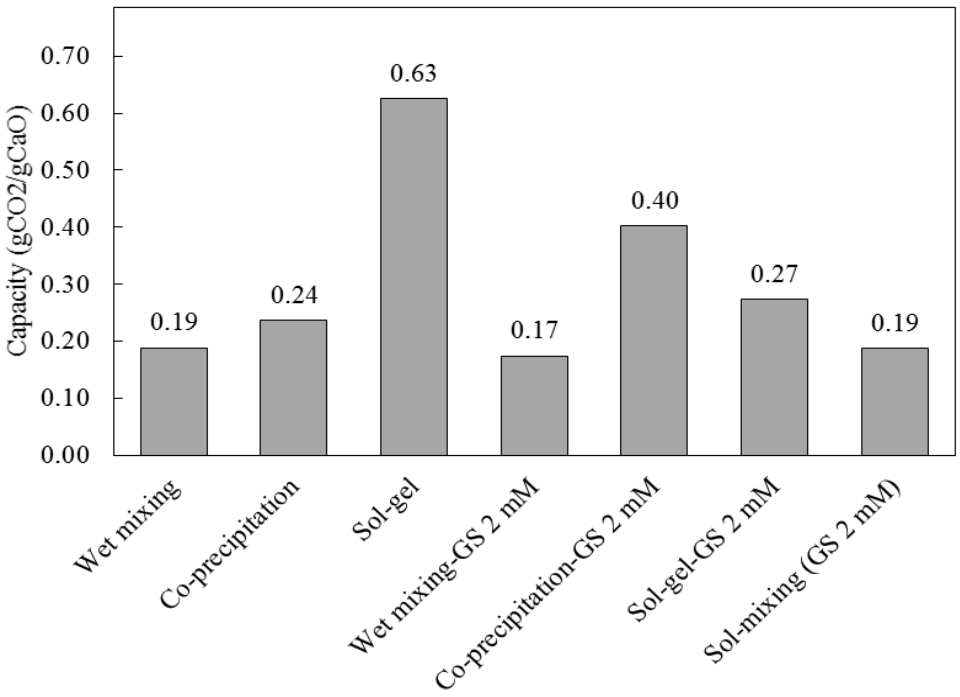

Fig. 6.6: CO_2 sorption capacity of CaO-based alumina sorbents

The CaO-based alumina sorbent prepared by sol-gel technique, which shows the highest capacity of CO_2 sorption, was further investigated its performance for multiple-cycle used as shown in Fig. 6.7. The results reveal that conversion of 53% (0.65 $gCO_2/gCaO$) in the 1^{st} cycle decreases to 34% (0.41 $gCO_2/gCaO$) in the 10^{th} cycle, which is considered as 36% reduction. Our results are comparable to that reported by Broda et al. (2012) whose the synthesized CaO-based by sol-gel method

that contained 90%CaO and $Ca_{12}Al_{14}O_{33}$ showed a reduction of 22% sorption capacity in the 10th cycle. This result shows that by incorporating CaO with Al_2O_3 can improve properties of the sorbent in term of stability.

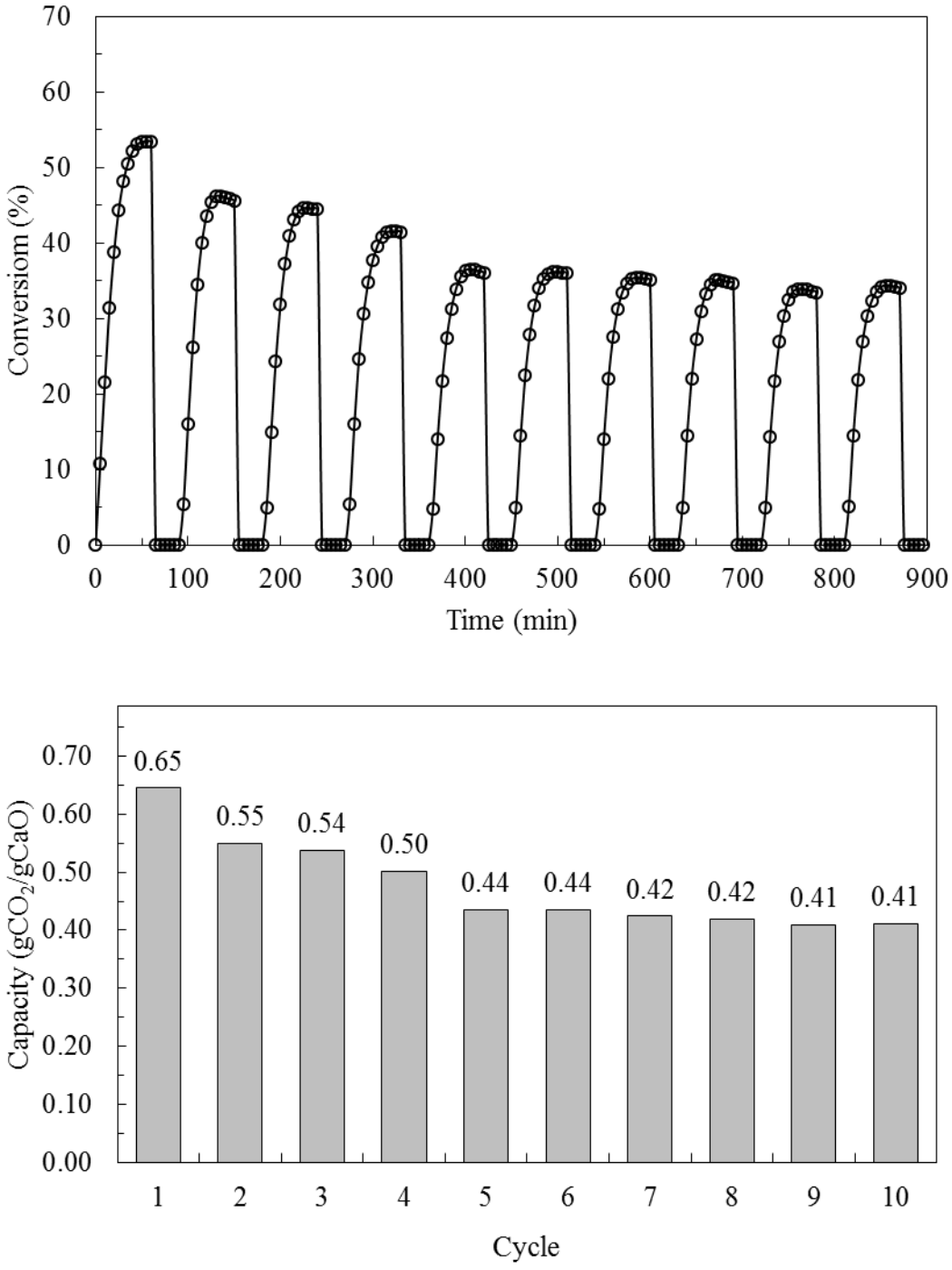

Fig. 6.7: Conversion and capacity of CaO-based sorbent synthesized by sol-gel method for 10th repeated cycles

6.6 Conclusion

CaO-based sorbents, which synthesized by different techniques, leads to different distinguish morphologies structure. The sorbent prepared by wet mixing and co-precipitation shows large particles and rough surface whereas sol-gel provided uniformly small particles and sol mixing formed small particles aggregation. Preparation CaO-based alumina with the addition of Gemini surfactant influences the morphologies of CaO-based alumina sorbent. The sorbents prepared by sol-gel method provides uniform small particles, which in turn offers good performance for CO_2 sorption capacity of 0.63 $gCO_2/gCaO$. Stability of the CaO-based sorbent prepared by sol-gel shows a reduction of 36% over 10 repeated cycles.

CHAPTER VII

CONCLUSIONS

This work is attempted to improve properties of CaO-based sorbent for high-temperature CO_2 sorption. Results obtained from the study are summarized as follows.

- Precipitation of $CaCO_3$ by using different precursors exhibits different morphologies and have effect on morphology of CaO sorbent as well as the ability to adsorb CO_2. The large network of connected particles obtained from $CaO_{Ac\text{-}urea}$ shows good performance for CO_2 sorption of 0.64 $gCO_2/gCaO$ at temperature 700°C. The kinetic model reveals that the sorption systems are controlled by both surface and diffusion through the layer.
- The addition of anionic surfactants, SDS and Gemini surfactant, has an influence on morphology of $CaCO_3$, of which rod-like structure is observed for SDS whereas needle-like is observed for Gemini surfactant.
- Concentration of surfactant on CaO-based sorbent exhibits either positive or negative impact on CO_2 sorption capacity: CaO-SDS 20 mM and CaO-GS 2 mM can increase sorption capacity to 0.27 and 0.29 $gCO_2/gCaO$, respectively, at carbonation temperature of 600°C due to connected small particles of CaO-SDS 20 mM and high surface area (16.3 m^2/g) of CaO-GS 2 mM. CaO-SDS 40 mM and CaO-GS 4 mM show negative effect because the interaction of surfactant on $CaCO_3$ promoted aggregation of small particles to large compact particle.
- CaO-based sorbents, which synthesized by different techniques, distinguish morphologies structure and have an influence on CO_2 capture. The sorbent prepared by wet mixing and co-precipitation show large particles and rough surface, sol-gel exhibit uniformly small particles, and sol mixing provide small particles aggregation. The sol-gel sorbent offers good performance for CO_2 sorption of 0.63 $gCO_2/gCaO$. The sorption is observed to reduce to 0.41 $gCO_2/gCaO$ for 10 cycles of adsorption at 600°C under 15%v/v CO_2 (balanced N_2).

REFERENCES

Abanades, J.C., Alvarez, D., 2003. Conversion Limits in the Reaction of CO_2 with Lime. *Energy & Fuels*, 17, 308-315.

Akgsornpeak, A., Witoon, T., Mungcharoen, T., Limtrakul, J., 2014. Development of synthetic CaO sorbents via CTAB-assisted sol–gel method for CO_2 capture at high temperature. *Chemical Engineering Journal*, 237, 189–198.

Blamey, J., Anthony, E.J., Wang, J., Fennel, P.S., 2010. The calcium looping cycle for large-scale CO_2 capture. *Progress in Energy and Combustion Science*, 36, 260–279.

Broda, M., Kierzkowska, A. M., Müller C. R., 2012. Influence of the Calcination and Carbonation Conditions on the CO_2 Uptake of Synthetic Ca-Based CO_2 Sorbents. *Environ. Sci. Technol.*, 46, 10849−10856.

Bruce, C.D., Berkowitz, M.L., Perera, L., and Forbes, M.D.E., 2002. Molecular Dynamics Simulation of Sodium Dodecyl Sulfate Micelle in Water: Micellar Structural Characteristics and Counterion Distribution. *J. Phys. Chem. B*, 106, 3788-3793.

Cazorla-Amorb, D., Joly, J. P., Linares-Solano, A., Marcilla-Gomis, A., Salinas-Martinez de Lecea, C., 1991 CO_2-CaO Surface and Bulk Reactions: Thermodynamic and Kinetic Approach. *J . Phys. Chem.*, 95, 6611-6617

Chen, C., Yang, S., Ahn W., 2012. Calcium oxide as high temperature CO_2 sorbent: Effect of textural properties. *Materials Letters*, 75, 140–142.

Chen, H., Zhao, C., Duan, L., Liang, C., Liu, D., Chen X., 2011. Enhancement of reactivity in surfactant-modified sorbent for CO_2 capture in pressurized carbonation. *Fuel Processing Technology*, 92, 493–499.

Chen, J., Xiang, L., 2009, Controllable synthesis of calcium carbonate polymorphs at different temperatures. *Powder Technology*, 189, 64–69.

Chen, Z., Li, C., Yang, Q., Nan, Z., 2010. Transformation of novel morphologies and polymorphs of $CaCO_3$ crystals induced by the anionic surfactant SDS. *Materials Chemistry and Physics*, 123, 534–539.

Chen, Z., Nan, Z., 2011. Controlling the polymorph and morphology of $CaCO_3$ crystals using surfactant mixtures. *Journal of Colloid and Interface Science*, 358, 416–422.

Cho, Y.B., Seo, G., Chang, D.R., 2009. Transesterification of tributyrin with methanol over calcium oxide catalysts prepared from various precursors. *Fuel Processing Technology*, 90, 1252–1258.

Coenen, A., Church, T. L., Harris A. T., 2012. Biological versus Synthetic Polymers as Templates for Calcium Oxide for CO_2 Capture. *Energy Fuels*, 26, 162−168.

Dou B., Song, Y., Liu, Y., Feng C., 2010. High temperature CO_2 capture using calcium oxide sorbent in a fixed-bed reactor. *Journal of Hazardous Materials*, 183, 759–765.

Filitz, R., Kierzkowska, A.M., Broda, M., and Muller, C.R., 2012. Highly Efficient CO_2 Sorbents: Development of Synthetic, Calcium-Rich Dolomites. *Environ. Sci. Technol*., 46, 559−565.

Florin, N. H., Blamey, J., Fennell P. S., 2010. Synthetic CaO-Based Sorbent for CO_2 Capture from Large-Point Sources. *Energy Fuels*, 24, 4598–4604.

Florin, N. H., Harris, A. T., 2008. Preparation and Characterization of a Tailored Carbon Dioxide Sorbent for Enhanced Hydrogen Synthesis in Biomass Gasifiers. *Ind. Eng. Chem. Res.*, 47, 2191-2202.

Florin, N.H., Harris, A.T., 2009. Reactivity of CaO derived from nano-sized $CaCO_3$ particles through multiple CO_2 capture-and-release cycles. *Chemical Engineering Science*, 64, 187-191.

Franchi, R. S., Harlick, P. J. E., Sayari A., 2005. Applications of Pore-Expanded Mesoporous Silica. 2. Development of a High-Capacity, Water-Tolerant Adsorbent for CO_2. *Ind. Eng. Chem. Res.*, 44, 8007-8013.

Grasa, G., González, B., Alonso, M., Abanades J. C., 2007. Comparison of CaO-Based Synthetic CO_2 Sorbents under Realistic Calcination Conditions. *Energy & Fuels*, 21, 3560–3562.

Gupta, H., Fan, L.S., 2002. Carbonation-Calcination Cycle Using High Reactivity Calcium Oxide for Carbon Dioxide Separation from Flue Gas. *Ind. Eng. Chem. Res.*, 41, 4035-4042.

Hadiko, G., Han, Y. S., Fuji, M., Takahashi M., 2005. Synthesis of hollow calcium carbonate particles by the bubble templating method. *Materials Letters*, 59, 2519–2522.

Hai-xin, B., Xiao-zhen, S., Xiao-hua, L., Sheng-yong, L., 2009. Synthesis of porous CaO microsphere and its application in catalyzing transesterification reaction for biodiesel. *Trans. Nonferrous Met. Soc. China*, 19, s674-s677.

Hongxia, G., Zhenping, Q., Peng, Q., Peng, Y., Suping, C., Wei W., 2011. Crystallization of aragonite $CaCO_3$ with complex structures. *Advanced Powder Technology*, 22, 777–783.

Huang, J.H., Mao, Z.F., Luo, M.F., 2007. Effect of anionic surfactant on vaterite $CaCO_3$. *Materials Research Bulletin*, 42, 2184–2191.

Hwang, D.J., Cho, K.H., Choi, M.K., Yu, Y.H., Lee, S.K., Ah, J.W., Lim, G.I., Han, C., Lee, J.D., 2011. Effects of sodium dodecyl benzenesulfonic acid (SDBS) on the

morphology and the crystal phase of $CaCO_3$, *Korean J. Chem. Eng.*, 28(9), 1927-1935.

Katsuyama, Y., Yamasaki, A., Iizuka, A., Fujii, M., Kumagai, K., and, Yanagisawa Y., Development of a Process for Producing High-Purity Calcium Carbonate ($CaCO_3$) from Waste Cement Using Pressurized CO_2. *Environmental Progress*, Vol.24, No.2

Kierzkowska, A.M., Poulikakos, L.V., Broda, M., Müller, C.R., 2013. Synthesis of calcium-based, Al_2O_3-stabilized sorbents for CO_2 capture using a co-precipitation technique. *International Journal of Greenhouse Gas Control*, 15, 48–54.

Liang, P., Zhao, Y., Shen, Q., Wang, D., Xu D., 2004. The effect of carboxymethyl chitosan on the precipitation of calcium carbonate, *Journal of Crystal Growth*, 261, 571–576.

Liu, C., Zhang, L., Deng, J., Mu, Q., Dai, H., He, H., 2008. Surfactant-Aided Hydrothermal Synthesis and Carbon Dioxide Adsorption Behavior of Three-Dimensionally Mesoporous Calcium Oxide Single-Crystallites with Tri-, Tetra-, and Hexagonal Morphologies. *J. Phys. Chem. C*, 112, 19248–19256.

Liu, F., Li, W., Liua B., Lia R., 2013. Synthesis, characterization, and high temperature CO_2 capture of new CaO based hollow sphere sorbents. *J. Mater. Chem. A*, 1, 8037–8044.

Liu, W., Low, N. W., Feng, B., Wang, G., Costa, J. C. D., 2010. Calcium Precursors for the Production of CaO Sorbents for Multicycle CO_2 Capture. *Environ. Sci. Technol.*, 44, 841–847.

López-Periago, A. M., Fraile, J., López-Aranguren, P., Vega, L. F., Domingo, C., 2013. CO_2 capture efficiency and carbonation/calcination kinetics of micro and nanosized particles of supercritically precipitated calcium carbonate. *Chemical Engineering Journal*, 226, 357–366.

Lu, H., Khan, A., Pratsinis, S.E., Smirniotis, P.G., *2009*. Flame-Made Durable Doped-CaO Nanosorbents for CO_2 Capture. *Energy & Fuels*, 23, 1093–1100.

Lu, H., Khan, A., Smirniotis, P. G., 2008. Relationship between Structural Properties and CO_2 Capture Performance of CaO-Based Sorbents Obtained from Different Organometallic Precursors. *Ind. Eng. Chem. Res.*, 47, 6216–6220.

Lu, H., Reddy, E. P., Smirniotis, P. G., 2006. Calcium Oxide Based Sorbents for Capture of Carbon Dioxide at High Temperatures. *Ind. Eng. Chem. Res.*, 45, 3944-3949.

Luo, C., Zheng, Y., Ding, N., Zheng, C., 2011. Enhanced cyclic stability of CO_2 adsorption capacity of CaO-based sorbents using La_2O_3 or $Ca_{12}Al_{14}O_{33}$ as additives. *Korean J. Chem. Eng*, 28(4), 1042-1046.

Lysikov, A.I., Salanov, A.N., Okunev, A.G., 2007. Change of CO_2 Carrying Capacity of CaO in Isothermal Recarbonation-Decomposition Cycles. *Ind. Eng. Chem. Res.*, 46, 4633-4638.

Martavaltzi[a], C.S., Lemonidou, A.A., 2008. Development of new CaO based sorbent materials for CO_2 removal at high temperature. *Microporous and Mesoporous Materials*, 110, 119–127.

Martavaltzi[b], C.S., Lemonidou, A.A., 2008. Parametric Study of the CaO-$Ca_{12}Al_{14}O_{33}$ Synthesis with Respect to High CO_2 Sorption Capacity and Stability on Multicycle Operation. *Ind. Eng. Chem. Res.*, 47, 9537–9543.

Naka, K., Tanaka, Y., Chujo, Y., 2002. Effect of Anionic Starburst Dendrimers on the Crystallization of $CaCO_3$ in Aqueous Solution: Size Control of Spherical Vaterite Particles. *Langmuir*, 18, 3655-3658.

Nan, Z., Chen, X., Yang, Q., Wang, X., Shi, Z., Hou, W., 2008. Structure transition from aragonite to vaterite and calcite by the assistance of SDBS. *Journal of Colloid and Interface Science*, 325, 331–336.

Ochoa-Fernandez, E., Rusten, H. K., Jakobsen, H. A., Rønning, M., Holmen, A., Chen D., 2005. Sorption enhanced hydrogen production by steam methane reforming using Li_2ZrO_3 as sorbent: Sorption kinetics and reactor simulation. *Catalysis Today*, 106, 41–46.

Olivares-Marín, M., Cuerda-Correa, E.M., Nieto-Sánchez, A., García, S., Pevida, C., Román, S., 2013. Influence of morphology, porosity and crystal structure of $CaCO_3$ precursors on the CO_2 capture performance of CaO-derived sorbents. *Chemical Engineering Journal*, 217, 71–81.

Qin, C., Liu, W., An, H., Yin, J., Feng B., 2012. Fabrication of CaO-Based Sorbents for CO_2 Capture by a Mixing Method. *Environ. Sci. Technol.*, 46, 1932−1939.

Ronald Barker, 1973. The Reversibility of the Reaction $CaCO_3 \rightarrow CaO+CO_2$, *J. appl. Chem. Biotechnol*., 23, 133-142.

Samanta, A., Zhao, A., Shimizu, G. K. H., Sarkar, P., Gupta R., 2012. Post-Combustion CO_2 Capture Using Solid Sorbents: A Review. *Ind. Eng. Chem. Res.*, 51, 1438–1463.

Sammalkorpi, M., Karttunen, M., Haataja, M., 2009. Ionic Surfactant Aggregates in Saline Solutions: Sodium Dodecyl Sulfate (SDS) in the Presence of Excess Sodium Chloride (NaCl) or Calcium Chloride ($CaCl_2$). *J. Phys. Chem. B*, 113, 5863–5870.

Santos, E.T., Alfonsín, C., Chambel, A.J.S., Fernandes, A., Soares Dias, A.P., Pinheiro, C.I.C., Ribeiro, M.F., 2012. Investigation of a stable synthetic sol–gel CaO sorbent for CO_2 capture. *Fuel*, 94, 624–628.

Shen, Q., Wei, H., Zhao, Y., Wang, D.,Zheng, L., Xu, D., 2004. Morphological control of calcium carbonate crystals by polyvinylpyrrolidone and sodium dodecyl benzene sulfonate. *Colloids and Surfaces A: Physicochem. Eng. Aspects*, 251 87–91.

Silaban, A., Narcida, M. Harrison, D.P., 1992. Calcium acetate as a sorbent precursor for the removal of carbon dioxide from gas streams at high temperature. *Conservation and Recycling*, 7, 139-l53.

Toftegaard, M. B., Brix, J., Jensen, P. A., Glarborg, P., Jensen A. D., 2010. Oxy-fuel combustion of solid fuels. *Progress in Energy and Combustion Science*, 36, 581-625.

Tsubone, K., Ogawa, T., Mimura, K., Surface and Aqueous Properties of Anionic Gemini Surfactants Having Dialkyl Amide, Carboxyl, and Carboxylate Groups. *Journal of Surfactants and Detergents*, Vol. 6, No.1.

Wada, N., Kanamura, K., Umegaki, T., 2001. Effects of Carboxylic Acids on the Crystallization of Calcium Carbonate. *Journal of Colloid and Interface Science*, 233, 65–72.

Wang, M., Lawal, A., Stephenson, P., Sidders, J., Ramshaw, C., 2011. Post-combustion CO_2 capture with chemical absorption: A state-of-the-art review. *Chemical engineering research and design*, 89, 1609–1624.

Wang, Y., Han, Y., Huang, X., Cao, M., Wang, Y., 2008. Aggregation behaviors of a series of anionic sulfonate gemini surfactants and their corresponding monomeric surfactant. *Journal of Colloid and Interface Science*, 319, 534–541.

Wei, H., Shen, Q., Zhao, Y., Zhou, Y., Wang, D., Xu, D., 2005. On the crystallization of calcium carbonate modulated by anionic surfactants. *Journal of Crystal Growth*, 279, 439–446.

Wen, Y., Xiang, L., Jin, Y., 2003. Synthesis of plate-like calcium carbonate via carbonation route. *Materials Letters*, 57, 2565–2571.

Witoon, T., Mungcharoen, T., Limtrakul, J., 2014. Biotemplated synthesis of highly stable calcium-based sorbents for CO_2 capture via a precipitation method. *Applied Energy*, 118, 32–40.

Xu, P., Xie, M., Cheng, Z., Zhou, Z., 2013. CO_2 Capture Performance of CaO-Based Sorbents Prepared by a Sol−Gel Method. *Ind. Eng. Chem. Res.*, 52, 12161−12169.

Yan, H., Yuan, S., Xu, G., Liu, C., 2010. Effect of Ca^{2+} and Mg^{2+} Ions on Surfactant Solutions Investigated by Molecular Dynamics Simulation. *Langmuir*, 26(13), 10448–10459.

Yang, Z., Zhao, M., Florin, N. H., Harris, A. T., 2009 Synthesis and Characterization of CaO Nanopods for High Temperature CO_2 Capture. *Ind. Eng. Chem. Res.*, 48, 10765–10770.

Yin, J., Zhang, C., Qin, C., Liu, W., An, H., Chen, G., Feng B., 2012. Reactivation of calcium-based sorbent by water hydration for CO_2 capture. *Chemical Engineering Journal*, 198–199, 38–44.

Yoshimura, T., Bong, M., Matsuoka, K., Honda, C., End, K., 2009. Surface properties and aggregate morphology of partially fluorinated carboxylate-type anionic gemini surfactants. *Journal of Colloid and Interface Science*, 339, 230–235.

Yu, J., Zhao, X., Cheng, B., Zhang, Q., 2005. Controlled synthesis of calcium carbonate in a mixed aqueous solution of PSMA and CTAB. *Journal of Solid State Chemistry*, 178, 861–867.

Zhang, C., Zhang, J., Feng, X., Li, W., Zhao, Y., Han, B., 2008. Influence of surfactants on the morphologies of $CaCO_3$ by carbonation route with compressed CO_2. *Colloids and Surfaces A: Physicochem. Eng. Aspects*, 324, 167–170.

Zhao, C., Zhou, Z., Cheng Z., 2014. Sol−gel-Derived Synthetic CaO-Based CO_2 Sorbents Incorporated with Different Inert Materials. *Ind. Eng. Chem. Res.*, 53, 14065−14074.

Zhou, Z., Qi, Y., Xie, M., Cheng, Z., Yuan W., 2012. Synthesis of CaO-based sorbents through incorporation of alumina/aluminate and their CO_2 capture performance. *Chemical Engineering Science*, 74, 172–180.

Zhu, Y., Wu, S., Wang, X., 2011. Nano CaO grain characteristics and growth model under calcination. *Chemical Engineering Journal*, 175, 512–518.

APPENDIX A

Calculation capacity from breakthrough curve

Mass balance of CO_2

$$Accmulation = In - Out$$

$$\frac{dm_{CO_2}}{dt} = QC_0M_{w,CO_2} - QCM_{w,CO_2}$$

Assumption: Volumetric flow rate related to composition of N_2 and CO_2

$$\int m_{CO_2} = \left(x_{N_2} + x_{CO_{2,t}}\right)QM_{w,CO_2}\int_0^t (C_0 - C)\,dt$$

Mass CO_2 accumulation

$$m_{CO_2} = \left(x_{N_2} + x_{CO_{2,t}}\right)QM_{w,CO_2}C_0\int_0^t \left(1 - \frac{C}{C_0}\right)dt$$

Capacity of CaO

$$Capacity\ of\ CaO = \frac{m_{CO_2}}{m_{CaO}} = \frac{\left(x_{N_2} + x_{CO_{2,t}}\right)QM_{w,CO_2}C_0}{m_{CaO}}\int_0^t \left(1 - \frac{C}{C_0}\right)dt$$

$m_{CO_2} = mass\ of\ CO_2\ (g\ CO_2)$
$m_{CaO} = mass\ of\ CaO\ (g\ CaO)$
$x_{N_2} = volume\ fraction\ of\ N_2$
$x_{CO_2} = volume\ fraction\ of\ CO_2$
$Q = volumetric\ flow\ rate\ of\ gas\ (\frac{ml}{min})$
$M_{w,CO_2} = molecular\ weight\ of\ CO_2\ (\frac{g}{mol})$
$C_0 = initial\ concentration\ of\ CO_2\ (\frac{mol}{ml})$

$C = Outlet\ concentration\ of\ CO_2\ at\ time\ (\frac{mol}{ml})$
$t = time\ (min)$

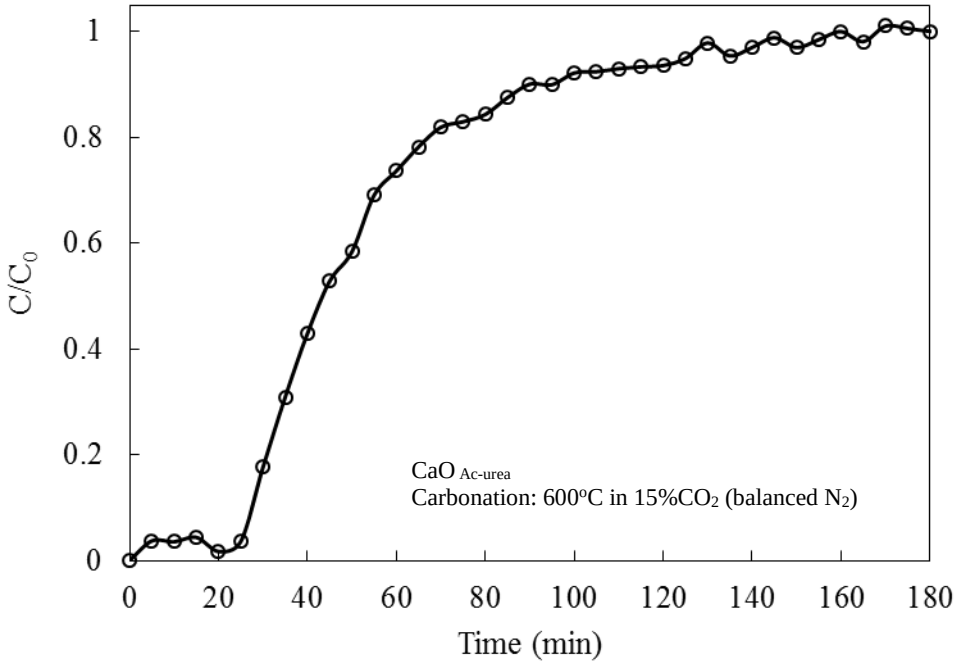

Fig. A.1: Breakthrough curve of $CaO_{Ac\text{-}urea}$ at 600ºC

Table A.1 Data experimental of $CaO_{Ac\text{-}urea}$ at 600°C

Time (min)	Area N_2	Area CO_2	Vol. N_2 (ml)	Vol. CO_2 (ml)	XCO_2	C/C_0	$1\text{-}C/C_0$	Int. $(1\text{-}C/C_0)$	Acc. CO_2 (gCO_2)	Capacity ($gCO_2/gCaO$)	ACC. Capa
0	0	0	0.00	0.00	0.00	0.00	1.00				0.00
5	23170	112	1.16	0.01	0.00	0.04	0.96	4.91	0.02	0.02	0.02
10	22934	105	1.15	0.01	0.00	0.04	0.96	4.82	0.02	0.02	0.04
15	23043	131	1.15	0.01	0.01	0.04	0.96	4.80	0.02	0.02	0.06
20	22892	51	1.14	0.00	0.00	0.02	0.98	4.85	0.02	0.02	0.08
25	22801	106	1.14	0.01	0.00	0.04	0.96	4.87	0.02	0.02	0.10
30	22404	520	1.12	0.03	0.02	0.18	0.82	4.47	0.01	0.02	0.12
35	22176	918	1.11	0.05	0.04	0.31	0.69	3.79	0.01	0.02	0.14
40	21684	1267	1.08	0.06	0.06	0.43	0.57	3.15	0.01	0.01	0.15
45	21577	1572	1.08	0.08	0.07	0.53	0.47	2.60	0.01	0.01	0.16
50	21333	1731	1.07	0.09	0.08	0.58	0.42	2.22	0.01	0.01	0.17
55	21147	2061	1.06	0.10	0.09	0.69	0.31	1.81	0.01	0.01	0.18
60	21032	2199	1.05	0.11	0.09	0.74	0.26	1.43	0.00	0.01	0.18
65	20862	2332	1.04	0.12	0.10	0.78	0.22	1.20	0.00	0.01	0.19
70	20661	2432	1.03	0.12	0.11	0.82	0.18	1.00	0.00	0.00	0.19
75	20618	2461	1.03	0.12	0.11	0.83	0.17	0.88	0.00	0.00	0.20
80	21047	2559	1.05	0.13	0.11	0.84	0.16	0.82	0.00	0.00	0.20
85	20632	2615	1.03	0.13	0.11	0.88	0.12	0.70	0.00	0.00	0.20
90	20684	2708	1.03	0.14	0.12	0.90	0.10	0.56	0.00	0.00	0.21
95	20725	2710	1.04	0.14	0.12	0.90	0.10	0.50	0.00	0.00	0.21
100	20649	2775	1.03	0.14	0.12	0.92	0.08	0.45	0.00	0.00	0.21
105	20777	2801	1.04	0.14	0.12	0.92	0.08	0.38	0.00	0.00	0.21
110	20709	2811	1.04	0.14	0.12	0.93	0.07	0.36	0.00	0.00	0.21

115	20669	2818	1.03	0.14	0.12	0.93	0.07	0.34	0.00	0.00	0.21
120	20679	2828	1.03	0.14	0.12	0.94	0.06	0.33	0.00	0.00	0.22
125	20676	2872	1.03	0.14	0.12	0.95	0.05	0.29	0.00	0.00	0.22
130	20356	2929	1.02	0.15	0.13	0.98	0.02	0.18	0.00	0.00	0.22
135	20766	2903	1.04	0.15	0.12	0.95	0.05	0.17	0.00	0.00	0.22
140	20803	2963	1.04	0.15	0.12	0.97	0.03	0.19	0.00	0.00	0.22
145	20649	3005	1.03	0.15	0.13	0.99	0.01	0.10	0.00	0.00	0.22
150	20747	2955	1.04	0.15	0.12	0.97	0.03	0.10	0.00	0.00	0.22
155	20873	3025	1.04	0.15	0.13	0.99	0.01	0.11	0.00	0.00	0.22
160	20842	3074	1.04	0.15	0.13	1.00	0.00	0.04	0.00	0.00	0.22
165	20964	3026	1.05	0.15	0.13	0.98	0.02	0.05	0.00	0.00	0.22
170	20871	3115	1.04	0.16	0.13	1.01	-0.01	0.02	0.00	0.00	0.22
175	20887	3102	1.04	0.16	0.13	1.01	-0.01	-0.04	0.00	0.00	0.22
180	21012	3101	1.05	0.16	0.13	1.00	0.00	-0.02	0.00	0.00	0.22
185	20909	3083	1.05	0.15	0.13	1.00	0.00	0.00	0.00	0.00	0.22

Find $\int_0^t \left(1 - \frac{C}{C_0}\right) dt$ from integrate area of breakthrough curve in 0-5

$$\int_0^t \left(1 - \frac{C}{C_0}\right) dt = Area\ above\ the\ graph$$

$$\int_0^5 \left(1 - \frac{C}{C_0}\right) dt = 4.91\ min$$

Calculation mass of CO_2 for 0-5 min

$$m_{CO_2} = \left(x_{N_2} + x_{CO_{2,t}}\right) Q M_{w,CO_2} C_0 \int_0^t \left(1 - \frac{C}{C_0}\right) dt$$

$$m_{CO_2} = (0.85 + 0)(15)(44)(0.00000504)(4.91)$$

$$m_{CO_2} = 0.02\ gCO_2$$

Capacity of CaO for 0-5 min

$$Capacity\ of\ CaO = \frac{0.02}{0.79} = 0.02\ gCO_2/gCaO$$

APPENDIX B

Experimental of investigated effect of CO_2 sorption in part 1 is analyzed by gas chromatography (Shimadzu GC-14B) that equipped with Porapak-Q column and TCD detector. Gas chromatography is used under operating condition that show in Table. B.1. The gas standard is injected to gas chromatography at different concentrations and the results obtained peak area from gas chromatography for each concentration. Then, peak area of gas chromatography and volume of injected gas are plotted, the calibration curves are showed in Fig. B.1.

Table B.1 Operating conditions for gas chromatography of Shimadzu

Gas Chromatography	Shimadzu GC-14B
Detector	TCD
Column	Porapak-Q
Carrier gas	Ar (99.999%)
Column temperature	
- initial (˚C)	40
- final (˚C)	40
Injector temperature (˚C)	150
Detector temperature (˚C)	150
Current (mA)	70 mA
Analyzed gas	N_2 and CO_2

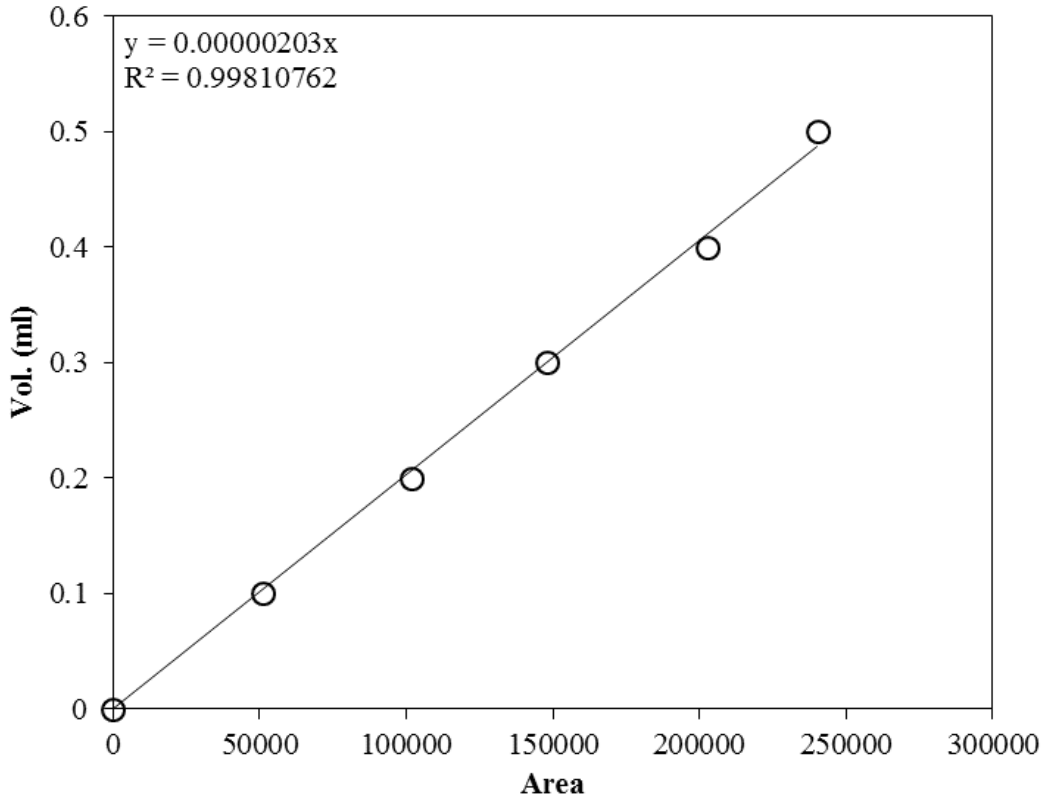

Fig. B.1: Calibration curve of CO_2 by Shimadzu GC-14B

Calibration curve is done from gas chromatography (SRI 8610C) equipped with two column that are Molecular Sieve and Porapak-Q column. Table B.2 shows the operating conditions for gas chromatography. The calibration curves are showed in Fig. B.2 and Fig. B.3.

Table B.2 Operating conditions for gas chromatography of SRI

Gas Chromatography	SRI 8610C	
Detector	TCD	
Column	Molecular sieve	Porapak-Q
Carrier gas	Ar (99.999%)	Ar (99.999%)
Column temperature		
- initial (˚C)	100	100
- final (˚C)	100	100
Injector temperature (˚C)	100	100
Detector temperature (˚C)	100	100
Current (mA)	High	High
Analyzed gas	N_2	CO_2

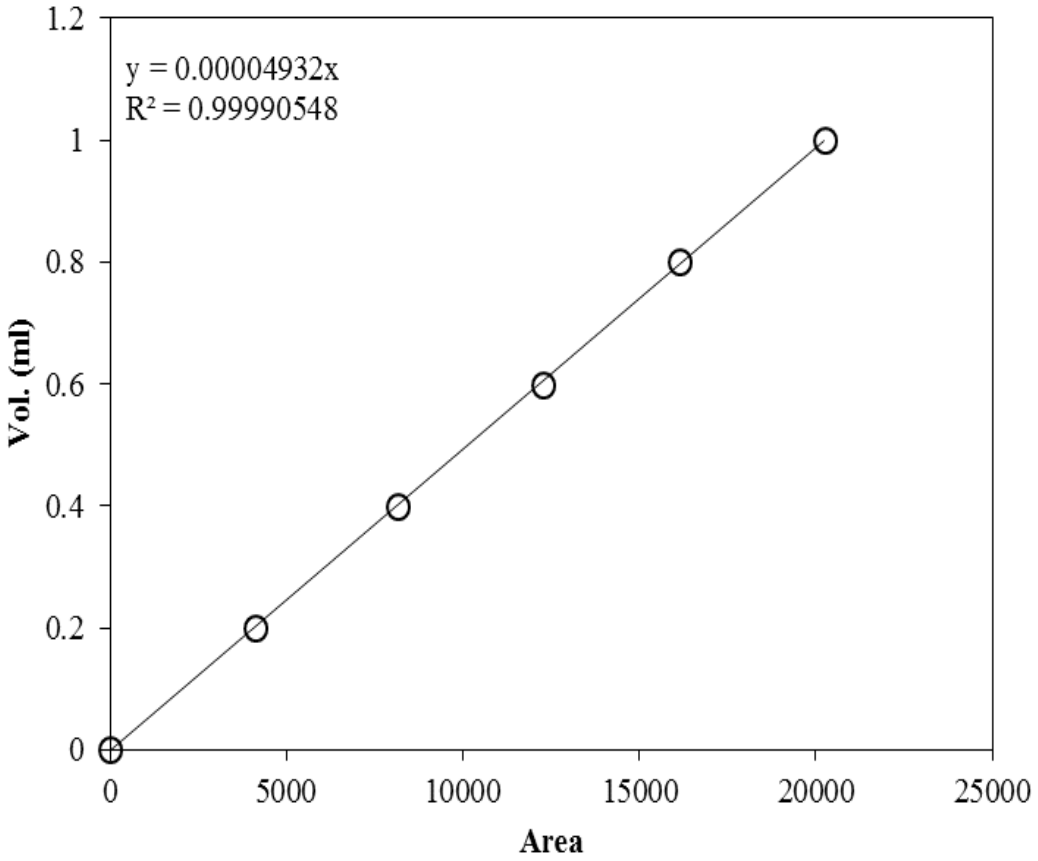

Fig. B.2: Calibration curve of N_2 by SRI 8610C

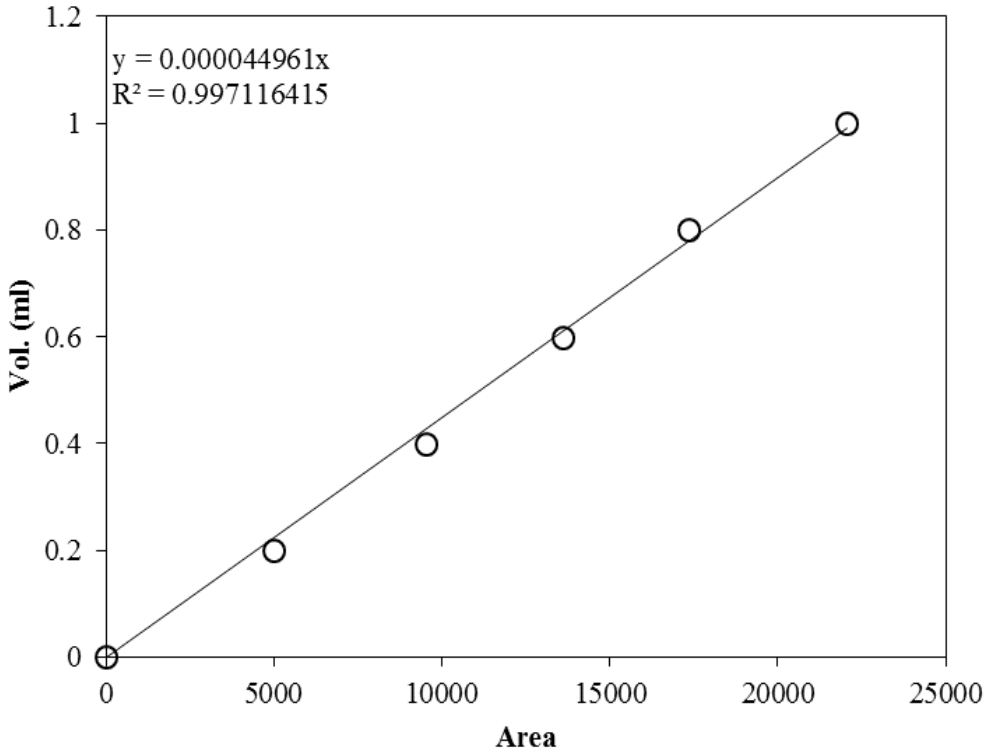

Fig. B.3: Calibration curve of CO_2 by SRI 8610C

Biography

Name-Surname	Panupong Jamrunroj
Birth	27th December 1990 in Chachoengsao, Thailand
Address	9/2, Village NO. 1, Tha Thonglang Sub-district, Bangkla District, Chachoengsao, 24110
Education Background	
2014-2015	Master's degree of Chemical Engineering, Department of Chemical engineering, Silpakorn University
2009-2013	Bachelor's degree of Chemical Engineering, Faculty of Engineering and Industrial Technology, Silpakorn University, GPA: 2.81
High school	Saint Louis School Chachoengsao